

Accepted Manuscript

On a family of numerical models for couple stress based flexoelectricity for continua and beams

Roman Poya, Antonio J. Gil, Rogelio Ortigosa, Roberto Palma

PII: S0022-5096(18)30986-4

DOI: <https://doi.org/10.1016/j.jmps.2019.01.013>

Reference: MPS 3548



To appear in: *Journal of the Mechanics and Physics of Solids*

Received date: 8 November 2018

Revised date: 21 January 2019

Accepted date: 22 January 2019

Please cite this article as: Roman Poya, Antonio J. Gil, Rogelio Ortigosa, Roberto Palma, On a family of numerical models for couple stress based flexoelectricity for continua and beams, *Journal of the Mechanics and Physics of Solids* (2019), doi: <https://doi.org/10.1016/j.jmps.2019.01.013>

This is a PDF file of an unedited manuscript that has been accepted for publication. As a service to our customers we are providing this early version of the manuscript. The manuscript will undergo copyediting, typesetting, and review of the resulting proof before it is published in its final form. Please note that during the production process errors may be discovered which could affect the content, and all legal disclaimers that apply to the journal pertain.

On a family of numerical models for couple stress based flexoelectricity for continua and beams

Roman Poya^a, Antonio J. Gil^b, Rogelio Ortigosa^b, Roberto Palma^c

^a*Digital Factory, Simulation & Test Solutions, Siemens PLM Software, Siemens Industry Software Limited, Cambridge, CB2 1PH, United Kingdom*

^a*Zienkiewicz Centre for Computational Engineering, College of Engineering, Swansea University, Bay Campus, SA1 8EN, United Kingdom*

^c*Department of Mechanical Engineering and Construction, Universitat Jaume I, Campus Riu Sec, 12071 Castellón, Spain*

Abstract

A family of numerical models for the phenomenological linear flexoelectric theory for continua and their particularisation to the case of three-dimensional beams based on a skew-symmetric couple stress theory is presented. In contrast to the standard strain gradient flexoelectric models which assume coupling between electric polarisation and strain gradients, we postulate an electric enthalpy in terms of linear invariants of curvature and electric field. This is achieved by introducing the axial (mean) curvature vector as a strain gradient measure. The physical implication of this assumption is many-fold. Firstly, analogous to the standard strain gradient models, for isotropic (non-piezoelectric) materials it allows constructing flexoelectric energies without breaking material's centrosymmetry. Secondly, unlike the standard strain gradient models, nonuniform distribution of volumetric part of strains (volumetric strain gradients) do not generate electric polarisation, as also confirmed by experimental evidence to be the case for some important classes of flexoelectric materials. Thirdly, a state of plane strain generates out of plane deformation through strain gradient effects. Finally, under this theory, extension and shear coupling modes cannot be characterised individually as they contribute to the generation of electric polarisation as a whole. As a first step, a detailed comparison of the developed couple stress based flexoelectric model with the standard strain gradient flexoelectric models is performed for the case of Barium Titanate where a myriad of simple analytical solutions are assumed in order to quantitatively describe the similarities and dissimilarities in effective electromechanical coupling under these two theories. From a physical point of view, the most notable insight gained is that, if the same experimental flexoelectric constants are fitted in to both theories, the presented theory in general, reports up to 200% stronger electromechanical conversion efficiency. From the formulation point of a view, the presented flexoelectric model is also competitively simpler as it eliminates the need for high order strain gradient and coupling tensors and can be characterised by a single flexoelectric coefficient. In addition, three distinct mixed flexoelectric variational principles are presented for both continuum and beam models that facilitate incorporation of strain gradient measures in to a standard finite element scheme while maintaining the C^0 continuity. Consequently, a series of low and high order mixed finite element schemes for couple stress based flexoelectricity are presented and thoroughly benchmarked against available closed form solutions in regards to electromechanical coupling efficiency. Finally, nanocompression of a complex flexoelectric conical pyramid for which analytical solution cannot be established is numerically studied where curvature induced necking of the specimen and vorticity around the frustum generate moderate electric polarisation.

Keywords: Flexoelectricity, size-dependent piezoelectricity, couple stress theory, curvature-induced polarisation, mixed high order finite elements

1. Introduction

Modelling linear piezoelectricity for actuation and energy harvesting purposes using the classical continuum mechanics theory is now well established in the literature, [Erturk and Inman \[2011\]](#); [duToit et al. \[2005\]](#); [Trindade et al. \[2001a,b\]](#); [Schröder and Gross \[2004\]](#); [Poya et al. \[2015\]](#). It is well known, that for a material to exhibit electric polarisation in the presence of mechanical strain (direct piezoelectric effect), it needs to have a noncentrosymmetric crystal structure, [Wooster \[1973\]](#). Recently, there has been a considerable research on producing piezoelectric effects from centrosymmetric (non-piezoelectric) materials, for instance, from perovskite ferroelectrics [Zubko et al. \[2007, 2013\]](#) and even graphene nano-shells and biological membranes, [Dumitrica et al. \[2002\]](#); [Petrov \[2006\]](#); [Maranganti et al. \[2006\]](#); [Kalinin and Meunier \[2008\]](#); [Maranganti and Sharma \[2009\]](#); [Zelisko et al. \[2014\]](#); [Deng et al. \[2014\]](#). To generate polarisation in centrosymmetric materials, the inversion symmetry of the material needs to be broken and this becomes achievable through the application of non-uniform strains (strain gradients). Theoretical and experimental evidence of this size-dependent phenomenon which is also termed “flexoelectricity” has been reported in [Tagantsev \[1986\]](#); [Ma and Cross \[2001, 2002\]](#); [Catalan et al. \[2005\]](#); [Ma and Cross \[2006\]](#); [Zubko et al. \[2007\]](#); [Sharma et al. \[2007, 2010\]](#); [Gharbi et al. \[2011\]](#); [Krichen and Sharma \[2016\]](#) for other classes of centrosymmetric cubic and isotropic materials; see [Tagantsev \[1986\]](#); [Yudin and Tagantsev \[2013\]](#) for a historical review. As discussed in [Yudin and Tagantsev \[2013\]](#) a crystalline material of any symmetry can be capable of producing electric polarisation under a nonuniform strain field or simply in the presence of strain gradient. The effective flexoelectric coefficients are certainly orders of magnitude smaller (in the range of $\mu\text{C/m}$, [Ma and Cross \[2001\]](#)) compared to their piezoelectric counterparts, however for nano-electromechanical systems where the device and material length scales are comparable, gradient of strain can have appreciable effects, [Deng et al. \[2014\]](#); [Jiang et al. \[2013\]](#).

From a generalised continuum mechanics point of view (c.f. [Eringen and Maugin \[1990\]](#) for related terminologies), flexoelectricity is considered as a higher order gradient theory where size effects are accounted for in a phenomenological sense. The study of higher order gradient theories and generalised continua dates back to the seminal work of [Cosserat and Cosserat \[1909\]](#) which was later revisited by [Mindlin and Tiersten \[1962\]](#); [Mindlin \[1964, 1965, 1968\]](#); [Mindlin and Eshel \[1968\]](#), [Toupin \[1962, 1964\]](#); [Eringen \[1966, 1972a,b, 1983, 1999\]](#); [Eringen and Maugin \[1990\]](#); [Ericksen and Truesdell \[1958\]](#) among others. In general, the fundamental kinematic assumption of these theories is in considering every material particle in the continuum to be equipped with a substructure (micro-continuum). Different models of strain gradient theory assume different kinematics, [Eringen \[1966\]](#); [Toupin \[1962, 1964\]](#); [Lam et al. \[2003\]](#); [Hadjesfandiari and Dargush \[2011\]](#). The micropolar continuum is one particular member of this class in which every micro-continuum is treated as a rigid body equipped with a rotational field emanating from the microstructure and termed as micro-rotation “*triédre mobile*”, [Cosserat and Cosserat \[1909\]](#). Since micro-rotations of discrete particles can not be considered continuous inside the matter, a different model of gradient theories called the couple stress theory considers macro-rotation “*triédre caché*” as a true continuum kinematical measure in order to study size effects, [Mindlin and Tiersten \[1962\]](#); [Toupin \[1962\]](#); [Koiter \[1964\]](#); [Yang et al. \[2002\]](#); [Park and Gao \[2008\]](#). The couple stress model can be considered as a constrained theory of the micropolar continuum, [Toupin \[1964\]](#); [Neff \[2006\]](#); [Neff and Jeong \[2009\]](#).

Generalisation of standard continuum in the case of couple stress theory is based on the following concepts: i) the deformation of substructure is measured based on a field of proper orthogonal rotations in the configurational space of the continuum and, ii) an additional kinematic measure related to the gradient of this rotation (curvature) is included to the set of thermodynamic state variables, [Simo et al. \[1992\]](#); [Steinmann \[1994\]](#); [Steinmann and Stein \[1997\]](#); [Neff \[2006\]](#); [Bauer](#)

et al. [2012]. Consequently, the work-conjugate to the curvature tensor, called the couple-stress enters the boundary value problem and in general the balance of angular momentum does not vanish.

State of the art flexoelectric models are however based on classical strain gradient theories of Mindlin [1965]; Mindlin and Eshel [1968]; Eringen [1972a,b]; Toupin [1964] where gradients of strain and electric field explicitly appear in the electric enthalpy of the system. As a result, a third order stress tensor (hyper stress) and a second order electric displacement tensor enter the boundary value problem, see Maranganti et al. [2006]; Maranganti and Sharma [2009]; Abdollahi et al. [2014, 2015]; Deng et al. [2018]. In order to close this system, the Gauss's law needs to be modified to facilitate balance equation for the newly arisen high order tensorial quantities. For instance, the models used in Maranganti et al. [2006]; Majdoub et al. [2008, 2009]; Sharma et al. [2007]; Gharbi et al. [2011]; Abdollahi et al. [2014]; Maranganti and Sharma [2009]; Mao and Purohit [2014] are all based on this approach. Certainly, this is a deviation from the true solution of the Maxwell equations. Whether, micropolar, couple stress or in general, formulations based on curvature energy have an advantage over classical strain gradient theories, is yet to be established Chen [2012]; Hadjesfandiari [2013].

Historically, flexoelectricity has been mainly studied in the context of beams. In fact, this is also reflected in the experimental set-ups for determining effective transverse flexoelectric coefficients (the bending piezoelectricity test), for example, in the works of Takayoshi [1974]; Fukada et al. [1987]; Ma and Cross [2001, 2002, 2005, 2006]. From the perspective of structural mechanics, amongst the many gradient theories, the couple stress theory has evolved as a competitive technique to model size effects in beams and plates Park and Gao [2006, 2008]; Ma et al. [2008]; Reddy [2011]; Reddy and El-Borgi [2014]; Srinivasa and Reddy [2013]; Tsiatas [2009]. The most successful implementation of couple stress theory for beams is based on the modified couple stress theory proposed by Yang et al. [2002]. The modified couple stress theory assumes that the moment of couples vanishes and as a result the underlying curvature tensor is symmetric (and deviatoric) and work conjugate to a deviatoric couple stress. For isotropic materials, this scenario yields only one material length scale (since the spherical part of the curvature energy vanishes) which is a practically desirable feature in the analysis of micro and nanobeams. In Jeong and Neff [2010] sense, this model corresponds to the *weakest* curvature energy allowable in linear Cosserat continuum.

Three competitive variants of the couple stress model can be considered to study flexoelectricity. The modified couple stress model of Yang et al. [2002], the skew-symmetric couple stress model of Hadjesfandiari and Dargush [2011] and the conformally invariant model of Ghiba et al. [2017]. As it will be shown later, in the model of Yang et al. [2002] the rotational kinematic measure namely, the symmetric deviatoric curvature tensor still contains diagonal terms that contribute to uniform contraction of the cross-section and torsional rigidity of the beam, although energetically (this curvature tensor is work-conjugate to the deviatoric couple stress) they are never activated. This effect has been mainly ignored in subsequent formulations of the modified couple stress theory for beam models, for instance in Park and Gao [2006, 2008]; Ma et al. [2008]; Reddy [2011]; Reddy and El-Borgi [2014]. For classical beam models, it is certainly desirable to choose a kinematic measure that excludes cross-sectional terms. The skew-symmetric Hadjesfandiari and Dargush [2011] and the conformal Ghiba et al. [2017] couple stress models specifically preclude such terms in the curvature tensor and are more suited for the particularisation of couple stress to the case of beams. Among the two, the skew-symmetric couple stress model can be easily extended to the case of isotropic flexoelectricity, as the skew-symmetric nature of the curvature tensor (i.e. the mean/axial curvature vector) makes it an ideal candidate for constructing linear invariants in

conjunction with the electric field without breaking material's centrosymmetry.

Following the authors' recent development on the analysis of linear piezoelectric beams Poya et al. [2015], in this manuscript, the theoretical formulation and the associated finite element implementation of linear flexoelectricity in piezoelectric and non-piezoelectric materials based on a skew-symmetric couple stress theory is presented in the context of continua and beams. For the case of beams, no particular assumption is made on the direction of anisotropy or electric polarisation and a consistent second order interpolation of the electric field across the cross section is utilised. Furthermore, as strain gradient theories in general lead to high continuity requirements in the choice of functional spaces (for a material of grade N , C^N continuity is required [see Toupin [1962]]) for finite element discretisation, by relying on mixed variational formulations this requirement is relaxed and standard C^0 continuous interpolation functions are utilised for finite element discretisation, leading to an extremely efficient computational implementation. It should be mentioned that, while in Hadjesfandiari and Dargush [2011] it is claimed that the skew-symmetric couple stress theory is a physically valid continuum theory of its own (where every kinematic and kinetic in the theory have a physical meaning), despite having followed the same theoretical development, the present manuscript mathematically starts from a micropolar theory point of view and poses the variational principles of linear flexoelectricity as constrained minimisation problems to facilitate standard finite element implementations. It should also be noted the theory of micropolar and couple stress flexoelectricity is not new and have already been presented in Romeo [2015]; Chen [2012]; Hadjesfandiari and Dargush [2011]; Anqing et al. [2016]. The contribution of this manuscript is in presenting a series of new variational formulations for continua and beams and their subsequent numerical (finite element) discretisations for flexoelectricity. In the context of beams specifically, mixed finite element formulations for flexoelectricity are not explored. Furthermore, the focus is on qualitative and quantitative comparison of strain gradient and couple stress flexoelectric theories which as discussed later have substantial physical impact in analysing flexoelectric structures, which to the best of the authors' knowledge have not been reported before.

The structure of the paper is as follows. In section 2, the balance equations of electromechanics in a generalised micropolar continuum is presented. In section 3, the skew-symmetric couple stress model as a rotationally constrained case of the micropolar theory is discussed and the corresponding variational formulations are presented in section 4. In section 5 the couple stress problem is cast under the kinematics and electrostatics of three-dimensional flexoelectric beams and the associated virtual work and governing equations are derived. Finally, in section 6 a set of analytical and numerical problems to study the electromechanical conversion efficiency of the theory with respect to other available work in the literature are reported.

2. Balance equations of electromechanics in micropolar continuum

Let $\Omega \subset \mathbb{R}^3$ be a bounded contractible domain occupied by a micropolar continuum during the time interval $[0, T]$ and Γ be its boundary, equipped with a unit outward normal \mathbf{n} , as shown in Figure 1. In this case, the static Faraday and Gauss laws can be summarised as follows

$$\nabla \times \mathbf{E} = \mathbf{0} \quad \text{and} \quad \operatorname{div} \tilde{\mathbf{D}} - \rho^e = 0 \quad \text{in } \Omega \times [0, T], \quad (1)$$

where $\nabla \times$ denotes the curl operator, \mathbf{E} is the electric field intensity vector, $\tilde{\mathbf{D}}$ is the electric displacement vector and ρ^e is the volume charge density. According to the Helmholtz decomposition (also known as the fundamental theorem of vector calculus) and in the absence of magnetic fields, the electric field vector \mathbf{E} can be reformulated as $\mathbf{E} = -\nabla\psi$, where ψ is a scalar potential field.

Dirichlet and Neumann boundary conditions can then be introduced as

$$\psi = \bar{\psi} \quad \text{on} \quad \Gamma^\psi \times [0, T], \quad (2a)$$

$$\tilde{\mathbf{D}} \cdot \mathbf{n} = -q_0 \quad \text{on} \quad \Gamma^D \times [0, T]. \quad (2b)$$

where $\Gamma = \Gamma^D \cup \Gamma^\psi$ and $\Gamma^D \cap \Gamma^\psi = \emptyset$. In the context of small deformations, the motion of the continuum can be defined by a displacement field $\mathbf{u} : \Omega \times [0, T] \rightarrow \mathbb{R}^3$, such that $(\mathbf{x}, t) \mapsto \mathbf{u}(\mathbf{x}, t)$, where $\mathbf{x} \in \Omega$ represents a material point and $t \in [0, T]$ the time. The conservation of linear momentum equation is defined as

$$\operatorname{div} \tilde{\boldsymbol{\sigma}} + \rho \mathbf{b} = \rho \ddot{\mathbf{u}} \quad \text{in } \Omega \times [0, T], \quad (3)$$

where ρ is the density of the continuum, $\tilde{\boldsymbol{\sigma}}$ is the non-symmetric force stress tensor, \mathbf{b} is a body force per unit of mass and a superimposed dot (double dot) indicates partial (double) differentiation with respect to time (e.g. $\dot{\cdot} := \frac{\partial}{\partial t}$ and $\ddot{\cdot} := \frac{\partial^2}{\partial t^2}$). Dirichlet, Neumann and initial conditions can be introduced as

$$\mathbf{u} = \bar{\mathbf{u}} \quad \text{on} \quad \Gamma^u \times [0, T], \quad (4a)$$

$$\tilde{\boldsymbol{\sigma}} \cdot \mathbf{n} = \mathbf{t} \quad \text{on} \quad \Gamma^\sigma \times [0, T], \quad (4b)$$

$$\mathbf{u} = \mathbf{u}_0 \quad \text{in} \quad \bar{\Omega} \times 0, \quad (4c)$$

$$\dot{\mathbf{u}} = \dot{\mathbf{u}}_0 \quad \text{in} \quad \bar{\Omega} \times 0, \quad (4d)$$

where $\Gamma = \Gamma^\sigma \cup \Gamma^u$ and $\Gamma^\sigma \cap \Gamma^u = \emptyset$. The vector \mathbf{t} in (4b) represents the force-traction. In the context of small rotations, the angular motion of the continuum can be defined by a field of proper orthogonal rotations $\boldsymbol{\omega} : \Omega \times [0, T] \rightarrow \mathbf{SO}(3)$, such that the mapping, $(\mathbf{x}, t) \mapsto \boldsymbol{\omega}(\mathbf{x}, t)$ is an isometric linear transformation. The conservation of angular momentum is defined as

$$\operatorname{div} \tilde{\boldsymbol{\mu}} + \boldsymbol{\xi} : \tilde{\boldsymbol{\sigma}}^T + \rho \mathbf{l} = \rho \mathbf{J} \ddot{\boldsymbol{\omega}} \quad \text{in } \Omega \times [0, T], \quad (5)$$

where $\tilde{\boldsymbol{\mu}}$ is the couple (hyperstress) stress tensor, \mathbf{l} is the body couple, \mathbf{J} is the rotational or spin inertia (determined by the shape and size of micro-continuum elements, [de Borst and Sluys \[1991\]](#)) and $\boldsymbol{\xi}$ is the third order permutation tensor¹. Dirichlet, Neumann and initial conditions can be introduced as

$$\boldsymbol{\omega} = \bar{\boldsymbol{\omega}} \quad \text{on} \quad \Gamma^\omega \times [0, T], \quad (6a)$$

$$\tilde{\boldsymbol{\mu}} \cdot \mathbf{n} = \mathbf{m} \quad \text{on} \quad \Gamma^\mu \times [0, T], \quad (6b)$$

$$\boldsymbol{\omega} = \boldsymbol{\omega}_0 \quad \text{in} \quad \bar{\Omega} \times 0, \quad (6c)$$

$$\dot{\boldsymbol{\omega}} = \dot{\boldsymbol{\omega}}_0 \quad \text{in} \quad \bar{\Omega} \times 0, \quad (6d)$$

¹Throughout the paper, the symbol (\cdot) is used to indicate the scalar product or contraction of a single index $\mathbf{a} \cdot \mathbf{b} = a_i b_i$; the symbol $(:)$ is used to indicate double contraction of two indices $\mathbf{A} : \mathbf{B} = A_{ij} B_{ij}$; the symbol (\times) is used to indicate the cross product $[\mathbf{a} \times \mathbf{b}]_i = \xi_{ijk} a_j b_k$ via the permutation tensor ξ_{ijk} and the symbol (\otimes) is used to indicate the outer or dyadic product $[\mathbf{a} \otimes \mathbf{b}]_{ij} = a_i b_j$. Whenever indices are used, unless otherwise stated, Einstein's summation convention will be assumed.

It is important to note that all tensor fields (\cdot) represent micropolar quantities, differentiating them with their counterparts in couple stress theory. In general, when the grapheme (\sim) does not appear, such as on electric field \mathbf{E} , it implies that the definition of the field/quantity is the same in both theories.

Furthermore, unless specified otherwise, all tensor fields (\cdot) represent skew-symmetric tensors dual to their corresponding axial vector (\cdot) .

where $\Gamma = \Gamma^\mu \cup \Gamma^\omega$ and $\Gamma^\mu \cap \Gamma^\omega = \emptyset$. The vector \mathbf{m} in (6b) represents the moment-traction, see Figure 1. For the full set of corrected boundary conditions in couple stress elasticity refer to Madeo et al. [2016]; Ghiba et al. [2017]. The coupled electro-mechanical initial boundary value problem, defined by equations (1) to (6), must be complemented with three closure equations related to the electro-mechanical nature of the generalised continuum. For a conservative material, the closure equations can be derived from the enthalpy density of the system Ψ defined in terms of the small strain tensor $\tilde{\boldsymbol{\varepsilon}}$, the curvature tensor $\tilde{\boldsymbol{\chi}}$ the electric field vector \mathbf{E} as follows

$$\tilde{\boldsymbol{\sigma}}(\tilde{\boldsymbol{\varepsilon}}, \tilde{\boldsymbol{\chi}}, \mathbf{E}) := \frac{\partial \tilde{\Psi}(\boldsymbol{\varepsilon}, \boldsymbol{\chi}, \mathbf{E})}{\partial \tilde{\boldsymbol{\varepsilon}}}, \quad (7)$$

$$\tilde{\boldsymbol{\mu}}(\tilde{\boldsymbol{\varepsilon}}, \tilde{\boldsymbol{\chi}}, \mathbf{E}) := \frac{\partial \tilde{\Psi}(\tilde{\boldsymbol{\varepsilon}}, \tilde{\boldsymbol{\chi}}, \mathbf{E})}{\partial \tilde{\boldsymbol{\chi}}}, \quad (8)$$

$$\tilde{\mathbf{D}}(\tilde{\boldsymbol{\varepsilon}}, \tilde{\boldsymbol{\chi}}, \mathbf{E}) := -\frac{\partial \tilde{\Psi}(\tilde{\boldsymbol{\varepsilon}}, \tilde{\boldsymbol{\chi}}, \mathbf{E})}{\partial \mathbf{E}}, \quad (9)$$

expressing the force stress tensor $\tilde{\boldsymbol{\sigma}}$, the couple stress tensor $\tilde{\boldsymbol{\mu}}$ and the electric displacement vector $\tilde{\mathbf{D}}$ in terms of the small strain tensor $\tilde{\boldsymbol{\varepsilon}}$, the curvature tensor $\tilde{\boldsymbol{\chi}}$ and the electric field \mathbf{E} where the compatibility equations (kinematic measures), are defined in the classical Cosserat sense Nowacki [1986]; Neff [2006]; Braun [2010]

$$\tilde{\boldsymbol{\varepsilon}} := \nabla \mathbf{u} - \hat{\boldsymbol{\omega}}, \quad \tilde{\boldsymbol{\chi}} := \nabla \boldsymbol{\omega}, \quad (10)$$

where the following relationships exist between the axial vector and its dual skew-symmetric tensor

$$\hat{\boldsymbol{\omega}} := \boldsymbol{\omega} \times \mathbf{I}, \quad \boldsymbol{\omega} = \text{axl}(\hat{\boldsymbol{\omega}})$$

where \mathbf{I} is the identity tensor and the symbol \times which appears in (10) is the tensor cross product, introduced for the first time by de Boer [1982] and recently brought in to the context of solid mechanics with its associated algebra by Bonet et al. [2015a,b,c] and further extensively used in the context large deformation electromechanics by Gil and Ortigosa [2016]; Ortigosa and Gil [2016a,b]. A variety of electro-mechanical constitutive models are available in the literature defined in terms of different enthalpy expressions, such as in Chen [2012]; Sharma et al. [2007]; Hadjesfandiari [2013]; Schröder and Gross [2004]; Gil and Ledger [2012]. In the case of linear flexoelectricity, $\tilde{\boldsymbol{\sigma}}$, $\tilde{\boldsymbol{\mu}}$ and $\tilde{\mathbf{D}}$ obtained this way render algebraic summations of mechanical (strain related) $(\cdot)^m$, micro-mechanical (curvature/strain gradient related) $(\cdot)^g$ and electrical $(\cdot)^e$ components. For instance, the electric displacement vector $\tilde{\mathbf{D}}$ can be expanded as

$$\tilde{\mathbf{D}} = \tilde{\mathbf{D}}^m + \tilde{\mathbf{D}}^g + \tilde{\mathbf{D}}^e; \quad \tilde{\mathbf{D}}^m := \tilde{\mathbf{e}} : \tilde{\boldsymbol{\varepsilon}}, \quad \tilde{\mathbf{D}}^g := \tilde{\mathbf{f}} : \tilde{\boldsymbol{\chi}}, \quad \mathbf{D}^e := \boldsymbol{\epsilon} \cdot \mathbf{E}, \quad (11)$$

where $\boldsymbol{\epsilon}$ is the symmetric second order dielectric permittivity tensor, $\tilde{\mathbf{e}}$ is the third order piezoelectric tensor and $\tilde{\mathbf{f}}$ is the third order flexoelectric tensor. Note that due to the asymmetric nature of strain and curvature tensors, there is no symmetry restriction on $\tilde{\mathbf{e}}$ and $\tilde{\mathbf{f}}$, thus allowing for more general electromechanical couplings, Chen [2012]. Analogously, the force stress tensor $\tilde{\boldsymbol{\sigma}}$ can be decomposed additively as

$$\tilde{\boldsymbol{\sigma}} = \tilde{\boldsymbol{\sigma}}^m + \tilde{\boldsymbol{\sigma}}^g + \tilde{\boldsymbol{\sigma}}^e; \quad \tilde{\boldsymbol{\sigma}}^m := \tilde{\mathcal{C}} : \tilde{\boldsymbol{\varepsilon}}, \quad \tilde{\boldsymbol{\sigma}}^g := \tilde{\mathcal{D}} : \tilde{\boldsymbol{\chi}}, \quad \tilde{\boldsymbol{\sigma}}^e := -\mathbf{E} \cdot \tilde{\mathbf{e}}, \quad (12)$$

and the couple stress tensor $\tilde{\boldsymbol{\chi}}$ can be additively decomposed as

$$\tilde{\boldsymbol{\mu}} = \tilde{\boldsymbol{\mu}}^m + \tilde{\boldsymbol{\mu}}^g + \tilde{\boldsymbol{\mu}}^e; \quad \tilde{\boldsymbol{\mu}}^m := \tilde{\boldsymbol{\varepsilon}} : \tilde{\mathcal{D}}, \quad \tilde{\boldsymbol{\mu}}^g := \tilde{\mathcal{B}} : \tilde{\boldsymbol{\chi}}, \quad \tilde{\boldsymbol{\mu}}^e := -\mathbf{E} \cdot \tilde{\mathbf{f}}. \quad (13)$$

where $\tilde{\mathcal{C}}$ is the fourth order anisotropic elasticity tensor and $\tilde{\mathcal{B}}$ and $\tilde{\mathcal{D}}$ are fourth order tensors characterising the behaviour of micro-continuum. Note that, for centrosymmetric materials, coupling between the strain tensor $\tilde{\boldsymbol{\varepsilon}}$ and the curvature tensor $\tilde{\boldsymbol{\chi}}$ is not possible as this breaks the point symmetry (centrosymmetry), and invariance of the strain energy requires $\tilde{\mathcal{D}} = \mathbf{0}$, Nowacki [1986]; Lakes [1995]. Finally, the initial boundary value problem of the coupled system is defined by equations (1)-(6), (11)-(13).

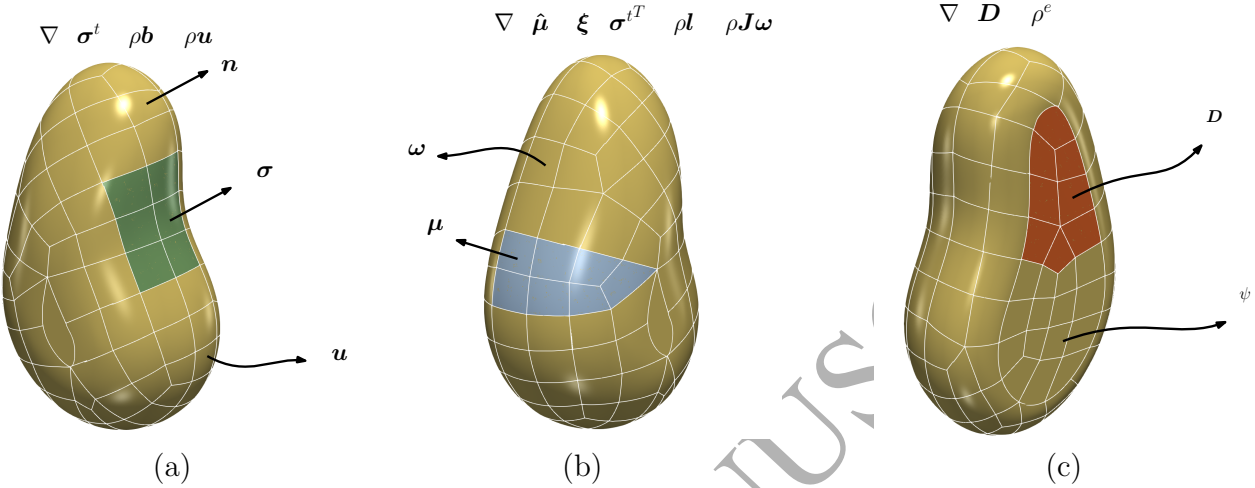


Figure 1: Schematic representation of the governing equations of couple stress and the decomposition of the boundary of a couple stress continua into a) displacements and tractions, $\Gamma = \Gamma^\sigma \cup \Gamma^u$ and $\Gamma^\sigma \cap \Gamma^u = \emptyset$, b) rotations and couples/moment $\Gamma = \Gamma^\mu \cup \Gamma^\omega$ and $\Gamma^\mu \cap \Gamma^\omega = \emptyset$ and, c) surface charge and electric flux, $\Gamma = \Gamma^D \cup \Gamma^\psi$ and $\Gamma^D \cap \Gamma^\psi = \emptyset$. Note that, while the boundary conditions associated with the electrostatics of the system are independent, in couple stress theory wherein the rotations are constrained and individual variations of the fields are not allowed, it is only possible to apply two tangential components of moments on a traction boundary Γ^σ , and/or two tangential components of rotations on a displacement boundary Γ^u Mindlin and Tiersten [1962]; Koiter [1964]; Neff et al. [2016]. Note that σ^t represents the non-symmetric stress tensor defined in section 3.)

3. The skew-symmetric couple stress theory

The classical linear couple stress theory is formally a limit case of linear micropolar theory. The fundamental assumption is to enforce the following constraint on the rotations of the substructure

$$\boldsymbol{\omega}(\mathbf{x}, t) = \frac{1}{2} \nabla \times \mathbf{u}(\mathbf{x}, t) \quad \text{in } \Omega \times [0, T]. \quad (14)$$

Equation (14) is in fact the infinitesimal rotation (vorticity) vector of Cauchy elasticity. As discussed in Appendix A, this limit model can be obtained from the linear isotropic Cosserat model. However, the consequence of imposing this constraint in general implies the indeterminacy of the couple stresses, as the spherical part of the curvature energy vanishes, see Appendix A. Furthermore, the strain tensor becomes symmetric, that is

$$\tilde{\boldsymbol{\varepsilon}} = \boldsymbol{\varepsilon}, \quad (15)$$

where $\boldsymbol{\varepsilon}$ represent the symmetric small strain tensor work conjugate to the force stress tensor of Cauchy elasticity $\boldsymbol{\sigma}$ and the curvature tensor in (10) remains unchanged. Furthermore, the grapheme (\sim) can be dropped from all quantities. The definition of the curvature tensor as the skew-symmetric part of gradient of rotation has been extensively studied in Hadjesfandiari and

Dargush [2011]; Hadjesfandiari [2013]; Darrall et al. [2014, 2015], giving rise to skew-symmetric couple stress theories, where it is claimed a skew-symmetric couple stress theory is a self-contained theory of its own and does not physically emanate as a limit case of the micropolar theory. The theory however can still be mathematically posed as such. Following this philosophy, the couple stress curvature χ will have a dual representation

$$\hat{\chi} = \nabla^{skew}\omega = \nabla^{skew}\nabla^{skew}\mathbf{u} \quad \text{or} \quad \chi = \frac{1}{4}\nabla \times \nabla \times \mathbf{u}, \quad (16)$$

where

$$\chi = \text{axl}(\hat{\chi}), \quad \hat{\chi} = \chi \times \mathbf{I},$$

where ∇^{skew} denotes the skew-symmetric part of the gradient and the curvature vector is also called the mean curvature vector in skew-symmetric couple stress theory. This definition of curvature vector opens new opportunities for modelling flexoelectricity in centrosymmetric materials, since the electric enthalpy can be defined in terms of linear invariants of the axial curvature vector and electric field, without breaking the centrosymmetry of material. This also shows that the isotropic modified couple stress models developed by Yang et al. [2002]; Park and Gao [2006]; Ma et al. [2008] cannot be generalised for the flexoelectric case as any linear invariant of symmetric curvature tensor in the enthalpy breaks the centrosymmetry.

In light of (15) and in order to further simplify the process of material characterisation, the most well established couple stress models assume an additive decomposition of the internal energy of the system into a macromechanical energy expressed in terms of the invariants of classical strain tensor, a micromechanical energy expressed in terms of the invariants of the curvature vector and a couple term imposing the couple stress constraint Yang et al. [2002]; Park and Gao [2006]; Ghica et al. [2017]. Extending this to the case of flexoelectricity, the total internal energy of the electromechanical system can be written as

$$\begin{aligned} \check{\Psi}(\nabla^{sym}\mathbf{u}, \nabla^{skew}\mathbf{u}, \omega, \mathbf{E}(\psi)) &= \Psi(\epsilon(\mathbf{u}), \nabla \times \mathbf{u}, \omega, \mathbf{E}(\psi)) \\ &= \Psi_{mac}(\epsilon(\mathbf{u}), \mathbf{E}(\psi)) + \Psi_{mic}(\chi(\omega), \mathbf{E}(\psi)) + \Psi_{con}(\nabla \times \mathbf{u}, \omega), \end{aligned} \quad (17)$$

where $\Psi_{con}(\nabla \times \mathbf{u}, \omega)$ typically takes the form shown in Appendix A if different variations of the fields are considered and vanishes if the couple stress constraint is strongly enforced.

Remark: When coupled invariants of strain and curvature are neglected the constitutive term \mathcal{D} in (13) vanishes and consideration of infinitesimal strain tensor ϵ leads to a symmetric local (Cauchy) stress and a symmetric constitutive tangent operator. However, a skew-symmetric non-local stress tensor $\hat{\sigma}^g$ (dual to vector σ^g) [see (12)] still emerges from the enforcement of the couple stress constraint which is not work-conjugate to ϵ . In other words, $\hat{\sigma}^g$ can be treated as a geometric term. This renders a non-symmetric total force stress tensor σ^t that contains both constitutive and geometric contributions. Certainly, this is also true for the classical indeterminate couple stress theory of Mindlin and Tiersten [1962] (i.e. the presence of body couples in the total force stress tensor); c.f. page 101 in Eringen [1967]. In essence, the equations of linear momentum and angular momentum can be re-written as

$$\text{div}\sigma^t + \rho\mathbf{b} = \rho\ddot{\mathbf{u}} \quad \text{in } \Omega \times [0, T], \quad (18)$$

$$\text{div}\hat{\mu} + \xi : \hat{\sigma}^g{}^T + \rho\mathbf{l} = \rho\mathbf{J}\ddot{\omega} \quad \text{in } \Omega \times [0, T]. \quad (19)$$

We note that, in couple stress theories the effect of micro-inertia (angular velocities) can be neglected due to their associated moment of inertia being quadratic in characteristic length scale,

Georgiadis and Velgaki [2003]. In addition, since it is emphasised that the couple stress theory is a continuum theory, the existence of micro-inertia cannot have a physical justification Hadjesfandiari and Dargush [2011]. Furthermore, since the body couple term $\rho\mathbf{l}$ performs work against $\delta\boldsymbol{\omega}$ and $\delta\boldsymbol{\omega}$ can be written in terms of $\delta\mathbf{u}$ (where $\delta\boldsymbol{\omega}$ and $\delta\mathbf{u}$ are possible boundary compatible variations of $\boldsymbol{\omega}$ and \mathbf{u} , respectively) the body couple can be transformed to a body force and a traction force contribution Hadjesfandiari and Dargush [2011]. This leaves us with angular momentum equation of the form

$$-\nabla \times \boldsymbol{\mu} + \boldsymbol{\xi} : \hat{\boldsymbol{\sigma}}^g{}^T = \boldsymbol{\xi} : (\hat{\boldsymbol{\sigma}}^g{}^T - \nabla \boldsymbol{\mu}) = \mathbf{0} \quad \text{in } \Omega \times [0, T], \quad (20)$$

which implies

$$\hat{\boldsymbol{\sigma}}^g{}^T = \nabla \boldsymbol{\mu} \quad \text{in } \Omega \times [0, T], \quad (21)$$

signifying that in skew-symmetric couple stress theory, $\hat{\boldsymbol{\sigma}}^g$ is not an independent quantity and can in fact be linked to the couple stress vector $\boldsymbol{\mu}$ which itself is a constitutive stress. As a consequence, $\hat{\boldsymbol{\sigma}}^g$, and $\hat{\boldsymbol{\mu}}$ contribute to the traction boundary condition. Subjected to the consideration of suitable boundary conditions, the skew-symmetric couple stress theory discussed here can be regarded as a restrictive case of the indeterminate couple stress theory of Mindlin and Tiersten, Neff et al. [2016]. However, as shown later, all the difficulties in boundary conditions can be circumvented if independent variations of the fields \mathbf{u} and $\boldsymbol{\omega}$ are considered.

4. Variational formulations in couple stress based electromechanics of continua

In this section, four different variational formulations for couple stress based electromechanics are described in the continuum setting namely, a displacement potential formulation, a lagrange multiplier formulation, an augmented Lagrangian formulation and a penalty formulation.

4.1. The displacement-potential variational formulation

A two-field variational formulation can be established by strongly imposing the couple stress constraint. Focusing on the electro-elastodynamics of the conservative flexoelectric system, the internal and external forces together with the motion between times $T_0 = 0$ and T , can be determined from a Hamilton's principle, Deng and Dargush [2017]; Sudeep et al. [2005]. To this effect, we introduce the Lagrangian \mathcal{L} as

$$\mathcal{L}(\mathbf{u}, \dot{\mathbf{u}}, \psi) = \mathcal{K}(\dot{\mathbf{u}}) - \Pi_{\text{int}}(\mathbf{u}, \psi) - \Pi_{\text{ext}}(\mathbf{u}, \psi) \quad (22)$$

where \mathcal{K} is the kinetic energy of the body expressed as a function of velocity $\dot{\mathbf{u}}$ and Π the total potential energy of the system, containing the work of internal and external electromechanical forces such that

$$\mathcal{K}(\dot{\mathbf{u}}) = \frac{1}{2} \int_{\Omega} \rho \dot{\mathbf{u}} \cdot \dot{\mathbf{u}} \, dV, \quad (23a)$$

$$\Pi_{\text{int}}(\mathbf{u}, \psi) = \int_{\Omega} \Psi(\boldsymbol{\varepsilon}(\mathbf{u}), \boldsymbol{\omega}(\mathbf{u}), \psi) \, dV = \int_{\Omega} \Psi_{\text{mac}}(\boldsymbol{\varepsilon}(\mathbf{u}), \mathbf{E}(\psi)) + \Psi_{\text{mic}}(\boldsymbol{\chi}(\mathbf{u}), \mathbf{E}(\psi)) \, dV, \quad (23b)$$

$$\Pi_{\text{ext}}(\mathbf{u}, \psi) = \int_{\Omega} \left(\rho(\mathbf{b} \cdot \mathbf{u} + \mathbf{l} \cdot \boldsymbol{\omega}(\mathbf{u})) - \rho_0 \psi \right) \, dV + \int_{\Gamma} \left(\mathbf{t} \cdot \mathbf{u} + \mathbf{m} \cdot \boldsymbol{\omega}(\mathbf{u}) - q_0 \psi \right) \, dA \quad (23c)$$

Considering the action integral as the integral of the Lagrangian over the time interval $t = [0, T]$, the Hamilton's principle states that the mapping satisfying the equations of motion and electrostatics can be obtained by making the action integral stationary with respect to all possible mappings which are compatible with the boundary conditions. In the present case this leads to the following Euler-Lagrange equations

$$\frac{\partial \mathcal{L}}{\partial \mathbf{u}} - \frac{d}{dt} \frac{\partial \mathcal{L}}{\partial \dot{\mathbf{u}}} = \mathbf{0}, \quad \frac{\partial \mathcal{L}}{\partial \psi} = 0. \quad (24)$$

Denoting the virtual and incremental variations of displacements and electric potential as $\delta \mathbf{u}$, $\Delta \mathbf{u}$, $\delta \psi$ and $\Delta \psi$ respectively leading to

$$\delta \boldsymbol{\omega} = \frac{1}{2} \nabla \times \delta \mathbf{u}, \quad \Delta \boldsymbol{\omega} = \frac{1}{2} \nabla \times \Delta \mathbf{u}. \quad (25)$$

The stationary condition of the kinetic energy then becomes

$$\frac{d}{dt} \frac{\partial \mathcal{L}}{\partial \dot{\mathbf{u}}} = \frac{d}{dt} \frac{\partial \mathcal{K}}{\partial \dot{\mathbf{u}}} = \int_{\Omega} \rho \ddot{\mathbf{u}} \cdot \delta \mathbf{u} \, dV. \quad (26)$$

The stationary conditions of the internal energy can be found by computing the directional derivative of the energy with respect to virtual variations of displacements and electric potential as

$$D\Pi_{\text{int}}[\delta \mathbf{u}] = \int_{\Omega} \left(\frac{\partial \Psi}{\partial \boldsymbol{\varepsilon}} : \delta \boldsymbol{\varepsilon} + \left(\frac{\partial \Psi}{\partial \boldsymbol{\omega}} \times \mathbf{I} \right) : \delta \hat{\boldsymbol{\omega}} + \frac{\partial \Psi}{\partial \boldsymbol{\chi}} \cdot \delta \boldsymbol{\chi} \right) \, dV = \int_{\Omega} \left(\boldsymbol{\sigma} : \delta \boldsymbol{\varepsilon} + \hat{\boldsymbol{\sigma}}^g : \delta \hat{\boldsymbol{\omega}} + \boldsymbol{\mu} \cdot \delta \boldsymbol{\chi} \right), \quad (27a)$$

$$D\Pi_{\text{int}}[\delta \psi] = \int_{\Omega} \frac{\partial \Psi}{\partial \mathbf{E}} \cdot \delta \mathbf{E} \, dV = - \int_{\Omega} \mathbf{D} \cdot \delta \mathbf{E} \, dV, \quad (27b)$$

where $\delta \boldsymbol{\varepsilon}$, $\delta \boldsymbol{\chi}$ and $\delta \mathbf{E}$ represent virtual variations of strain tensor, curvature vector and electric field vector respectively. Moreover, without loss of generality, $\boldsymbol{\sigma}$ now represents the total constitutive tensor which might or might not include gradient effects depending on material symmetry; see (12).² Analogously, consistent linearisation of the external work leads to

$$D\Pi_{\text{ext}}[\delta \mathbf{u}] = \int_{\Omega} \rho \left(\mathbf{b} \cdot \delta \mathbf{u} + \mathbf{l} \cdot \delta \boldsymbol{\omega} \right) \, dV + \int_{\Gamma} \left(\mathbf{t} \cdot \delta \mathbf{u} + \mathbf{m} \cdot \delta \boldsymbol{\omega} \right) \, dA, \quad (28a)$$

$$D\Pi_{\text{ext}}[\delta \psi] = - \int_{\Omega} \rho_0 \psi \, dV - \int_{\Gamma} q_0 \psi \, dA, \quad (28b)$$

where $\delta \boldsymbol{\omega}$ is defined in (25). It is also necessary to compute the relevant tangent operators through further consistent linearisation of (28) which can be written as (the symmetric terms are omitted)

$$D\Pi_{\text{int}}[\delta \mathbf{u}; \Delta \mathbf{u}] = \int_{\Omega} \left(\Delta \boldsymbol{\varepsilon} : \frac{\partial^2 \Psi}{\partial \boldsymbol{\varepsilon} \partial \boldsymbol{\varepsilon}} : \delta \boldsymbol{\varepsilon} + \Delta \boldsymbol{\chi} \cdot \frac{\partial^2 \Psi}{\partial \boldsymbol{\chi} \partial \boldsymbol{\chi}} \cdot \delta \boldsymbol{\chi} \right) \, dV$$

²Depending on the notation, the work-conjugacy between $\delta \boldsymbol{\chi}$ and $\boldsymbol{\mu}$ can also be written in terms of their dual representation $\hat{\mu}_{ij} : \delta \hat{\chi}_{ij} = \xi_{ijk} \xi_{ijl} \mu_k \delta \chi_l = 2\mu_k \delta \chi_k$,

which shows that the proper work-conjugate to $\delta \boldsymbol{\chi}$ is in fact $2\boldsymbol{\mu}$. For notational convenience, here it is assumed that this factor is embedded in the definition of the axial couple stress vector $\boldsymbol{\mu}$.

$$\begin{aligned}
& + \int_{\Omega} \left(\Delta \boldsymbol{\varepsilon} : \frac{\partial^2 \Psi}{\partial \boldsymbol{\varepsilon} \partial \boldsymbol{\chi}} \cdot \delta \boldsymbol{\chi} + \Delta \boldsymbol{\chi} \cdot \frac{\partial^2 \Psi}{\partial \boldsymbol{\chi} \partial \boldsymbol{\varepsilon}} : \delta \boldsymbol{\varepsilon} \right) dV \\
& = \int_{\Omega} \left(\Delta \boldsymbol{\varepsilon} : \mathbf{C} : \delta \boldsymbol{\varepsilon} + \Delta \boldsymbol{\chi} \cdot \mathbf{B} \cdot \delta \boldsymbol{\chi} \right) dV \\
& + \int_{\Omega} \left(\Delta \boldsymbol{\varepsilon} : \mathbf{D} \cdot \delta \boldsymbol{\chi} + \Delta \boldsymbol{\chi} \cdot \mathbf{D}^T : \delta \boldsymbol{\varepsilon} \right) dV,
\end{aligned} \tag{29a}$$

$$\begin{aligned}
D\Pi_{\text{int}}[\delta \mathbf{u}; \Delta \psi] &= \int_{\Omega} \left(\Delta \mathbf{E} \cdot \frac{\partial^2 \Psi}{\partial \boldsymbol{\varepsilon} \partial \mathbf{E}} : \delta \boldsymbol{\varepsilon} + \Delta \mathbf{E} \cdot \frac{\partial^2 \Psi}{\partial \boldsymbol{\chi} \partial \mathbf{E}} \cdot \delta \boldsymbol{\chi} \right) dV \\
&= - \int_{\Omega} \left(\Delta \mathbf{E} \cdot \mathbf{e} : \delta \boldsymbol{\varepsilon} + \Delta \mathbf{E} \cdot \mathbf{f} \cdot \delta \boldsymbol{\chi} \right) dV,
\end{aligned} \tag{29b}$$

$$D\Pi_{\text{int}}[\delta \psi, \Delta \psi] = \int_{\Omega} \Delta \mathbf{E} \cdot \frac{\partial^2 \Psi}{\partial \mathbf{E} \partial \mathbf{E}} \cdot \delta \mathbf{E} dV = - \int_{\Omega} \Delta \mathbf{E} \cdot \boldsymbol{\epsilon} \cdot \delta \mathbf{E} dV, \tag{29c}$$

where $\Delta \boldsymbol{\varepsilon}$, $\Delta \boldsymbol{\chi}$ and $\Delta \mathbf{E}$ represent incremental variations of strain tensor, curvature vector and electric field vector respectively. Furthermore, the coupled terms in (29a) vanish for isotropic materials. Note that upon performing further integration by part on (27) new boundary terms emerge that contribute to traction force and couple force Neff et al. [2016]. In general, the total force stress can be written as

$$\boldsymbol{\sigma}^t = \boldsymbol{\sigma} + \hat{\boldsymbol{\sigma}}^g, \quad \text{where} \quad \hat{\boldsymbol{\sigma}}^g = \frac{1}{2} (\nabla \times \boldsymbol{\mu}) \times \mathbf{I}. \tag{30}$$

The set of equations in (27), (28) and (29) facilitate straightforward finite element discretisation in terms of displacements and electric potential. This formulation however, dictates C^1 continuity for displacements which inevitably requires the use of non-standard function spaces and is not pursued here.

4.2. The penalty formulation

A natural way to formulate the couple stress flexoelectric problem is to treat the vorticity of the substructure \mathbf{w} as an independent field and impose the couple stress constraint weakly through a penalty approximation. In this case the potential energy of the system is given by

$$\hat{\Pi}_{\text{int}}(\mathbf{u}, \boldsymbol{\omega}, \psi) = \int_{\Omega} \hat{\Psi}(\boldsymbol{\varepsilon}(\mathbf{u}), \boldsymbol{\chi}(\boldsymbol{\omega}), \mathbf{E}(\psi)) dV + \int_{\Omega} \frac{\kappa}{2} \left\| \frac{1}{2} \nabla \times \mathbf{u} - \boldsymbol{\omega} \right\|^2 dV, \tag{31}$$

where $\|\cdot\|$ is the Frobenius norm. As shown in Appendix A, the elegance of this formulation comes from the fact that κ can be treated as the Cosserat modulus and hence, the formulation adheres to a physically meaningful treatment of couple stress flexoelectricity.

Avoiding redundant derivations of stationary conditions of kinetic and external energies and focussing only on the internal energy, the first directional derivative of the (31) with respect to the virtual variations of displacements, vorticity and electric potential yields

$$D\hat{\Pi}_{\text{int}}[\delta \mathbf{u}] = \int_{\Omega} \boldsymbol{\sigma} : \delta \boldsymbol{\varepsilon} dV + \int_{\Omega} \kappa \left(\frac{1}{2} \nabla \times \mathbf{u} - \boldsymbol{\omega} \right) \cdot \left(\frac{1}{2} \nabla \times \delta \mathbf{u} \right) dV, \tag{32a}$$

$$D\hat{\Pi}_{\text{int}}[\delta \boldsymbol{\omega}] = \int_{\Omega} \boldsymbol{\mu} \cdot \delta \boldsymbol{\chi} dV - \int_{\Omega} \kappa \left(\frac{1}{2} \nabla \times \mathbf{u} - \boldsymbol{\omega} \right) \cdot \delta \boldsymbol{\omega} dV, \tag{32b}$$

$$D\hat{\Pi}_{\text{int}}[\delta \psi] = - \int_{\Omega} \mathbf{D} \cdot \delta \mathbf{E} dV, \tag{32c}$$

It is also necessary to compute the relevant tangent operators through further consistent linearisation of (32)

$$D\bar{\Pi}_{\text{int}}[\delta\mathbf{u}; \Delta\mathbf{u}] = \int_{\Omega} \Delta\boldsymbol{\varepsilon} : \mathcal{C} : \delta\boldsymbol{\varepsilon} \, dV + \int_{\Omega} \kappa \left(\frac{1}{2} \nabla \times \Delta\mathbf{u} \right) \cdot \left(\frac{1}{2} \nabla \times \delta\mathbf{u} \right) \, dV, \quad (33a)$$

$$D\bar{\Pi}_{\text{int}}[\delta\mathbf{u}; \Delta\boldsymbol{\omega}] = - \int_{\Omega} \kappa \Delta\boldsymbol{\omega} \cdot \left(\frac{1}{2} \nabla \times \delta\mathbf{u} \right) \, dV + \int_{\Omega} \Delta\boldsymbol{\chi} \cdot \mathcal{D}^T : \delta\boldsymbol{\varepsilon} \, dV, \quad (33b)$$

$$D\bar{\Pi}_{\text{int}}[\delta\mathbf{u}; \Delta\psi] = - \int_{\Omega} \delta\mathbf{E} \cdot \mathbf{e} : \delta\boldsymbol{\varepsilon} \, dV, \quad (33c)$$

$$D\bar{\Pi}_{\text{int}}[\delta\boldsymbol{\omega}; \Delta\boldsymbol{\omega}] = \int_{\Omega} \Delta\boldsymbol{\chi} \cdot \mathcal{B} \cdot \delta\boldsymbol{\chi} \, dV + \int_{\Omega} \kappa \Delta\boldsymbol{\omega} \cdot \delta\boldsymbol{\omega} \, dV, \quad (33d)$$

$$D\bar{\Pi}_{\text{int}}[\delta\boldsymbol{\omega}; \Delta\psi] = - \int_{\Omega} \Delta\mathbf{E} \cdot \mathbf{f} \cdot \delta\boldsymbol{\chi} \, dV, \quad (33e)$$

$$D\bar{\Pi}_{\text{int}}[\delta\psi, \Delta\psi] = - \int_{\Omega} \Delta\mathbf{E} \cdot \boldsymbol{\epsilon} \cdot \delta\mathbf{E} \, dV, \quad (33f)$$

where the second integrand in (33b) vanishes for isotropic materials. Note that, with a slight abuse of notation the kinematic variables and their work-conjugates have not been renamed, although strictly speaking their description under displacement-potential and penalty formulations are not the same. Analogous to displacement potential formulation, the total force stress tensor in the penalty formulation can be written as

$$\boldsymbol{\sigma}^t = \boldsymbol{\sigma} + \hat{\boldsymbol{\sigma}}^g, \quad \text{where} \quad \hat{\boldsymbol{\sigma}}^g = \kappa \left(\frac{1}{2} \nabla \times \mathbf{u} - \boldsymbol{\omega} \right) \times \mathbf{I}, \quad (34)$$

which shows that the penalty parameter κ is indeed the Cosserat modulus and the constraint will be imposed if $\kappa \rightarrow \infty$. In essence, this is an approximate enforcement, however the advantage of this formulation certainly, lies in the fact that it does not introduce a new variable for the enforcement of the constraint.

4.3. The Lagrange multiplier formulation

The couple stress constraint can also be imposed exactly albeit in a weak sense through the so-called Lagrange multiplier approach. In this formulation, a new variable is introduced to impose the constraint and the internal energy of the system is given by

$$\bar{\Pi}_{\text{int}}(\mathbf{u}, \boldsymbol{\omega}, \mathbf{s}, \psi) = \int_{\Omega} \bar{\Psi}(\boldsymbol{\varepsilon}(\mathbf{u}), \boldsymbol{\chi}(\boldsymbol{\omega}), \mathbf{E}(\psi)) \, dV + \int_{\Omega} \mathbf{s} \cdot \left(\frac{1}{2} \nabla \times \mathbf{u} - \boldsymbol{\omega} \right) \, dV, \quad (35)$$

where \mathbf{s} is the vector of Lagrange multipliers enforcing the constraint. Focussing only on the internal energy, the first directional derivative of the (39) with respect to the virtual variations of displacements, vorticity, Lagrange multiplier and electric potential yields

$$D\bar{\Pi}_{\text{int}}[\delta\mathbf{u}] = \int_{\Omega} \boldsymbol{\sigma} : \delta\boldsymbol{\varepsilon} \, dV + \int_{\Omega} \mathbf{s} \cdot \left(\frac{1}{2} \nabla \times \delta\mathbf{u} \right) \, dV, \quad (36a)$$

$$D\bar{\Pi}_{\text{int}}[\delta\boldsymbol{\omega}] = \int_{\Omega} \boldsymbol{\mu} \cdot \delta\boldsymbol{\chi} \, dV - \int_{\Omega} \mathbf{s} \cdot \delta\boldsymbol{\omega} \, dV, \quad (36b)$$

$$D\bar{\Pi}_{\text{int}}[\delta\mathbf{s}] = \int_{\Omega} \delta\mathbf{s} \cdot \left(\frac{1}{2} \nabla \times \mathbf{u} - \boldsymbol{\omega} \right) \, dV, \quad (36c)$$

$$D\bar{\Pi}_{\text{int}}[\delta\psi] = - \int_{\Omega} \boldsymbol{D} \cdot \delta\boldsymbol{E} \, dV, \quad (36d)$$

It is also necessary to compute the relevant tangent operators through further consistent linearisation of (36)

$$D\bar{\Pi}_{\text{int}}[\delta\boldsymbol{u}; \Delta\boldsymbol{u}] = \int_{\Omega} \Delta\boldsymbol{\varepsilon} : \mathcal{C} : \delta\boldsymbol{\varepsilon} \, dV, \quad (37a)$$

$$D\bar{\Pi}_{\text{int}}[\delta\boldsymbol{u}; \Delta\boldsymbol{\omega}] = \int_{\Omega} \Delta\boldsymbol{\chi} \cdot \boldsymbol{\mathcal{D}}^T : \delta\boldsymbol{\varepsilon} \, dV, \quad (37b)$$

$$D\bar{\Pi}_{\text{int}}[\delta\boldsymbol{u}; \Delta\boldsymbol{s}] = \int_{\Omega} \Delta\boldsymbol{s} \cdot (\frac{1}{2}\nabla \times \delta\boldsymbol{u}) \, dV, \quad (37c)$$

$$D\bar{\Pi}_{\text{int}}[\delta\boldsymbol{u}; \Delta\psi] = - \int_{\Omega} \delta\boldsymbol{E} \cdot \boldsymbol{e} : \delta\boldsymbol{\varepsilon} \, dV, \quad (37d)$$

$$D\bar{\Pi}_{\text{int}}[\delta\boldsymbol{\omega}; \Delta\boldsymbol{\omega}] = \int_{\Omega} \Delta\boldsymbol{\chi} \cdot \boldsymbol{\mathcal{B}} \cdot \delta\boldsymbol{\chi} \, dV + \int_{\Omega} \kappa \Delta\boldsymbol{\omega} \cdot \delta\boldsymbol{\omega} \, dV, \quad (37e)$$

$$D\bar{\Pi}_{\text{int}}[\delta\boldsymbol{\omega}; \Delta\boldsymbol{s}] = - \int_{\Omega} \Delta\boldsymbol{s} \cdot \delta\boldsymbol{\omega} \, dV, \quad (37f)$$

$$D\bar{\Pi}_{\text{int}}[\delta\boldsymbol{\omega}; \Delta\psi] = - \int_{\Omega} \Delta\boldsymbol{E} \cdot \boldsymbol{f} \cdot \delta\boldsymbol{\chi} \, dV, \quad (37g)$$

$$D\bar{\Pi}_{\text{int}}[\delta\boldsymbol{s}; \Delta\boldsymbol{s}] = 0, \quad (37h)$$

$$D\bar{\Pi}_{\text{int}}[\delta\psi, \Delta\psi] = - \int_{\Omega} \Delta\boldsymbol{E} \cdot \boldsymbol{\epsilon} \cdot \delta\boldsymbol{E} \, dV, \quad (37i)$$

where (37b) vanishes for isotropic materials. Note that, with a slight abuse of notation, the kinematic variables and their work-conjugates have not been renamed, although strictly speaking their description compared to the last two variational formulations have changed. The total force stress tensor can now be written as

$$\boldsymbol{\sigma}^t = \boldsymbol{\sigma} + \hat{\boldsymbol{\sigma}}^g, \quad \text{where} \quad \hat{\boldsymbol{\sigma}}^g = \frac{1}{2}\boldsymbol{s} \times \boldsymbol{I}, \quad (38)$$

which shows that the Lagrange multiplier \boldsymbol{s} can be interpreted as the skew-symmetric part of total force stress tensor emanating from microstructural contribution.

4.4. The augmented Lagrangian formulation

From a numerical implementation point of view, the Lagrange multiplier approach leads to the popular saddle point problem that typically occurs in constrained energy minimisation problems such as incompressibility. Hence, it is at times advantageous to add a penalty type *regularisation* term to the internal energy of the system. This approach is termed as the augmented Lagrangian formulation and the internal energy of the system is given by

$$\check{\Pi}_{\text{int}}(\boldsymbol{u}, \boldsymbol{\omega}, \boldsymbol{s}, \psi) = \int_{\Omega} \check{\Psi}(\boldsymbol{\varepsilon}(\boldsymbol{u}), \boldsymbol{\chi}(\boldsymbol{\omega}), \boldsymbol{E}(\psi)) \, dV + \int_{\Omega} \boldsymbol{s} \cdot \left(\frac{1}{2}\nabla \times \boldsymbol{u} - \boldsymbol{\omega} \right) \, dV + \int_{\Omega} \frac{1}{2\kappa} \boldsymbol{s} \cdot \boldsymbol{s} \, dV. \quad (39)$$

Consistent linearisation of this energy is similar to the Lagrange multiplier formulation and the only two new terms arising are

$$D\check{\Pi}_{\text{int}}[\delta\boldsymbol{s}] = \int_{\Omega} \delta\boldsymbol{s} \cdot \left(\frac{1}{2}\nabla \times \boldsymbol{u} - \boldsymbol{\omega} \right) \, dV + \int_{\Omega} \frac{1}{\kappa} \boldsymbol{s} \cdot \delta\boldsymbol{s} \, dV, \quad (40)$$

$$D\check{\Pi}_{\text{int}}[\delta \mathbf{s}; \Delta \mathbf{s}] = \int_{\Omega} \frac{1}{\kappa} \Delta \mathbf{s} \cdot \delta \mathbf{s} \, dV, \quad (41)$$

and the total force stress tensor remains unchanged.

5. Couple-stress flexoelectric theory for three-dimensional beams

Having established a curvature-induced flexoelectric theory through couple stress formulation for the continua, in this section, we turn our attention to couple stress flexoelectricity in three-dimensional beams. Extending the work of Poya et al. [2015] on piezoelectric beams to flexoelectricity, we start with kinematics and electrostatics of a generic three-dimensional beam. Work-conjugates and area resultants are then introduced to facilitate similar variational formulations for beams. The Euler-Lagrange equations of three-dimensional beams are then derived in a compact form to facilitate interested readers with their closed form solutions.

5.1. Kinematics of three-dimensional flexoelectric beams

Let us consider the motion of a beam $\Omega \subset \mathbb{R}^3$ as shown in Figure 2. The beam in the undeformed configuration has a straight axis of length l and is completely characterised with an orthonormal reference triad $\{\mathbf{e}_1, \mathbf{e}_2, \mathbf{e}_3\}$, where \mathbf{e}_3 is parallel to the beam axis and $\{\mathbf{e}_\alpha\}(\alpha = 1, 2)$ lie in the plane which defines the cross sectional area A (with boundary ∂A) of the beam $\Omega = A \times l$ ³. Assuming for simplicity that this reference frame (placed at $[0, 0, x_3]^T$) coincides with the global one (placed at $[0, 0, 0]^T$), as shown in Figure 2, the displacements of the beam considering small rotations can be described as; see Poya et al. [2015]

$$(\mathbf{x}, t) \mapsto \mathbf{u}(\mathbf{x}, t) = \mathbf{w}(x_3, t) + \boldsymbol{\theta}(x_3, t) \times \mathbf{p}(x_1, x_2), \quad (42)$$

where $\mathbf{p}(x_1, x_2) := x_\alpha \mathbf{e}_\alpha$ is the position vector of a material point within the cross section A with

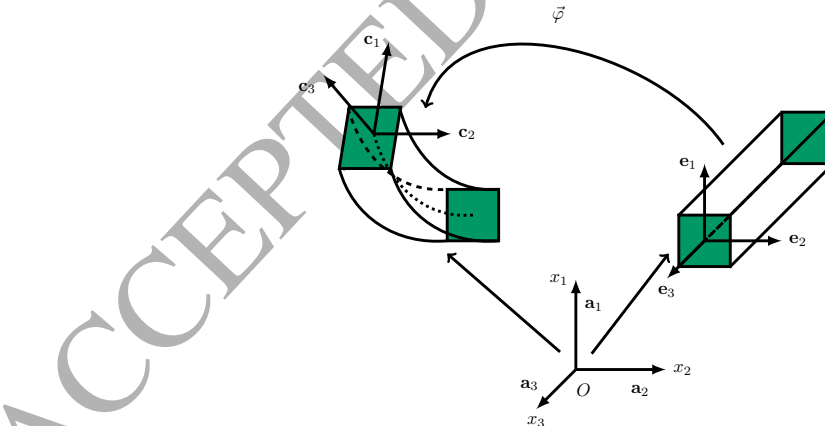


Figure 2: Motion of Beam in \mathbb{R}^3 . The initial orthonormal triad $\{\mathbf{e}_1, \mathbf{e}_2, \mathbf{e}_3\}$ transforms to the orthonormal triad $\{\mathbf{c}_1, \mathbf{c}_2, \mathbf{c}_3\}$.

respect to the origin of the triad $\{\mathbf{e}_1, \mathbf{e}_2, \mathbf{e}_3\}$. Vectors $\mathbf{w} = w_i \mathbf{e}_i$ and $\boldsymbol{\theta} = \theta_i \mathbf{e}_i$ are collectively called the generalised beam displacements. Expression (42) represents a time dependent affine mapping

³Throughout the remainder of the paper, any Greek indices will be assumed to vary in the integer interval [1,2] and Latin indices to vary in the integer interval [1,2,3].

for any material point contained within the cross sectional area A of the beam. Noticing that $\nabla \mathbf{u} = \frac{\partial \mathbf{u}}{\partial x_i} \otimes \mathbf{e}_i$ and $\frac{\partial \mathbf{p}}{\partial x_\alpha} = \mathbf{e}_\alpha$, the small strain tensor $\boldsymbol{\varepsilon}$ can be rewritten as

$$\boldsymbol{\varepsilon} = \frac{1}{2} \left[(\boldsymbol{\epsilon}^m + \boldsymbol{\kappa}^m \times \mathbf{p}) \otimes \mathbf{e}_3 + \mathbf{e}_3 \otimes (\boldsymbol{\epsilon}^m + \boldsymbol{\kappa}^m \times \mathbf{p}) \right], \quad (43)$$

where

$$\boldsymbol{\epsilon}^m := \frac{\partial \mathbf{w}}{\partial x_3} + \mathbf{e}_3 \times \boldsymbol{\theta}, \quad \boldsymbol{\kappa}^m := \frac{\partial \boldsymbol{\theta}}{\partial x_3}, \quad (44)$$

are called the strain measures of the linear beam model, which characterise translational deformation and rotational deformation, respectively. The explicit form of the strain tensor is

$$\boldsymbol{\varepsilon} = \frac{1}{2} \begin{bmatrix} 0 & 0 & \frac{\partial w_1}{\partial x_3} - \theta_2 - \frac{\partial \theta_3}{\partial x_3} \\ 0 & 0 & \frac{\partial w_2}{\partial x_3} + \theta_1 + \frac{\partial \theta_3}{\partial x_3} \\ sym & \frac{\partial w_3}{\partial x_3} + x_2 \frac{\partial \theta_1}{\partial x_3} - x_1 \frac{\partial \theta_2}{\partial x_3} & \end{bmatrix}. \quad (45)$$

As it is well known in classical beam theories and can also be seen clearly from (45), there is no deformation within the cross-section of the beam ($\mathbf{e}_\alpha \cdot \boldsymbol{\varepsilon} \mathbf{e}_\beta = 0$). Following our argument in subsection 4.1, and with finding the beam balance equations of flexoelectric beams in mind, from the onset, we strongly impose the couple stress constraint (14), to obtain

$$(\mathbf{x}, t) \mapsto \boldsymbol{\omega}(\mathbf{x}, t) = \frac{1}{2} \nabla \times \left(\mathbf{w}(x_3, t) + \boldsymbol{\theta}(x_3, t) \times \mathbf{p}(x_1, x_2) \right), \quad (46)$$

where on the right hand side of (46) we have substituted the continuum displacements in terms of beam's generalised displacements using (42). Similar to the strain tensor, the symmetric and skew-symmetric parts of gradient of $\boldsymbol{\omega}$ can be written in their matrix form as

$$\nabla^{sym} \boldsymbol{\omega} = \frac{1}{4} \begin{bmatrix} -\frac{\partial \theta_3}{\partial x_3} & 0 & \omega_{1,3} \\ 0 & -\frac{\partial \theta_3}{\partial x_3} & \omega_{2,3} \\ sym & 2\frac{\partial \theta_3}{\partial x_3} & \end{bmatrix}, \quad \nabla^{skew} \boldsymbol{\omega} = \frac{1}{4} \begin{bmatrix} 0 & 0 & \omega_{1,3} \\ 0 & 0 & \omega_{2,3} \\ -\omega_{1,3} & -\omega_{2,3} & 0 \end{bmatrix}, \quad (47)$$

where

$$\omega_{1,3} = \frac{\partial \theta_1}{\partial x_3} - \frac{\partial^2 w_2}{\partial x_3^2} - x_1 \frac{\partial^2 \theta_3}{\partial x_3^2}, \quad \omega_{2,3} = \frac{\partial \theta_2}{\partial x_3} + \frac{\partial^2 w_1}{\partial x_3^2} - x_2 \frac{\partial^2 \theta_3}{\partial x_3^2}.$$

From (47) we observe that the symmetric part vorticity gradient is deviatoric i.e. $\text{tr}(\nabla^{sym} \boldsymbol{\omega}) = 0$. However, the non-zero diagonal components of symmetric part of the gradient still contribute to the uniform contraction of the cross section by an amount proportional to $(-\frac{\partial \theta_3}{\partial x_3})$ and increase the torsional rigidity of the beam by an amount proportional to $(2\frac{\partial \theta_3}{\partial x_3})$. From the point of view of classical beam theories, it is essential that the strain measures should not include cross-sectional deformation. This further justifies the use of a skew-symmetric curvature tensor as a fundamental kinematic measure however, it should be noted that, the conformal variant of the couple stress theory recently reported by Ghiba et al. [2017] based on the kinematic measure $\nabla \times \boldsymbol{\varepsilon}$ also excludes these cross-sectional rotational modes. The axial curvature vector defined in (16) can now be written in terms of the beam kinematics

$$\boldsymbol{\chi} = \frac{1}{4} \mathbf{e}_3 \times \left(\mathbf{e}_3 \times (\boldsymbol{\epsilon}^g + \boldsymbol{\kappa}^g \times \mathbf{p}) \right) = \frac{1}{4} \bar{\mathbf{I}}(\boldsymbol{\epsilon}^g + \boldsymbol{\kappa}^g \times \mathbf{p}), \quad (48)$$

where

$$\boldsymbol{\epsilon}^g = \frac{\partial^2 \mathbf{w}}{\partial x_3^2} + \boldsymbol{\kappa}^m \times \mathbf{e}_3, \quad \boldsymbol{\kappa}^g = \frac{\partial^2 \boldsymbol{\theta}}{\partial x_3^2}, \quad (49)$$

are the strain gradient measures of the linear beam model, augmenting the classical strain measures (44) and

$$\bar{\mathbf{I}} = \mathbf{e}_3 \otimes \mathbf{e}_3 - \mathbf{I}. \quad (50)$$

The symmetric part of the gradient of rotation utilised in the purely mechanical planar beam theories developed by Park and Gao [2006, 2008], Ma et al. [2008]; Reddy [2011]; Şişmek and Reddy [2012, 2013]; Li and Luo [2017] can also be represented in a compact form including the torsional terms as

$$(\nabla^{sym} \boldsymbol{\omega})_3 = \text{axl}(\nabla^{skew} \boldsymbol{\omega}) \times \mathbf{e}_3 + 2\boldsymbol{\kappa}_3^m \mathbf{e}_3, \quad (51)$$

where the subscript 3 in (51) represents the longitudinal (\mathbf{e}_3) direction.⁴

5.2. Electrical Mapping

Following our recent development in Poya et al. [2015], similar to the beam kinematics, we approximate electric potential $\psi : \Omega \times [0, T] \rightarrow \mathbb{R}$ across the cross section of the beam through a Taylor series expansion, defined as

$$(\mathbf{x}, t) \mapsto \psi(\mathbf{x}, t) := \phi(x_3, t) + \mathbf{p}(x_1, x_2) \cdot \boldsymbol{\beta}(x_3, t) + \frac{1}{2} \mathbf{p}(x_1, x_2) \cdot \boldsymbol{\gamma}(x_3, t) \mathbf{p}(x_1, x_2), \quad (52)$$

where ψ represents a parabolic expansion across the cross sectional area A of the beam, completely defined in terms of ϕ the electric potential at the reference triad origin $[0, 0, x_3]^T$, its gradient $\boldsymbol{\beta}$ and its Hessian $\boldsymbol{\gamma}$, namely scalar, vector and symmetric second order tensor beam axis-varying functions. It is important to remark that the only approximation for the distribution of the electric potential is established across the section of the beam (see Figure 3).

The electric field vector \mathbf{E} can now be obtained by computing the gradient of the newly introduced electric potential ψ as $\mathbf{E} := -\nabla\psi$ yielding (refer to equation (52)), after some algebraic manipulation

$$\mathbf{E} = -\boldsymbol{\epsilon}^e - (\mathbf{e}_3 \otimes \mathbf{p}) \boldsymbol{\kappa}^e - \mathbf{V} : \boldsymbol{\varsigma}^e - \mathbf{W} : \boldsymbol{\gamma}, \quad (53)$$

where

$$\boldsymbol{\epsilon}^e := \frac{\partial \phi}{\partial x_3} \mathbf{e}_3 + \boldsymbol{\beta}, \quad \boldsymbol{\kappa}^e := \frac{\partial \boldsymbol{\beta}}{\partial x_3}, \quad \boldsymbol{\varsigma}^e := \frac{\partial \boldsymbol{\gamma}}{\partial x_3}, \quad (54)$$

with the third order tensors \mathbf{V} and \mathbf{W} defined by

$$\mathbf{V} := \mathbf{e}_3 \otimes \frac{1}{2} (\mathbf{p} \otimes \mathbf{p}), \quad \mathbf{W} := \mathbf{e}_\alpha \otimes \frac{1}{2} (\mathbf{p} \otimes \mathbf{e}_\alpha + \mathbf{e}_\alpha \otimes \mathbf{p}). \quad (55)$$

Considering equation (53), it is interesting to notice the similarities with the definition of the small strain tensor $\boldsymbol{\epsilon}$ (43). Notice how the first two terms on the right hand side of equation (53)

⁴Interestingly, a direct consequence of (50) for the case of skew-symmetric couple stress theory is that, the couple stress resultants are first projected on to the axis of the beam prior to area integration. In classical beam theory, this projection vanishes due to the symmetry of Cauchy stresses i.e. $\mathbf{e}_i \times (\boldsymbol{\sigma} \mathbf{e}_i) = \mathbf{0}$; see Hjelmstad [2005].

stem from the linear contribution in (52) (as in formula (43)) whereas the last two terms stem from the quadratic contribution in (52).

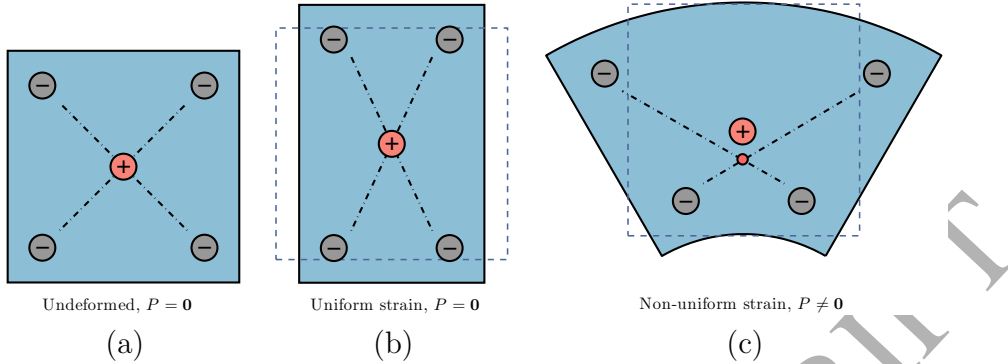


Figure 3: A schematic representation of electric polarisation in a centrosymmetric lattice beam, (a) undeformed state - no polarisation, (b) when uniformly strained, the atomic displacements of the centrosymmetric lattice will follow the elastic medium approximation resulting in no polarisation, (c) when strained non-uniformly, the atomic displacements no longer follow the elastic medium approximation and the symmetry restriction (symmetrical movement of ions) is broken resulting in electric polarisation opposite to the direction of applied strain, [Zubko et al. \[2013\]](#); [Deng et al. \[2014\]](#).

The new initial boundary value problem, adapted to a three-dimensional beam problem, is then defined by equations (1,3,5) and (42,52), which combine the governing equations of both elastodynamics and electrostatics, initial and boundary conditions, the coupling electro-mechanical equations for $\boldsymbol{\sigma}$, $\boldsymbol{\chi}$ and \boldsymbol{D} , the beam kinematics assumption \boldsymbol{u} and the electric potential spatial distribution ψ .

5.3. Displacement-potential variational formulation for flexoelectric beams

In order to establish the variational formulation of the problem at a beam level, we consider virtual variations of displacements and electric potential $\delta\boldsymbol{u}$ and $\delta\psi$, satisfying appropriate boundary conditions. Analogous to continuum formulation and following [Poya et al. \[2015\]](#), we can rewrite the variational form (virtual work) of the initial boundary value problem at beam level as

$$\delta W(\boldsymbol{u}, \psi; \delta\boldsymbol{u}, \delta\psi) := \delta W_{iner} + \delta W_{int}^m + \delta W_{int}^g + \delta W_{int}^e - \delta W_{ext}^m - \delta W_{ext}^g - \delta W_{ext}^e = 0, \quad (56)$$

where W represents the total work including strain-induced, curvature-induced and polarisation-induced internal and their corresponding external work, such that

$$\delta W_{iner} := \int_{\Omega} \rho \ddot{\boldsymbol{u}} \cdot \delta \boldsymbol{u} \, d\Omega, \quad (57a)$$

$$\delta W_{int}^m := \int_{\Omega} \boldsymbol{\sigma} : \delta \boldsymbol{\varepsilon} \, d\Omega + \int_{\Omega} \hat{\boldsymbol{\sigma}}^g : \delta \hat{\boldsymbol{\omega}} \, d\Omega, \quad (57b)$$

$$\delta W_{int}^g := \int_{\Omega} \boldsymbol{\mu} \cdot \delta \boldsymbol{\chi} \, d\Omega, \quad (57c)$$

$$\delta W_{ext}^m := \int_{\Omega} \rho \boldsymbol{b} \cdot \delta \boldsymbol{u} \, d\Omega + \int_{\Gamma^{\sigma}} \boldsymbol{t} \cdot \delta \boldsymbol{u} \, d\Gamma, \quad (57d)$$

$$\delta W_{ext}^g := \frac{1}{2} \left[\int_{\Omega} \rho \boldsymbol{b} \cdot (\nabla \times \delta \boldsymbol{u}) \, d\Omega + \int_{\Gamma^{\mu}} \boldsymbol{m} \cdot (\nabla \times \delta \boldsymbol{u}) \, d\Gamma \right], \quad (57e)$$

$$\delta W_{int}^e := - \int_{\Omega} \mathbf{D} \cdot \delta \mathbf{E} \, d\Omega, \quad (57f)$$

$$\delta W_{ext}^e := \int_{\Omega} \rho^e \delta \psi \, d\Omega + \int_{\Gamma^D} q_0 \delta \psi \, d\Gamma, \quad (57g)$$

represent the different contributions (e.g. inertial, internal, external, mechanical, electrical) to the total virtual work. Substituting the expressions for $\delta \mathbf{u}$ (42) and $\delta \psi$ (52) into equation (43), (48) and (53) results in

$$\delta \boldsymbol{\varepsilon} = \frac{1}{2} \left[(\delta \boldsymbol{\epsilon}^m + \delta \boldsymbol{\kappa}^m \times \mathbf{p}) \otimes \mathbf{e}_3 + \mathbf{e}_3 \otimes (\delta \boldsymbol{\epsilon}^m + \delta \boldsymbol{\kappa}^m \times \mathbf{p}) \right], \quad (58a)$$

$$\delta \boldsymbol{\chi} = \frac{1}{4} \bar{\mathbf{I}} (\delta \boldsymbol{\epsilon}^g + \delta \boldsymbol{\kappa}^g \times \mathbf{p}), \quad (58b)$$

$$\delta \mathbf{E} = -\delta \boldsymbol{\epsilon}^e - (\mathbf{e}_3 \otimes \mathbf{p}) \delta \boldsymbol{\kappa}^e - \mathbf{V} : \delta \boldsymbol{\varsigma}^e - \mathbf{W} : \delta \boldsymbol{\gamma}, \quad (58c)$$

where

$$\delta \boldsymbol{\epsilon}^m := \frac{\partial \delta \mathbf{w}}{\partial x_3} + \mathbf{e}_3 \times \delta \boldsymbol{\theta}, \quad \delta \boldsymbol{\kappa}^m := \frac{\partial \delta \boldsymbol{\theta}}{\partial x_3}, \quad (59a)$$

$$\delta \boldsymbol{\epsilon}^g := \frac{\partial^2 \delta \mathbf{w}}{\partial x_3^2} + \delta \boldsymbol{\kappa}^m \times \mathbf{e}_3, \quad \delta \boldsymbol{\kappa}^g := \frac{\partial^2 \delta \boldsymbol{\theta}}{\partial x_3^2}, \quad (59b)$$

$$\delta \boldsymbol{\epsilon}^e := \frac{\partial \delta \phi}{\partial x_3} \mathbf{e}_3 + \delta \boldsymbol{\beta}, \quad \delta \boldsymbol{\kappa}^e := \frac{\partial \delta \boldsymbol{\beta}}{\partial x_3}, \quad \delta \boldsymbol{\varsigma}^e := \frac{\partial \delta \boldsymbol{\gamma}}{\partial x_3}, \quad (59c)$$

represent the virtual mechanical and electrical beam strains. Substituting the expressions for \mathbf{u} and $\delta \mathbf{u}$ (42) into (57a) yields (after integration over the cross sectional area A) the inertial virtual work

$$\delta W_{iner} = \int_l \left[\delta \mathbf{w} \cdot (\mathbf{A}_D \ddot{\mathbf{w}} + \mathbf{S}_D \ddot{\boldsymbol{\theta}}) + \delta \boldsymbol{\theta} \cdot (\mathbf{S}_D^T \ddot{\mathbf{w}} + \mathbf{I}_D \ddot{\boldsymbol{\theta}}) \right] dx_3, \quad (60)$$

where

$$\mathbf{A}_D := \int_A \rho \mathbf{I} \, dA, \quad \mathbf{S}_D := \int_A \rho \hat{\mathbf{p}} \, dA, \quad \mathbf{I}_D := \int_A \rho \hat{\mathbf{p}} \hat{\mathbf{p}}^T \, dA, \quad (61)$$

represent the mass \mathbf{A}_D , first area moment \mathbf{S}_D and second area moment \mathbf{I}_D tensors of the cross sectional area A . Notice that $\hat{\mathbf{p}}$ represents the skew symmetric tensor associated with the axial vector \mathbf{p} . When considering a reference frame whose origin coincides with the centre of mass of the cross sectional area A , then $\mathbf{S}_D = \mathbf{0}$. Moreover, if the reference frame is aligned along the so-called principal directions, the second area moment tensor \mathbf{I}_D becomes diagonal.

Analogously, substituting the expression for $\delta \boldsymbol{\varepsilon}$ (58a) into (57b) yields (after integration over the cross sectional area A) the internal mechanical virtual work

$$\delta W_{int}^m = \int_l [\delta \boldsymbol{\epsilon}^m \cdot \mathbf{Q}^m + \delta \boldsymbol{\kappa}^m \cdot \mathbf{M}^m] \, dx_3, \quad (62)$$

with

$$\mathbf{Q}^m := \int_A \boldsymbol{\sigma} \mathbf{e}_3 \, dA, \quad \mathbf{M}^m := \int_A \mathbf{p} \times (\boldsymbol{\sigma} \mathbf{e}_3) \, dA. \quad (63)$$

In the above equation (62), \mathbf{Q}^m represents the internal shear/axial force whereas \mathbf{M}^m represents the internal bending/torsion moment.

Substituting the expression for $\delta\mathbf{u}$ (42) into (57d) yields (after integration over the cross sectional area A) the standard mechanical external virtual work

$$\delta W_{ext}^m = [\delta\mathbf{w} \cdot \mathbf{Q}^m + \delta\boldsymbol{\theta} \cdot \mathbf{M}^m]_0^l + \int_l [\delta\mathbf{w} \cdot \mathbf{q}^m + \delta\boldsymbol{\theta} \cdot \mathbf{m}^m] dx_3, \quad (64)$$

where

$$\mathbf{q}^m := \int_A \rho\mathbf{b} dA + \int_{\partial A} \mathbf{t} d\Gamma, \quad \mathbf{m}^m := \int_A (\mathbf{p} \times \rho\mathbf{b}) dA + \int_{\partial A} (\mathbf{p} \times \mathbf{t}) d\Gamma. \quad (65)$$

In above equations (64) and (65), \mathbf{q}^m and \mathbf{m}^m represent a possible external distributed force and moment, respectively, acting along the beam axis. The first term in squared brackets on the right hand side of equation (64) represents mechanical actions (force and moment) applied at both ends of the beam, namely $x_3 = 0$ and $x_3 = l$.

For the strain gradient (curvature) quantities, substituting the expression for $\delta\chi$ (58b) into (57c) yields the micro-mechanical internal virtual work

$$\delta W_{int}^g = \int_l [\delta\boldsymbol{\epsilon}^g \cdot \mathbf{Q}^g + \delta\boldsymbol{\kappa}^g \cdot \mathbf{M}^g] dx_3, \quad (66)$$

with

$$\mathbf{Q}^g := \int_A \frac{1}{2} \bar{\mathbf{I}}\boldsymbol{\mu} dA, \quad \mathbf{M}^g := \int_A \mathbf{p} \times \left(\frac{1}{2} \bar{\mathbf{I}}\boldsymbol{\mu} \right) dA. \quad (67)$$

where \mathbf{Q}^g and \mathbf{M}^g can be interpreted as size-dependent shear force and bending/torsion moment emanating from the micro-structure. Comparing (63) and (67), it is evident that unlike the standard force stress resultants (based on $\sigma\mathbf{e}_3$), couple-stress resultants are integrated in the plane ($\mathbf{e}_3 \otimes \mathbf{e}_3 - \mathbf{I} = \bar{\mathbf{I}}$) which is the direct consequence of couple stress constraint $2\boldsymbol{\omega} = \nabla \times \mathbf{u}$ and the axial curvature vector (48).

Substituting the expression for $\delta\mathbf{u}$ (42) into (57e) yields (after integration over the cross sectional area A) the micro-mechanical external virtual work

$$\delta W_{ext}^g = [\delta\mathbf{w} \cdot \mathbf{Q}^g + \delta\boldsymbol{\theta} \cdot \mathbf{M}^g]_0^l + \int_l [\delta\mathbf{w} \cdot \mathbf{q}^g + \delta\boldsymbol{\theta} \cdot \mathbf{m}^g] dx_3, \quad (68)$$

where

$$\begin{aligned} \mathbf{q}^g &:= \int_A \frac{\rho}{2} \nabla \times \mathbf{l} dA + \int_{\partial A} \frac{1}{2} \nabla \times \mathbf{m} d\Gamma, \\ \mathbf{m}^g &:= \int_A \left(\mathbf{p} \times \left(\frac{\rho}{2} \nabla \times \mathbf{l} \right) \right) dA + \int_{\partial A} \frac{1}{2} \left(\mathbf{p} \times (\nabla \times \mathbf{m}) \right) d\Gamma. \end{aligned} \quad (69)$$

In the above equations (68) and (69), \mathbf{q}^g and \mathbf{m}^g can be interpreted as the micro-mechanical external distributed force and moment, respectively, acting along the beam axis. We can merge the contribution of external forces of δW_{ext}^m (68) with δW_{ext}^g (64), as these are prescribed quantities carrying the same units, whose effects cannot be distinguished individually. Hence, in what follows, with slight abuse of notation, we assume

$$\mathbf{q}^m = \mathbf{q}^m + \mathbf{q}^g, \quad \mathbf{m}^m = \mathbf{m}^m + \mathbf{m}^g.$$

From the electrical point of view, substituting the expression for $\delta\mathbf{E}$ (58c) into (57f) yields (after integration over the cross sectional area A) the internal electrical virtual work

$$\delta W_{int}^e = \int_l [\delta\boldsymbol{\epsilon}^e \cdot \mathbf{Q}^e + \delta\boldsymbol{\kappa}^e \cdot \mathbf{M}^e + \delta\boldsymbol{\varsigma}^e : \mathbf{O}^e + \delta\boldsymbol{\gamma} : \mathbf{P}^e] dx_3, \quad (70)$$

where

$$\mathbf{Q}^e := \int_A \mathbf{D} dA, \quad \mathbf{M}^e := \int_A (\mathbf{D} \cdot \mathbf{e}_3) \mathbf{p} dA, \quad (71a)$$

$$\mathbf{P}^e := \int_A \mathbf{D} \cdot \mathcal{W} dA, \quad \mathbf{O}^e := \int_A \mathbf{D} \cdot \mathbf{V} dA. \quad (71b)$$

In the above equations (70) and (71a), it is interesting to observe the similarities between \mathbf{Q}^e and \mathbf{M}^e and their mechanical counterparts (63), namely \mathbf{Q}^m and \mathbf{M}^m , respectively. In addition, due to the quadratic nature of the electric potential distribution, two extra second order tensors arise, that is \mathbf{P}^e and \mathbf{O}^e expressed in terms of the third order tensors \mathcal{W} and \mathbf{V} already defined in (55).

Finally, substituting the expression for $\delta\psi$ (52) into (57g) yields (after integration over the cross sectional area A) the electrical external virtual work as

$$\delta W_{ext}^e = [\delta\phi (\mathbf{Q}^e \cdot \mathbf{e}_3) + \delta\beta \cdot \mathbf{M}^e + \delta\gamma : \mathbf{O}^e]_0^l + \int_l [\delta\phi q^e + \delta\beta \cdot \mathbf{m}^e + \delta\gamma : \mathbf{o}^e] dx_3, \quad (72)$$

where

$$q^e := \int_A \rho^e dA + \int_{\partial A} q_0 d\Gamma, \quad (73a)$$

$$\mathbf{m}^e := \int_A \rho^e \mathbf{p} dA + \int_{\partial A} q_0 \mathbf{p} d\Gamma, \quad (73b)$$

$$\mathbf{o}^e := \int_A \frac{\rho^e}{2} (\mathbf{p} \otimes \mathbf{p}) dA + \int_{\partial A} \frac{q_0}{2} (\mathbf{p} \otimes \mathbf{p}) d\Gamma. \quad (73c)$$

Again, it is interesting to note the similarities between the above expressions q^e , \mathbf{m}^e (73) and those of q^m , \mathbf{m}^m (65). In equation (72), q^e , \mathbf{m}^e and \mathbf{o}^e represent possible distributed electrical effects per unit of length. Moreover, $(\mathbf{Q}^e \cdot \mathbf{e}_3)$, \mathbf{M}^e and \mathbf{O}^e represent electrical actions applied at both ends of the beam, namely $x_3 = 0$ and $x_3 = L$.

For completeness, the final virtual work expression characterising the behaviour of the piezoelectric beam can be written as

$$\delta W := \delta W_{iner} + \delta W_{int} - \delta W_{ext} = 0, \quad (74)$$

$$\delta W_{iner} = \int_l [\delta \mathbf{w} \cdot (\mathbf{A}_D \ddot{\mathbf{w}} + \mathbf{S}_D \ddot{\boldsymbol{\theta}}) + \delta \boldsymbol{\theta} \cdot (\mathbf{S}_D^T \ddot{\mathbf{w}} + \mathbf{I}_D \ddot{\boldsymbol{\theta}})] dx_3, \quad (75a)$$

$$\begin{aligned} \delta W_{int} &= \int_l [\delta \boldsymbol{\epsilon}^m \cdot \mathbf{Q}^m + \delta \boldsymbol{\kappa}^m \cdot \mathbf{M}^m] + [\delta \boldsymbol{\epsilon}^g \cdot \mathbf{Q}^g + \delta \boldsymbol{\kappa}^g \cdot \mathbf{M}^g] dx_3 \\ &\quad + \int_l [\delta \boldsymbol{\epsilon}^e \cdot \mathbf{Q}^e + \delta \boldsymbol{\kappa}^e \cdot \mathbf{M}^e + \delta \boldsymbol{\varsigma}^e : \mathbf{P}^e + \delta \boldsymbol{\gamma} : \mathbf{O}^e] dx_3, \end{aligned} \quad (75b)$$

$$\begin{aligned} \delta W_{ext} &= [\delta \mathbf{w} \cdot \mathbf{Q}^m + \delta \boldsymbol{\theta} \cdot \mathbf{M}^m]_0^l + \int_l [\delta \mathbf{w} \cdot \mathbf{q}^m + \delta \boldsymbol{\theta} \cdot \mathbf{m}^m] dx_3 \\ &\quad + \left[\delta \mathbf{w} \cdot \frac{\partial \mathbf{Q}^g}{\partial x_3} + \delta \boldsymbol{\theta} \cdot \frac{\partial \mathbf{M}^g}{\partial x_3} \right]_0^l + \int_l \left[\delta \mathbf{w} \cdot \frac{\partial \mathbf{q}^g}{\partial x_3} + \delta \boldsymbol{\theta} \cdot \frac{\partial \mathbf{m}^g}{\partial x_3} \right] dx_3 \\ &\quad + [\delta\phi (\mathbf{Q}^e \cdot \mathbf{e}_3) + \delta\beta \cdot \mathbf{M}^e + \delta\gamma : \mathbf{O}^e]_0^l + \int_l [\delta\phi q^e + \delta\beta \cdot \mathbf{m}^e + \delta\gamma : \mathbf{o}^e] dx_3. \end{aligned} \quad (75c)$$

5.4. Internal area resultants for displacement-potential formulation

From the mechanical standpoint, having introduced the additive decomposition of the total Cauchy stress tensor $\boldsymbol{\sigma}$ in equation (12), we now proceed to find the traction vector acting in a cross sectional area A of the beam defined by the outward unit normal \mathbf{e}_3 , namely $\boldsymbol{\sigma}\mathbf{e}_3$. For the mechanical contribution $\boldsymbol{\sigma}^m$, referring to Appendix B, (43) yields

$$\boldsymbol{\sigma}^m \mathbf{e}_3 = \boldsymbol{\Xi}(\boldsymbol{\epsilon}^m + \hat{\mathbf{p}}^T \boldsymbol{\kappa}^m), \quad [\boldsymbol{\Xi}]_{ij} = [\mathcal{C}]_{ikjl} [\mathbf{e}_3]_k [\mathbf{e}_3]_l. \quad (76)$$

For the nonlocal contribution of the force stress tensor $\hat{\boldsymbol{\sigma}}^g$, (48) yields

$$\hat{\boldsymbol{\sigma}}^g \mathbf{e}_3 = \boldsymbol{\Upsilon}_1(\boldsymbol{\epsilon}^m + \hat{\mathbf{p}}^T \boldsymbol{\kappa}^m), \quad \boldsymbol{\Upsilon}_1 = \frac{1}{2} \hat{\boldsymbol{\sigma}}^g \hat{\mathbf{I}}, \quad (77)$$

where $\hat{\mathbf{I}}$ is the skew-symmetric tensor dual to \mathbf{e}_3 given by

$$\hat{\mathbf{I}} = \begin{bmatrix} 0 & -1 & 0 \\ 1 & 0 & 0 \\ 0 & 0 & 0 \end{bmatrix}.$$

For anisotropic materials the nonlocal contribution of the force stress tensor $\hat{\boldsymbol{\sigma}}^g$ also includes constitutive terms

$$\hat{\boldsymbol{\sigma}}^g \mathbf{e}_3 = \boldsymbol{\Upsilon}_2(\boldsymbol{\epsilon}^g + \hat{\mathbf{p}}^T \boldsymbol{\kappa}^g), \quad [\boldsymbol{\Upsilon}_2]_{ij} = \frac{1}{4} [\mathcal{D}]_{ikl} [\mathbf{e}_3]_k [\bar{\mathbf{I}}]_{lj}. \quad (78)$$

Analogously, for the electrical contribution $\boldsymbol{\sigma}^e$, (53) yields

$$\boldsymbol{\sigma}^e \mathbf{e}_3 = \boldsymbol{\Theta} (\boldsymbol{\epsilon}^e + (\mathbf{e}_3 \otimes \mathbf{p}) \boldsymbol{\kappa}^e + \boldsymbol{\mathcal{V}} : \boldsymbol{\varsigma}^e + \boldsymbol{\mathcal{W}} : \boldsymbol{\gamma}), \quad [\boldsymbol{\Theta}]_{ij} = [\mathbf{e}]_{jik} [\mathbf{e}_3]_k. \quad (79)$$

The first internal area resultant \mathbf{Q}^m , also known as the axial/shear force, can now be computed from equations (63), (76-79) as

$$\mathbf{Q}^m = \mathbf{A}^m \boldsymbol{\epsilon}^m + \mathbf{S}^m \boldsymbol{\kappa}^m + \mathbf{A}^{mg} \boldsymbol{\epsilon}^g + \mathbf{S}_1^{mg} \boldsymbol{\kappa}^g + \mathbf{A}_1^e \boldsymbol{\epsilon}^e + \mathbf{S}_1^e \boldsymbol{\kappa}^e + \mathbf{S}_2^e : \boldsymbol{\gamma} + \mathbf{I}_1^e : \boldsymbol{\varsigma}^e, \quad (80)$$

where

$$\begin{aligned} \mathbf{A}^m &:= \int_A \boldsymbol{\Xi} \, dA + \int_A \boldsymbol{\Upsilon}_1 \, dA, & \mathbf{S}^m &:= \int_A \boldsymbol{\Xi} \hat{\mathbf{p}}^T \, dA + \int_A \boldsymbol{\Upsilon}_1 \hat{\mathbf{p}}^T \, dA, & \mathbf{A}^{mg} &:= \int_A \boldsymbol{\Upsilon}_2 \, dA, \\ \mathbf{S}_1^{mg} &:= \int_A \boldsymbol{\Upsilon}_2 \hat{\mathbf{p}}^T \, dA, & \mathbf{A}_1^e &:= \int_A \boldsymbol{\Theta} \, dA, & \mathbf{S}_1^e &:= \int_A \boldsymbol{\Theta} (\mathbf{e}_3 \otimes \mathbf{p}) \, dA, \\ \mathbf{I}_1^e &:= \int_A \boldsymbol{\Theta} \boldsymbol{\mathcal{V}} \, dA, & \mathbf{S}_2^e &:= \int_A \boldsymbol{\Theta} \boldsymbol{\mathcal{W}} \, dA, \end{aligned}$$

The first two terms on the right hand side of (80) stem from strain contributions, the third and fourth terms stem from curvature contribution and the remainder stem from electrical contribution. The second internal area resultant \mathbf{M}^m , also known as bending/torsion moment, can also be computed from equations (63), (76) and (79) as

$$\mathbf{M}^m = (\mathbf{S}^m)^T \boldsymbol{\epsilon}^m + \mathbf{I}^m \boldsymbol{\kappa}^m + \mathbf{S}_2^{mg} \boldsymbol{\epsilon}^g + \mathbf{I}^{mg} \boldsymbol{\kappa}^g + \mathbf{S}_3^e \boldsymbol{\epsilon}^e + \mathbf{I}_2^e \boldsymbol{\kappa}^e + \mathbf{I}_3^e : \boldsymbol{\gamma} + \mathbf{G}_1^e : \boldsymbol{\varsigma}^e, \quad (82)$$

where

$$\mathbf{I}^m := \int_A \hat{\mathbf{p}} \boldsymbol{\Xi} \hat{\mathbf{p}}^T \, dA + \int_A \hat{\mathbf{p}} \boldsymbol{\Upsilon}_1 \hat{\mathbf{p}}^T \, dA, \quad \mathbf{S}_2^{mg} := \int_A \hat{\mathbf{p}} \boldsymbol{\Upsilon}_2 \, dA, \quad \mathbf{I}^{mg} := \int_A \hat{\mathbf{p}} \boldsymbol{\Upsilon}_2 \hat{\mathbf{p}}^T \, dA,$$

$$\begin{aligned} S_3^e &:= \int_A \hat{\mathbf{p}}\boldsymbol{\Theta} dA, & I_2^e &:= \int_A \hat{\mathbf{p}}\boldsymbol{\Theta}(\mathbf{e}_3 \otimes \mathbf{p}) dA, & G_1^e &:= \int_A \hat{\mathbf{p}}\boldsymbol{\Theta}\mathbf{V} dA, \\ I_3^e &:= \int_A \hat{\mathbf{p}}\boldsymbol{\Theta}\mathbf{W} dA. \end{aligned}$$

As mentioned before, couple-stress resultants are integrated in the cross-sectional plane $\bar{\mathbf{I}}$. For mechanical contribution $\boldsymbol{\mu}^m$ referring to [Appendix B](#), (43) yields

$$\frac{1}{2}\bar{\mathbf{I}}\boldsymbol{\mu}^m = \boldsymbol{\Upsilon}^T(\boldsymbol{\epsilon}^m + \hat{\mathbf{p}}^T\boldsymbol{\kappa}^m), \quad (84)$$

For micro-mechanical contributions $\boldsymbol{\mu}^g$, (48) yields

$$\frac{1}{2}\bar{\mathbf{I}}\boldsymbol{\mu}^g = \boldsymbol{\varrho}(\boldsymbol{\epsilon}^g + \hat{\mathbf{p}}^T\boldsymbol{\kappa}^g), \quad [\boldsymbol{\varrho}]_{ij} = \frac{1}{16}[\bar{\mathbf{I}}]_{ik}[\mathcal{B}]_{kl}[\bar{\mathbf{I}}]_{lj}. \quad (85)$$

Analogously, for electrical contributions $\boldsymbol{\mu}^e$, (53) yields

$$\frac{1}{2}\bar{\mathbf{I}}\boldsymbol{\mu}^e = \boldsymbol{\aleph}(\boldsymbol{\epsilon}^e + (\mathbf{e}_3 \otimes \mathbf{p})\boldsymbol{\kappa}^e + \mathbf{V} : \boldsymbol{\varsigma}^e + \mathbf{W} : \boldsymbol{\gamma}), \quad \boldsymbol{\aleph} = \frac{1}{4}\bar{\mathbf{I}}\mathbf{f}^T. \quad (86)$$

The couple stress area resultants \mathbf{Q}^g and \mathbf{M}^g , can now be computed from equations (67), (84-79) as

$$\mathbf{Q}^g = (\mathbf{A}^{mg})^T\boldsymbol{\epsilon}^m + (S_2^{mg})^T\boldsymbol{\kappa}^m + \mathbf{A}^g\boldsymbol{\epsilon}^g + S^g\boldsymbol{\kappa}^g + \mathbf{A}^{ge}\boldsymbol{\epsilon}^e + S_1^{ge}\boldsymbol{\kappa}^e + S_2^{ge} : \boldsymbol{\gamma} + \mathbf{I}_1^{ge} : \boldsymbol{\varsigma}^e, \quad (87)$$

where

$$\begin{aligned} \mathbf{A}^g &:= \int_A \boldsymbol{\varrho} dA, & S^g &:= \int_A \boldsymbol{\varrho}\hat{\mathbf{p}}^T dA, & \mathbf{A}_1^{ge} &:= \int_A \boldsymbol{\aleph} dA, \\ S_1^{ge} &:= \int_A \boldsymbol{\aleph}(\mathbf{e}_3 \otimes \mathbf{p}) dA, & \mathbf{I}_1^{ge} &:= \int_A \boldsymbol{\aleph}\mathbf{V} dA, & S_2^{ge} &:= \int_A \boldsymbol{\aleph}\mathbf{W} dA, \end{aligned}$$

and analogously for \mathbf{M}^g

$$\mathbf{M}^g = (S_1^{mg})^T\boldsymbol{\epsilon}^m + (I_2^{mg})^T\boldsymbol{\kappa}^m + (S^g)^T\boldsymbol{\epsilon}^g + I^{mg}\boldsymbol{\kappa}^g + S_3^{ge}\boldsymbol{\epsilon}^e + I_2^{ge}\boldsymbol{\kappa}^e + I_3^{ge} : \boldsymbol{\gamma} + G_1^{ge} : \boldsymbol{\varsigma}^e, \quad (89)$$

where

$$\begin{aligned} I^g &:= \int_A \hat{\mathbf{p}}\boldsymbol{\varrho}\hat{\mathbf{p}}^T dA, & S_3^{ge} &:= \int_A \hat{\mathbf{p}}\boldsymbol{\aleph} dA, & I_2^{ge} &:= \int_A \hat{\mathbf{p}}\boldsymbol{\aleph}(\mathbf{e}_3 \otimes \mathbf{p}) dA, \\ G_1^{ge} &:= \int_A \hat{\mathbf{p}}\boldsymbol{\aleph}\mathbf{V} dA, & I_3^{ge} &:= \int_A \hat{\mathbf{p}}\boldsymbol{\aleph}\mathbf{W} dA. \end{aligned}$$

From the electrical standpoint, having introduced the additive decomposition of the electric displacement \mathbf{D} in equation (11) and [Appendix B](#), we can obtain after combining equations (11), (43), (48) and (53)

$$\mathbf{D}^m = \boldsymbol{\Theta}^T(\boldsymbol{\epsilon}^m + \hat{\mathbf{p}}^T\boldsymbol{\kappa}^m), \quad (91)$$

$$\mathbf{D}^g = \boldsymbol{\aleph}^T(\boldsymbol{\epsilon}^g + \hat{\mathbf{p}}^T\boldsymbol{\kappa}^g), \quad (92)$$

$$\mathbf{D}^e = -\boldsymbol{\epsilon}(\boldsymbol{\epsilon}^e + (\mathbf{e}_3 \otimes \mathbf{p})\boldsymbol{\kappa}^e + \mathbf{V} : \boldsymbol{\varsigma}^e + \mathbf{W} : \boldsymbol{\gamma}). \quad (93)$$

The third internal area resultant \mathbf{Q}^e can now be computed from equations (71a), (91) and (93) as

$$\mathbf{Q}^e = (\mathbf{A}_1^e)^T \boldsymbol{\epsilon}^m + (\mathbf{S}_3^e)^T \boldsymbol{\kappa}^m + (\mathbf{A}^{ge})^T \boldsymbol{\epsilon}^g + (\mathbf{S}_3^{ge})^T \boldsymbol{\kappa}^g - \mathbf{A}_2^e \boldsymbol{\epsilon}^e - \mathbf{S}_4^e \boldsymbol{\kappa}^e - \mathbf{S}_5^e : \boldsymbol{\gamma} - \mathbf{I}_4^e : \boldsymbol{\varsigma}^e, \quad (94)$$

where

$$\begin{aligned} \mathbf{A}_2^e &:= \int_A \boldsymbol{\epsilon} dA, & \mathbf{S}_4^e &:= \int_A \boldsymbol{\epsilon} (\mathbf{e}_3 \otimes \mathbf{p}) dA, \\ \mathbf{I}_4^e &:= \int_A \boldsymbol{\epsilon} \mathbf{V} dA, & \mathbf{S}_5^e &:= \int_A \boldsymbol{\epsilon} \mathbf{W} dA. \end{aligned}$$

Analogously, the fourth \mathbf{M}^e , fifth \mathbf{P}^e and sixth \mathbf{O}^e internal area resultants can be computed from equations (71a-71b), (91) and (93) as

$$\begin{aligned} \mathbf{M}^e &= (\mathbf{S}_1^e)^T \boldsymbol{\epsilon}^m + (\mathbf{I}_2^e)^T \boldsymbol{\kappa}^m + (\mathbf{S}_1^{ge})^T \boldsymbol{\epsilon}^g + (\mathbf{I}_2^{ge})^T \boldsymbol{\kappa}^g \\ &\quad - (\mathbf{S}_4^e)^T \boldsymbol{\epsilon}^e - \mathbf{I}_5^e \boldsymbol{\kappa}^e - \mathbf{I}_6^e : \boldsymbol{\gamma} - \mathbf{G}_2^e : \boldsymbol{\varsigma}^e, \\ \mathbf{P}^e &= (\mathbf{S}_2^e)^T \boldsymbol{\epsilon}^m + (\mathbf{I}_3^e)^T \boldsymbol{\kappa}^m + (\mathbf{S}_2^{ge})^T \boldsymbol{\epsilon}^g + (\mathbf{I}_3^{ge})^T \boldsymbol{\kappa}^g \\ &\quad - (\mathbf{S}_5^e)^T \boldsymbol{\epsilon}^e - (\mathbf{I}_6^e)^T \boldsymbol{\kappa}^e - \mathbf{I}_7^e : \boldsymbol{\gamma} - \mathbf{G}_3^e : \boldsymbol{\varsigma}^e, \\ \mathbf{O}^e &= (\mathbf{I}_1^e)^T \boldsymbol{\epsilon}^m + (\mathbf{G}_1^e)^T \boldsymbol{\kappa}^m + (\mathbf{I}_1^{ge})^T \boldsymbol{\epsilon}^g + (\mathbf{G}_1^{ge})^T \boldsymbol{\kappa}^g \\ &\quad - (\mathbf{I}_4^e)^T \boldsymbol{\epsilon}^e - (\mathbf{G}_2^e)^T \boldsymbol{\kappa}^e - (\mathbf{G}_3^e)^T : \boldsymbol{\gamma} - \mathbf{J}^e : \boldsymbol{\varsigma}^e, \end{aligned}$$

where

$$\begin{aligned} \mathbf{I}_5^e &:= \int_A (\mathbf{p} \otimes \mathbf{e}_3) \boldsymbol{\epsilon} (\mathbf{e}_3 \times \mathbf{p}) dA, & \mathbf{J}^e &:= \int_A \mathbf{V}^{*T} \boldsymbol{\epsilon} \mathbf{V} dA, & \mathbf{I}_6^e &:= \int_A (\mathbf{p} \otimes \mathbf{e}_3) \boldsymbol{\epsilon} \mathbf{W} dA, \\ \mathbf{G}_2^e &:= \int_A (\mathbf{p} \otimes \mathbf{e}_3) \boldsymbol{\epsilon} \mathbf{V} dA, & \mathbf{G}_3^e &:= \int_A \mathbf{W}^{*T} \boldsymbol{\epsilon} \mathbf{V} dA, & \mathbf{I}_7^e &:= \int_A \mathbf{W}^{*T} \boldsymbol{\epsilon} \mathbf{W} dA. \end{aligned}$$

Finally, we can summarise all of the above relationships between internal area resultants and mechanical/electrical strains in the following table matrix format⁵

$$\left\{ \begin{array}{l} \mathbf{Q}^m \\ \mathbf{M}^m \\ \mathbf{Q}^g \\ \mathbf{M}^g \\ \mathbf{Q}^e \\ \mathbf{M}^e \\ \mathbf{P}^e \\ \mathbf{O}^e \end{array} \right\} = \left[\begin{array}{cccccccc} \mathbf{A}^m & \mathbf{S}^m & \mathbf{A}^{mg} & \mathbf{S}_1^{mg} & \mathbf{A}_1^e & \mathbf{S}_1^e & \mathbf{S}_2^e & \mathbf{I}_1^e \\ \mathbf{I}^m & \mathbf{S}_2^{mg} & \mathbf{I}^{mg} & \mathbf{S}_3^g & \mathbf{I}^{ge} & \mathbf{I}_2^e & \mathbf{I}_3^e & \mathbf{G}_1^e \\ & & & \mathbf{A}^g & & \mathbf{S}_3^e & \mathbf{S}_2^{ge} & \mathbf{I}_1^{ge} \\ & & & & \mathbf{I}^g & & & \\ & & & & \mathbf{S}_3^{ge} & \mathbf{I}_2^{ge} & \mathbf{I}_3^{ge} & \mathbf{G}_1^{ge} \\ & & & & & -\mathbf{A}_2^e & -\mathbf{S}_4^e & -\mathbf{S}_5^e & -\mathbf{I}_4^e \\ & & & & & & -\mathbf{I}_5^e & -\mathbf{I}_6^e & -\mathbf{G}_2^e \\ & & & & & & & -\mathbf{I}_7^e & -\mathbf{G}_3^e \\ & & & & & & & & -\mathbf{J}^e \end{array} \right] \left\{ \begin{array}{l} \boldsymbol{\epsilon}^m \\ \boldsymbol{\kappa}^m \\ \boldsymbol{\epsilon}^g \\ \boldsymbol{\kappa}^g \\ \boldsymbol{\epsilon}^e \\ \boldsymbol{\kappa}^e \\ : \boldsymbol{\gamma} \\ : \boldsymbol{\varsigma}^e \end{array} \right\} \quad (97)$$

This resulting Hessian operator is symmetric indefinite since it emanates from the enthalpy density of the system. In case of dealing with a homogeneous material across the section of the beam, namely constant mechanical and electrical properties within the area section A , if the origin of the reference triad $\{\mathbf{e}_1, \mathbf{e}_2, \mathbf{e}_3\}$ is chosen as the centre of mass of the section, then the tensors \mathbf{S}^m , \mathbf{S}_k^e ($k = 1 \dots 5$) and \mathbf{G}_k^e ($k = 1 \dots 3$) vanish (e.g. their integrand is of odd order in the position vector \mathbf{p}). Finally, the initial boundary value problem representing the behaviour of a flexoelectric three-dimensional beam is defined by equations (110), (111), (112) and (97).

⁵Notice that the entries in columns one to four correspond to second order tensors whereas the entries in columns five and six correspond to third order tensors. Also note that for a third order tensor $[\mathcal{A}]_{ijk}$, we have defined a transpose operator $\mathcal{A}^{*T} = [\mathcal{A}]_{kij}$

5.5. The penalty formulation for flexoelectric beams

So far in the development of flexoelectric beam theory, we have assumed a strong enforcement of the couple stress constraint in order to be able to find the area resultants and balance equations governing the physics of flexoelectric beams. However, similar to the continuum formulation, the couple stress constraint can be imposed weakly through a penalty formulation. This essentially implies that the vorticity vector must be treated as an independent field and must have a description compatible with the rest of beam kinematic and electrostatic measures. In essence, $\boldsymbol{\omega}$ can be described through the mapping

$$(\mathbf{x}, t) \mapsto \boldsymbol{\omega}(\mathbf{x}, t) = \boldsymbol{\omega}_c(x_3, t) + \boldsymbol{\omega}_p(x_3, t) \times \mathbf{p}(x_1, x_2), \quad (98)$$

where $\boldsymbol{\omega}_c$ and $\boldsymbol{\omega}_p$ characterise the vorticity of the beam along the axis and across the cross section of the beam, respectively. The curvature vector can now be written as

$$\boldsymbol{\chi} = \frac{1}{2} \mathbf{e}_3 \times \left(\boldsymbol{\epsilon}^g + \boldsymbol{\kappa}^g \times \mathbf{p} \right) = \frac{1}{2} \hat{\mathbf{I}} \left(\boldsymbol{\epsilon}^g + \boldsymbol{\kappa}^g \times \mathbf{p} \right), \quad (99)$$

where

$$\boldsymbol{\epsilon}^g = \frac{\partial \boldsymbol{\omega}_c}{\partial x_3}, \quad \boldsymbol{\kappa}^g = \frac{\partial \boldsymbol{\omega}_p}{\partial x_3} \times \mathbf{p}, \quad (100)$$

If we assume a slight abuse of notation in order not to rename the variables, interestingly, the variational formulation for the penalty approach in the beam setting remains the same as the displacement-potential formulation presented in (75). The changes that will have to be reflected are minor and in the area resultants emanating from (32) taking into account the total stress tensor (34). In principle, this also means substituting the new value of $\boldsymbol{\chi}$ which entails exchanging the term $\frac{1}{4} \bar{\mathbf{I}}$ with $\frac{1}{2} \hat{\mathbf{I}}$. Furthermore, the contribution of geometric stiffness in \mathbf{A}^m and \mathbf{S}^m in (80) and in \mathbf{I}^m in (82) disappear, as these contribution now explicitly perform work against $\delta \boldsymbol{\omega}_c$ and $\delta \boldsymbol{\omega}_p$, respectively (the third term in square brackets in (102b)). Under this settings we can write the variational form as

$$\delta W := \delta W_{iner} + \delta W_{int} - \delta W_{ext} = 0, \quad (101)$$

$$\delta W_{iner} = \int_l \left[\delta \boldsymbol{w} \cdot (\mathbf{A}_D \ddot{\boldsymbol{w}} + \mathbf{S}_D \ddot{\boldsymbol{\theta}}) + \delta \boldsymbol{\theta} \cdot (\mathbf{S}_D^T \ddot{\boldsymbol{w}} + \mathbf{I}_D \ddot{\boldsymbol{\theta}}) \right] dx_3, \quad (102a)$$

$$\begin{aligned} \delta W_{int} &= \int_l [\delta \boldsymbol{\epsilon}^m \cdot \mathbf{Q}^m + \delta \boldsymbol{\kappa}^m \cdot \mathbf{M}^m] + [\delta \boldsymbol{\epsilon}^g \cdot \mathbf{Q}^g + \delta \boldsymbol{\kappa}^g \cdot \mathbf{M}^g] + [\delta \boldsymbol{\omega}_c \cdot \bar{\mathbf{Q}}^m + \delta \boldsymbol{\omega}_p \cdot \bar{\mathbf{M}}^m] dx_3 \\ &\quad + \int_l [\delta \boldsymbol{\epsilon}^e \cdot \mathbf{Q}^e + \delta \boldsymbol{\kappa}^e \cdot \mathbf{M}^e + \delta \boldsymbol{\varsigma}^e : \mathbf{P}^e + \delta \boldsymbol{\gamma} : \mathbf{O}^e] dx_3, \end{aligned} \quad (102b)$$

$$\begin{aligned} \delta W_{ext} &= [\delta \boldsymbol{w} \cdot \mathbf{Q}^m + \delta \boldsymbol{\theta} \cdot \mathbf{M}^m]_0^l + \int_l [\delta \boldsymbol{w} \cdot \mathbf{q}^m + \delta \boldsymbol{\theta} \cdot \mathbf{m}^m] dx_3 \\ &\quad + [\delta \boldsymbol{\omega}_c \cdot \mathbf{Q}^g + \delta \boldsymbol{\omega}_p \cdot \mathbf{M}^g]_0^l + \int_l [\delta \boldsymbol{\omega}_c \cdot \mathbf{q}^g + \delta \boldsymbol{\omega}_p \cdot \mathbf{m}^g] dx_3 \\ &\quad + [\delta \phi(\mathbf{Q}^e \cdot \mathbf{e}_3) + \delta \boldsymbol{\beta} \cdot \mathbf{M}^e + \delta \boldsymbol{\gamma} : \mathbf{O}^e]_0^l + \int_l [\delta \phi q^e + \delta \boldsymbol{\beta} \cdot \mathbf{m}^e + \delta \boldsymbol{\gamma} : \mathbf{o}^e] dx_3. \end{aligned} \quad (102c)$$

where

$$\bar{\mathbf{Q}}^m := \int_A \hat{\boldsymbol{\sigma}}^g \mathbf{e}_3 dA, \quad \bar{\mathbf{M}}^m := \int_A \mathbf{p} \times (\hat{\boldsymbol{\sigma}}^g \mathbf{e}_3) dA. \quad (103)$$

5.6. The Lagrange multiplier and augmented Lagrangian formulations for flexoelectric beams

In case of beams, the variational form of the Lagrange multiplier and augmented Lagrangian formulations remain sufficiently similar to that of a penalty formulation. However, the Lagrange multiplier itself is treated as an independent quantity and should be described to have a description compatible to the vorticity vector. This implies that the Lagrange multiplier must the vorticity along the axis as well as across the cross-section of the beam. In other words the Lagrange multiplier \mathbf{s} can be prescribed through the following mapping

$$(\mathbf{x}, t) \mapsto \mathbf{s}(\mathbf{x}, t) = \mathbf{s}_c(x_3, t) + \mathbf{s}_p(x_3, t) \times \mathbf{p}(x_1, x_2), \quad (104)$$

where \mathbf{s}_c and \mathbf{s}_p characterise the variation of Lagrange multiplier along the axis and across the cross section of the beam, respectively. The variational form of the problem now takes the form

$$\delta W := \delta W_{iner} + \delta W_{int} - \delta W_{ext} = 0, \quad (105)$$

$$\delta W_{iner} = \int_l [\delta \mathbf{w} \cdot (\mathbf{A}_D \ddot{\mathbf{w}} + \mathbf{S}_D \ddot{\boldsymbol{\theta}}) + \delta \boldsymbol{\theta} \cdot (\mathbf{S}_D^T \ddot{\mathbf{w}} + \mathbf{I}_D \ddot{\boldsymbol{\theta}})] dx_3, \quad (106a)$$

$$\begin{aligned} \delta W_{int} &= \int_l [\delta \boldsymbol{\epsilon}^m \cdot \mathbf{Q}^m + \delta \boldsymbol{\kappa}^m \cdot \mathbf{M}^m] + [\delta \boldsymbol{\epsilon}^g \cdot \mathbf{Q}^g + \delta \boldsymbol{\kappa}^g \cdot \mathbf{M}^g] \\ &\quad + [\delta \boldsymbol{\omega}_c \cdot \bar{\mathbf{Q}}^g + \delta \boldsymbol{\omega}_p \cdot \bar{\mathbf{M}}^g] + [\delta \mathbf{s}_c \cdot \mathbf{Q}^s + \delta \mathbf{s}_p \cdot \mathbf{M}^s] dx_3 \\ &\quad + \int_l [\delta \boldsymbol{\epsilon}^e \cdot \mathbf{Q}^e + \delta \boldsymbol{\kappa}^e \cdot \mathbf{M}^e + \delta \boldsymbol{\varsigma}^e : \mathbf{P}^e + \delta \boldsymbol{\gamma} : \mathbf{O}^e] dx_3, \end{aligned} \quad (106b)$$

$$\begin{aligned} \delta W_{ext} &= [\delta \mathbf{w} \cdot \mathbf{Q}^m + \delta \boldsymbol{\theta} \cdot \mathbf{M}^m]_0^l + \int_l [\delta \mathbf{w} \cdot \mathbf{q}^m + \delta \boldsymbol{\theta} \cdot \mathbf{m}^m] dx_3 \\ &\quad + [\delta \boldsymbol{\omega}_c \cdot \mathbf{Q}^g + \delta \boldsymbol{\omega}_p \cdot \mathbf{M}^g]_0^l + \int_l [\delta \boldsymbol{\omega}_c \cdot \mathbf{q}^g + \delta \boldsymbol{\omega}_p \cdot \mathbf{m}^g] dx_3 \\ &\quad + [\delta \mathbf{s}_c \cdot \mathbf{Q}^s + \delta \mathbf{s}_p \cdot \mathbf{M}^s]_0^l + \int_l [\delta \mathbf{s}_c \cdot \mathbf{q}^s + \delta \mathbf{s}_p \cdot \mathbf{m}^s] dx_3 \\ &\quad + [\delta \phi(\mathbf{Q}^e \cdot \mathbf{e}_3) + \delta \boldsymbol{\beta} \cdot \mathbf{M}^e + \delta \boldsymbol{\gamma} : \mathbf{O}^e]_0^l + \int_l [\delta \phi q^e + \delta \boldsymbol{\beta} \cdot \mathbf{m}^e + \delta \boldsymbol{\gamma} : \mathbf{o}^e] dx_3. \end{aligned} \quad (106c)$$

where

$$\bar{\mathbf{Q}}^m := - \int_A \hat{\boldsymbol{\sigma}}^g \mathbf{e}_3 dA, \quad \bar{\mathbf{M}}^m := - \int_A \mathbf{p} \times (\hat{\boldsymbol{\sigma}}^g \mathbf{e}_3) dA, \quad (107)$$

and for Lagrange multiplier approach we have

$$\mathbf{Q}^s := \int_A (\nabla^{skew} \mathbf{u} - \hat{\boldsymbol{\omega}}) \mathbf{e}_3 dA, \quad \mathbf{M}^s := \int_A \mathbf{p} \times ((\nabla^{skew} \mathbf{u} - \hat{\boldsymbol{\omega}}) \mathbf{e}_3) dA, \quad (108a)$$

$$\mathbf{q}^s := \int_A (\nabla^{skew} \mathbf{u} - \hat{\boldsymbol{\omega}}) \mathbf{n} dA, \quad \mathbf{m}^s := \int_A \mathbf{p} \times ((\nabla^{skew} \mathbf{u} - \hat{\boldsymbol{\omega}}) \mathbf{n}) dA. \quad (108b)$$

whereas for augmented Lagrangian we obtain

$$\mathbf{Q}^s := \int_A [(\nabla^{skew} \mathbf{u} - \hat{\boldsymbol{\omega}}) + \frac{1}{\kappa} \mathbf{s} \times \mathbf{I}] \mathbf{e}_3 dA, \quad \mathbf{M}^s := \int_A \mathbf{p} \times ([(\nabla^{skew} \mathbf{u} - \hat{\boldsymbol{\omega}}) + \frac{1}{\kappa} \mathbf{s} \times \mathbf{I}] \mathbf{e}_3) dA, \quad (109a)$$

$$\mathbf{q}^s := \int_A [(\nabla^{skew} \mathbf{u} - \hat{\boldsymbol{\omega}}) + \frac{1}{\kappa} \mathbf{s} \times \mathbf{I}] \mathbf{n} dA, \quad \mathbf{m}^s := \int_A \mathbf{p} \times ([(\nabla^{skew} \mathbf{u} - \hat{\boldsymbol{\omega}}) + \frac{1}{\kappa} \mathbf{s} \times \mathbf{I}] \mathbf{n}) dA. \quad (109b)$$

5.7. Governing equations of three-dimensional flexoelectric beams

As it is well known in standard beam theory, further manipulation of the displacement-potential variational form (74)-(75) can lead to the so-called beam balance equations Hjelmstad [2005], which are written as

$$\left(\frac{\partial^2 \mathbf{Q}^g}{\partial x_3^2} \right) + \frac{\partial \mathbf{Q}^m}{\partial x_3} + \mathbf{q}^m = \mathbf{A}_D \ddot{\mathbf{w}} + \mathbf{S}_D \ddot{\boldsymbol{\theta}}, \quad \text{in } l \times [0, T], \quad (110a)$$

$$\begin{aligned} & \left(\frac{\partial^2 \mathbf{M}^g}{\partial x_3^2} - \mathbf{e}_3 \times \frac{\partial \mathbf{Q}^g}{\partial x_3} \right) + \frac{\partial \mathbf{M}^m}{\partial x_3} \\ & - \mathbf{Q}^m \times \mathbf{e}_3 + \mathbf{m}^m = \mathbf{S}_D^T \ddot{\mathbf{w}} + \mathbf{I}_D \ddot{\boldsymbol{\theta}}, \quad \text{in } l \times [0, T], \end{aligned} \quad (110b)$$

$$\frac{\partial (\mathbf{Q}^e \cdot \mathbf{e}_3)}{\partial x_3} + q^e = 0, \quad \text{in } l \times [0, T], \quad (110c)$$

$$\frac{\partial \mathbf{M}^e}{\partial x_3} + \bar{\mathbf{I}} \mathbf{Q}^e + \mathbf{m}^e = \mathbf{0}, \quad \text{in } l \times [0, T], \quad (110d)$$

$$\frac{\partial \mathbf{O}^e}{\partial x_3} - \mathbf{P}^e + \mathbf{o}^e = \mathbf{0}, \quad \text{in } l \times [0, T], \quad (110e)$$

The above set of equations represent a set of balance equations in terms of internal area resultants \mathbf{Q}^g , \mathbf{M}^g , \mathbf{Q}^m , \mathbf{M}^m , \mathbf{Q}^e , \mathbf{M}^e , \mathbf{P}^e and \mathbf{O}^e . If we drop the terms in the bracket, the piezoelectric beam model of Poya et al. [2015] is recovered. Initial conditions in (4), boundary conditions (2-4-6), strains measures (43-44), strain gradient measures (48-49) and the electrical counterparts (53-54) complement the above system of partial differential equations (110) to form the initial boundary value problem of the three-dimensional flexoelectric beam. Specifically, compatible initial conditions can be defined in terms of axis varying functions $\mathbf{w}_0, \dot{\mathbf{w}}_0, \boldsymbol{\theta}_0, \dot{\boldsymbol{\theta}}_0 : [0, l] \rightarrow \mathbb{R}^3$ as

$$\mathbf{u}(x_1, x_2, x_3, t) = \mathbf{w}_0(x_3) + \boldsymbol{\theta}_0(x_3) \times \mathbf{p}(x_1, x_2) \quad \text{in } \Omega \times 0, \quad (111a)$$

$$\dot{\mathbf{u}}(x_1, x_2, x_3, t) = \dot{\mathbf{w}}_0(x_3) + \dot{\boldsymbol{\theta}}_0(x_3) \times \mathbf{p}(x_1, x_2) \quad \text{in } \Omega \times 0, \quad (111b)$$

Dirichlet (and corresponding Neumann) boundary conditions can be defined at either end of the beam $x_3 = 0$ or $x_3 = l$ by

$$\mathbf{w} = \bar{\mathbf{w}}, \quad \boldsymbol{\theta} = \bar{\boldsymbol{\theta}}, \quad \phi = \bar{\phi}, \quad \boldsymbol{\beta} = \bar{\boldsymbol{\beta}}, \quad \boldsymbol{\gamma} = \bar{\boldsymbol{\gamma}}, \quad (112a)$$

$$\mathbf{Q}^m = \bar{\mathbf{Q}}^m, \quad \mathbf{M}^m = \bar{\mathbf{M}}^m, \quad \mathbf{Q}^e \cdot \mathbf{e}_3 = \bar{\mathbf{Q}}^e, \quad \mathbf{M}^e = \bar{\mathbf{M}}^e, \quad \mathbf{O}^e = \bar{\mathbf{O}}^e, \quad (112b)$$

$$\mathbf{Q}^g = \bar{\mathbf{Q}}^g, \quad \mathbf{M}^g = \bar{\mathbf{M}}^g. \quad (112c)$$

If we consider a purely mechanical couple stress beam model, equations (110) and (112) can be reduced to those of Ma et al. [2008](Eqs. 21-22) and Park and Gao [2006](Eqs. 22-23) for planar beams, by dropping the torsional term $\frac{\partial^2 \mathbf{M}^g}{\partial x_3^2}$ from (110b). Thus, the present beam model (110) is a fourth order differential equation in both \mathbf{w} and $\boldsymbol{\theta} \cdot \mathbf{e}_3$. It should be emphasised however, that the kinematics and constitutive relations of the present beam model are different. Due to the effect of couple stress quantities, namely moment-tractions and body couples having been merged with force-tractions and body forces, complicated boundary conditions (especially the body couple) of Ma et al. [2008]; Reddy [2011]; Sişmek and Reddy [2012] do not appear in our formulation.

6. Numerical experiments

6.1. A detailed comparison of couple stress based and strain gradient based flexoelectric models: vanishing volumetric strain gradients, the presence of reverse coupling modes and material characterisation for BaTiO₃

The objective of this first study is to qualitatively and quantitatively compare the present couple stress based flexoelectric model with the standard strain gradient based flexoelectric models in terms of their effectiveness in predicting size-dependent electric polarisation produced from non-uniform strain distribution. The point of departure is to study the fundamental theoretical differences in kinematics and governing equations of these two theories and their subsequent physical impact, as a similar study is not reported elsewhere in the literature. The study primarily focusses on BaTiO₃ whose piezoelectric and flexoelectric material properties are known from Berlincourt and Jaffe [1958] and Maranganti and Sharma [2009], respectively as

Elastic constants	Dielectric constants	Piezoelectric constants	Flexoelectric constants
$C_{11} = 275$ GPa	$\epsilon_{11} = 12.5$ nC/Vm	$e_{31} = -2.7$ C/m ²	$f_{11} = 0.15$ nC/m
$C_{12} = 179$ GPa	$\epsilon_{33} = 14.4$ nC/Vm	$e_{33} = 3.65$ C/m ²	$\bar{f}_{12} = 100$ nC/m
$C_{13} = 152$ GPa		$e_{15} = 21.3$ C/m ²	$\bar{f}_{44} = -1.9$ nC/m
$C_{33} = 165$ GPa			
$C_{44} = 54$ GPa			

Table 1: Material constants for BaTiO₃

where these constitutive tensors can be spherically parametrised to form the so-called indicator surfaces of BaTiO₃, as shown in Figure 4. Indicator surface is a convenient way to visualise the major axes of material symmetry as can be clearly seen in the case of piezoelectric tensor in Figure 4c. As an essential part of the comparison, this parametrisation is also used later to compare the flexoelectric tensors of couple stress based and standard strain gradient based models.

For the purpose of clarity, let us consider only the flexoelectric coupling mechanisms under both (couple stress and standard strain gradient) theories, in a two dimensional setting. The point of departure, is the flexoelectric enthalpy of the system which under standard strain gradient theories is given in terms of the gradient of strains $\bar{\chi} = \nabla^{sym}\nabla^{sym}\mathbf{u}$ and the electric field \mathbf{E} as

$$\Psi_{sg}(\mathbf{E}, \bar{\chi}) = -\mathbf{E} \cdot \bar{\mathbf{f}} : \bar{\chi} = -E_i f_{ijkl} \bar{\chi}_{ijkl}, \quad (113)$$

where $\bar{\mathbf{f}}$ is the fourth order flexoelectric tensor with one symmetry i.e. $\bar{f}_{ijkl} = \bar{f}_{ikjl}$ and in the general three-dimensional case can be characterised with 54 material constants, as shown in Figure 5a (for the case of BaTiO₃). Under a two-dimensional setting, only 12 material constants are required to fully characterise the flexoelectric tensor. The strain gradient tensor $\bar{\chi}$ and the flexoelectric tensor under Voigt notations can be written as Abdollahi et al. [2015]; Nanthakumar et al. [2017]

$$\bar{\chi} = \nabla^{sym}\nabla^{sym}\mathbf{u} = \left[\frac{\partial^2 u_x}{\partial x^2}, \frac{\partial^2 u_y}{\partial y \partial x}, \frac{\partial^2 u_x}{\partial y \partial x} + \frac{\partial^2 u_y}{\partial x^2}, \frac{\partial^2 u_x}{\partial x \partial y}, \frac{\partial^2 u_y}{\partial y^2}, \frac{\partial^2 u_x}{\partial y^2} + \frac{\partial^2 u_y}{\partial x \partial y} \right]^T, \quad (114)$$

$$\bar{\mathbf{f}} = \begin{bmatrix} \bar{f}_{11} & \bar{f}_{12} & 0 & 0 & 0 & \bar{f}_{44} \\ 0 & 0 & \bar{f}_{44} & \bar{f}_{12} & \bar{f}_{11} & 0 \end{bmatrix}, \quad (115)$$

where (114) is the so-called mean or engineering strain gradients, wherein the multiplication factor ($\frac{1}{4}$) is omitted for simplicity. This in general implies that the produced electric displacement must

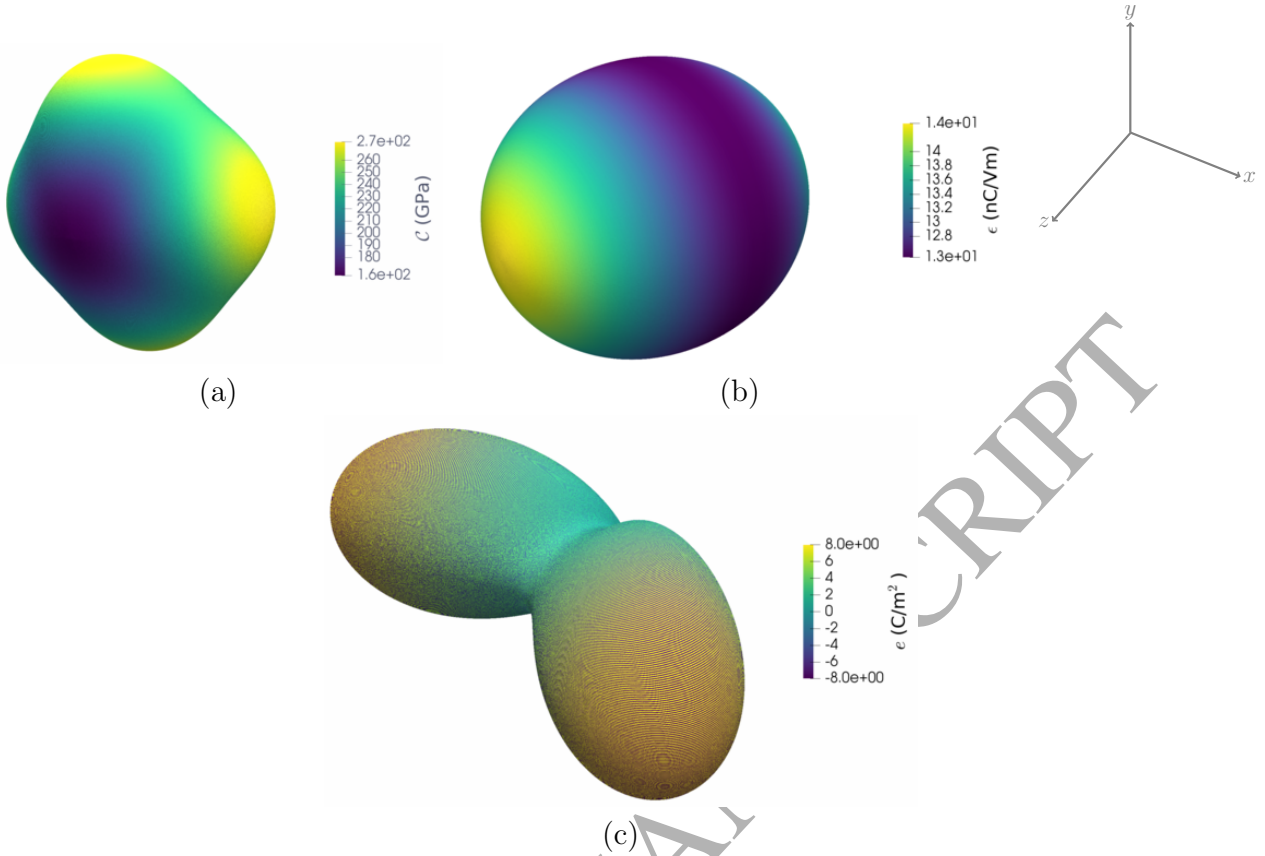


Figure 4: Indicator surfaces of BaTiO₃ constitutive tensors namely, a) the elasticity tensor \mathbf{C} , b) the dielectric tensor ϵ and, c) the piezoelectric tensor e

take the form

$$\mathbf{D}_{sg} = -\frac{\partial \Psi_{sg}}{\partial \mathbf{E}} = \begin{bmatrix} \bar{f}_{11} \frac{\partial^2 u_x}{\partial x^2} + \bar{f}_{12} \frac{\partial^2 u_y}{\partial y \partial x} + \bar{f}_{44} \left(\frac{\partial^2 u_x}{\partial y^2} + \frac{\partial^2 u_y}{\partial x \partial y} \right) \\ \bar{f}_{11} \frac{\partial^2 u_y}{\partial y^2} + \bar{f}_{12} \frac{\partial^2 u_x}{\partial x \partial y} + \bar{f}_{44} \left(\frac{\partial^2 u_x}{\partial y \partial x} + \frac{\partial^2 u_y}{\partial x^2} \right) \end{bmatrix}. \quad (116)$$

On the other hand, in the case of couple stress based flexoelectric model, as presented earlier the flexoelectric enthalpy can be written as

$$\Psi_{cs}(\mathbf{E}, \boldsymbol{\chi}) = -\mathbf{E} \cdot \mathbf{f} \cdot \boldsymbol{\chi} = -E_i f_{ij} \chi_j, \quad (117)$$

where \mathbf{f} is the second order flexoelectric tensor with no general symmetries. It is characterised by 9 constants in the three-dimensional case and 4 constants in the two-dimensional case. Comparing (113) and (117) their number of material constants and indicator surfaces in Figure 5 it is evident that, certain modes of deformations are inevitably combined in the couple stress flexoelectric theory. The explicit forms of $\boldsymbol{\chi}$ and \mathbf{f} are given as

$$\boldsymbol{\chi} = \nabla \times \nabla \times \mathbf{u} = \left[\frac{\partial^2 u_y}{\partial y \partial x} - \frac{\partial^2 u_x}{\partial y^2}, \frac{\partial^2 u_x}{\partial x \partial y} - \frac{\partial^2 u_y}{\partial x^2} \right]^T, \quad (118)$$

$$\mathbf{f} = \begin{bmatrix} f_{11} & f_{12} \\ f_{21} & f_{22} \end{bmatrix}, \quad (119)$$

where χ is the mean or engineering curvature vector presented earlier, wherein the multiplication factor ($\frac{1}{4}$) is omitted for simplicity. Note that no correspondence is established between the tensors \mathbf{f} and $\bar{\mathbf{f}}$ yet. This in general implies that the produced electric displacement must take the form

$$\mathbf{D}_{cs} = -\frac{\partial \Psi_{cs}}{\partial \mathbf{E}} = \begin{bmatrix} f_{11}\left(\frac{\partial^2 u_y}{\partial y \partial x} - \frac{\partial^2 u_x}{\partial y^2}\right) + f_{12}\left(\frac{\partial^2 u_x}{\partial x \partial y} - \frac{\partial^2 u_y}{\partial x^2}\right) \\ f_{21}\left(\frac{\partial^2 u_y}{\partial y \partial x} - \frac{\partial^2 u_x}{\partial y^2}\right) + f_{22}\left(\frac{\partial^2 u_x}{\partial x \partial y} - \frac{\partial^2 u_y}{\partial x^2}\right) \end{bmatrix}. \quad (120)$$

Comparing \mathbf{D}_{sg} in (116) and \mathbf{D}_{cs} in (120), one can observe that, in the case of couple stress flexoelectric theory, the variation of volumetric strains (volumetric strain gradients namely the components $\frac{\partial^2 u_x}{\partial x^2}$ and $\frac{\partial^2 u_y}{\partial y^2}$) do not generate electric polarisation, as they are fundamentally nonexistent. This is true for all variants of couple stress theories (i.e. classical, modified, conformal and skew-symmetric couple stress theories) as the spherical part of strain always vanishes. In other words, the \bar{f}_{11} coupling mode cannot be characterised under this theory. In the case of BaTiO₃, we observe that \bar{f}_{11} parameter corresponds to the weakest coupling mode which can be up to three orders of magnitude smaller than the flexural mode and can be neglected even in the case of standard strain gradient flexoelectricity. Moreover, it can be noticed that, if present, the f_{12} and f_{21} give rise to a completely reversed coupling mode in comparison to strain gradient theory. Further comparison of (116) and (120) for BaTiO₃ constants shown in Table 1, reveals that the flexoelectric coupling modes is in fact dominant in \bar{f}_{12} and one can consequently write

$$\mathbf{D}_{sg} \approx \begin{bmatrix} \bar{f}_{12} \frac{\partial^2 u_y}{\partial y \partial x} \\ \bar{f}_{12} \frac{\partial^2 u_x}{\partial x \partial y} \end{bmatrix}. \quad (121)$$

If we were to establish a correspondence between \mathbf{f} and $\bar{\mathbf{f}}$, then the most plausible relationship would be to assume $f_{11} = f_{22} = \bar{f}_{12}$ and $f_{12} = f_{21} = 0$ in which case we can write

$$\mathbf{f} \approx \bar{f}_{12} \mathbf{I} = \begin{bmatrix} \bar{f}_{12} & 0 \\ 0 & \bar{f}_{12} \end{bmatrix}, \quad \mathbf{D}_{cs} \approx \begin{bmatrix} \bar{f}_{12} \left(\frac{\partial^2 u_y}{\partial y \partial x} - \frac{\partial^2 u_x}{\partial y^2} \right) \\ \bar{f}_{12} \left(\frac{\partial^2 u_x}{\partial x \partial y} - \frac{\partial^2 u_y}{\partial x^2} \right) \end{bmatrix}. \quad (122)$$

Equation (122) establishes the closest possible algebraic relationships between flexoelectric constants of couple stress based and strain gradient based flexoelectric theories, without the need for a nonlinear optimisation process to characterise the constants of one theory with respect to the other. The need for this optimisation can also be negated by noting the significant discrepancies present between atomistic simulations and experimental observations in determining flexoelectric constants Ma and Cross [2006]; Maranganti and Sharma [2009]; Zubko et al. [2013], as result of which most authors assume the flexural constant \bar{f}_{12} in the wide range of 1nC/m-100μC/m. Under this setting, the indicatory surfaces of flexoelectric tensors $\bar{\mathbf{f}}$ and \mathbf{f} can be represented as shown in Figure 5 where the axes of symmetry for both tensors can be clearly seen. Figure 5, once again confirms that characterising the flexoelectric constants of \mathbf{f} with respect to $\bar{\mathbf{f}}$ is in general impractical owing to the fact that the tensors belong to two different vector spaces.

In what follows, we consider simplified cases of flexoelectric coupling of nano-specimen under different coupling modes with various boundary conditions and present simple analytical solutions in order to quantify the electromechanical coupling efficiency of couple stress based and standard strain gradient based flexoelectric theories. The analytical solutions are not derived but rather designed (in terms of beam displacements and hence strains and strain gradients) such that the specimen will experience a non-uniform strain distribution, assumed to be enough to break the inversion symmetry of BaTiO₃ to produce electric polarisation. While inspired by simple analytical solutions of beams these studies are performed at a continuum level. The studies here are in line with and complement the ones reported in Abdollahi et al. [2014, 2015].

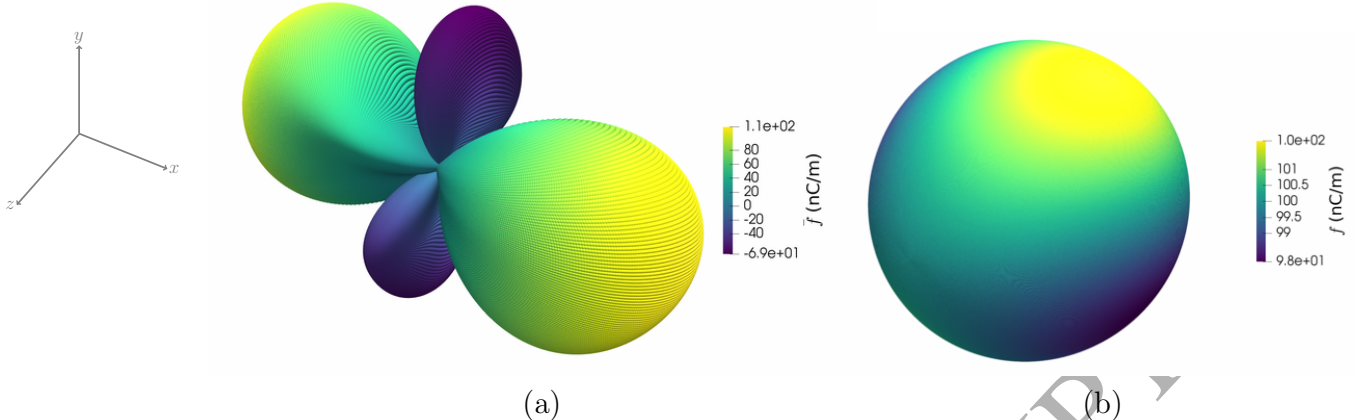


Figure 5: Indicator surface of BaTiO₃ flexoelectric constitutive tensor under, a) standard strain gradient based flexoelectric theory (i.e. \bar{f}), b) couple stress based flexoelectric theory (i.e. f)

6.1.1. Case 1. Simply supported nanobeam under uniformly distributed load

As a first case, let us consider a nanobeam shown in Figure 6. Under the action of uniformly distributed load the beam undergoes bending and as a result, a non-uniform distribution of strains across the cross section of the beam is observed. A simple analytical solution for the bending of

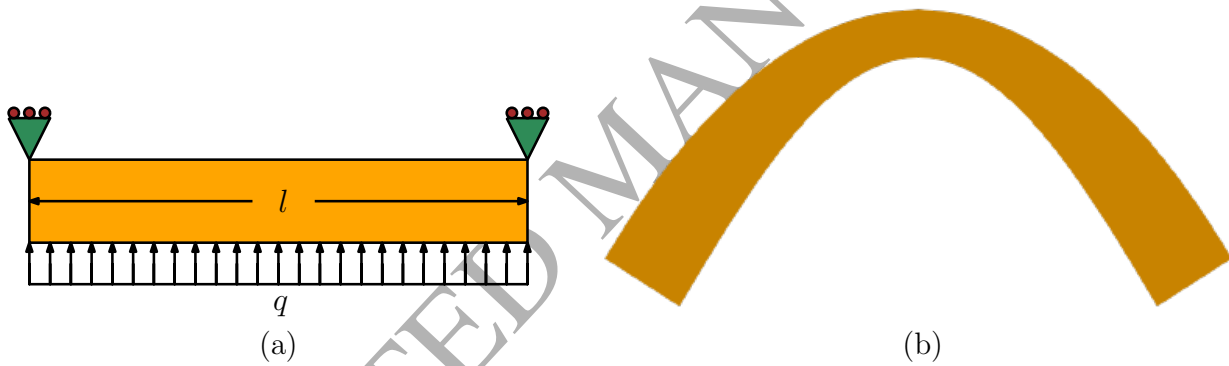


Figure 6: Original and deformed shape of nanobeam

the nanobeam shown in Figure 6b can be simply computed using the beam kinematics presented in (44), as

$$u_x = -\alpha(l^3 - 6lx^2 + 4x^3)y, \quad (123a)$$

$$u_y = \beta(l^3x - 2lx^3 + x^4) + \gamma x(l - x), \quad (123b)$$

where the parameters $\alpha = 1.25 \times 10^{20}$, $\beta = 1.25 \times 10^{20}$ and $\gamma = 1330$ are chosen for convenience. This in fact corresponds to a load of $100\mu\text{N}/\text{m}$. l denotes the length of the beam which is chosen to be 10nm and the thickness of the beam is retained as $t = 1\text{nm}$. The material constants of BaTiO₃ shown in Table 1 are chosen for the study. The electric displacement vectors \mathbf{D}_{sg} and \mathbf{D}_{cs} can now be computed using equations (116) and (120), respectively.

Figure 7 compares the generated electric displacement of the couple stress model computed using (122) with that of the standard strain gradient model computed using (116) (i.e. the fully coupled electric displacement vector), along the length of the beam (i.e. for all x such that y coincides with the neutral axis). The figures also compares the electric displacements generated with the standard strain gradient model ignoring the \bar{f}_{11} parameter which is not present in the

couple stress model. Notice that when \bar{f}_{11} parameter is discarded both couple stress and strain gradient models generate the same (zero) electric displacement component D_x , in this case. The electric displacement D_x is zero in the latter two cases, due to the fact the corresponding second derivatives vanish. This generated electric displacement is extremely small owing the fact that \bar{f}_{11} is significantly weaker in BaTiO₃. On the other hand, extremely high electric displacement D_y is generated. Under this coupling mode, it can be observed that the couple stress model generates approximately twice (200%) more the amount of electric displacement as compared to the strain gradient model and the contribution of \bar{f}_{11} and \bar{f}_{44} parameters while present are small enough, that they can be neglected. Given the discrepancies in theoretical and experimental findings in flexoelectric theory, we can say that this result provides yet another significantly positive physical insight in to this field. However, the profile of generated electric displacement along the beam is in general similar for both models.

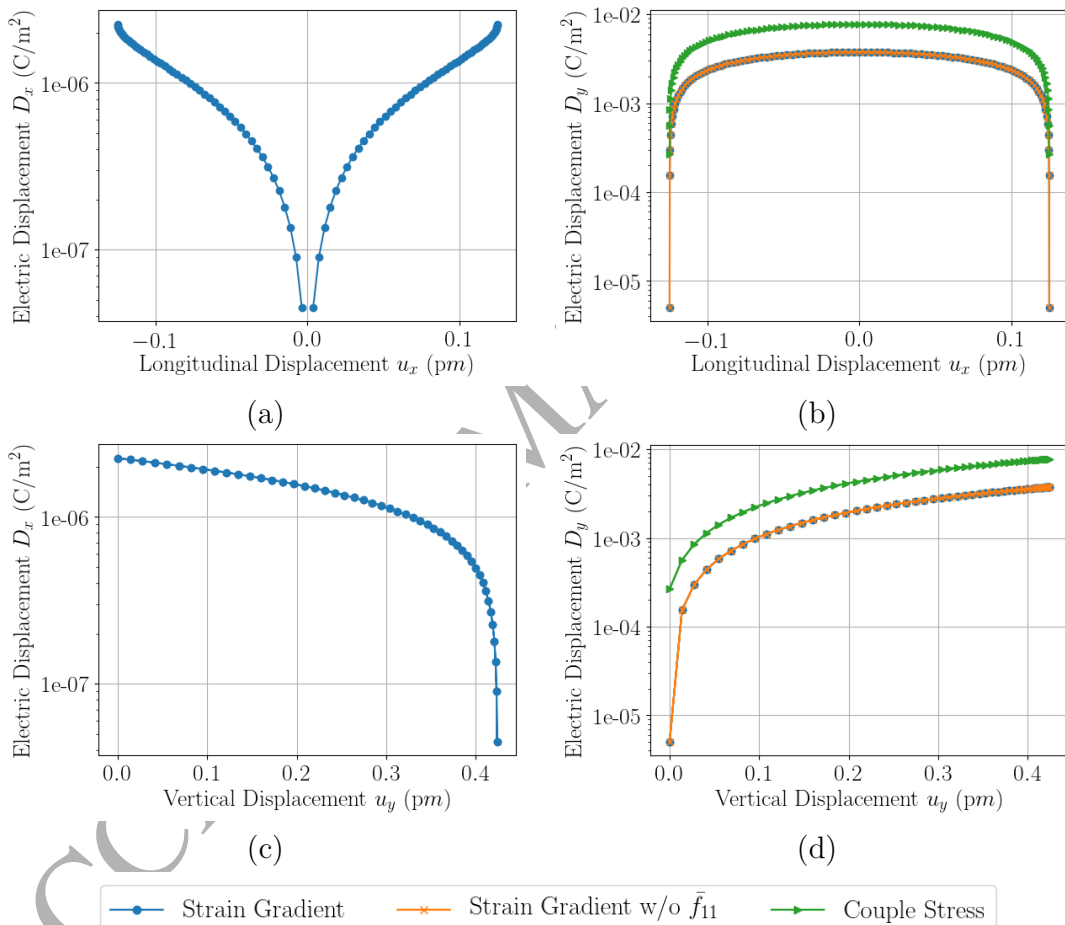


Figure 7: Comparison of couple stress based and strain gradient based flexoelectric models for the case of (123), when material constants are fitted according to (122)

6.1.2. Cantilever nanobeam undergoing bending and complex cross sectional thinning

Let us next consider a nanobeam undergoing complex cross sectional thinning and bending, as shown in [Figure 8](#). The analytical formula describing this morphology is given by

$$u_x = -\alpha(3l^2x - 3lx^2 + x^3)y, \quad (124a)$$

$$u_y = \beta(3l^2x^2 - 4lx^3 + x^4) + \gamma x(2l - x), \quad (124b)$$

where the parameter $\alpha = 5.21 \times 10^{18}$ is now chosen. Under this setting, the beam experiences nonuniform distribution of strains across the cross section and along the length and as a result the flexoelectric coupling mechanism is more complex now. Note that the form of loading q must be coordinate dependent and not generally uniform, in order to produce the aforementioned analytical formula.

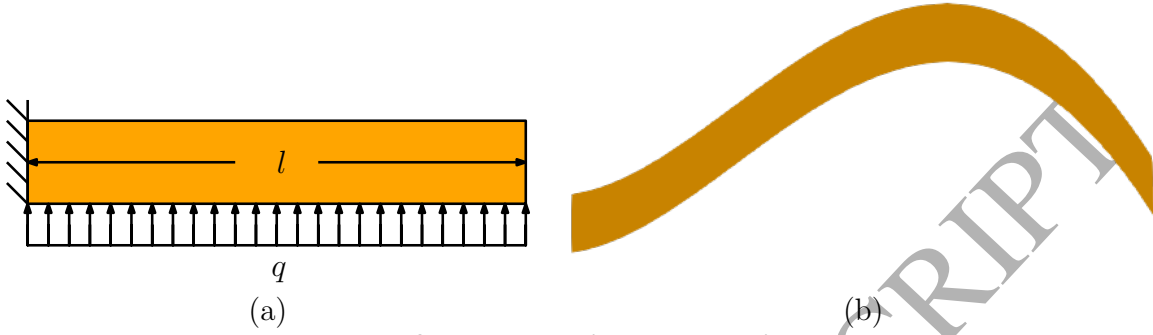


Figure 8: Original and deformed shape of nanobeam

Figure 9 compares the generated electric displacement of the couple stress model with that of the standard strain gradient model with and without consideration of the \bar{f}_{11} coupling modes. A similar conclusion can be drawn in this case in that, when \bar{f}_{11} parameter is discarded both couple stress and strain gradient models generate the same (zero) electric displacement component D_x , which is negligible regardless. However an extremely high electric displacement D_y is generated with the couple stress model, which in this case is up to two orders higher than that of strain gradient model. This is due to the strong presence of second derivatives (curvature effect) in the couple stress model, which gives rise to extremely high bending coupling mode. However, the profile of generated electric displacement is in general similar for both models.

6.1.3. Cantilever nanobeam undergoing extension and thinning

The third and final case considers an even more complex deformation scenario under extension to ensure that there are no vanishing component in the strain gradient tensor/curvature vector. This study also considers the extension coupling mechanism in flexoelectricity. To this effect a nanobeam undergoing complex cross sectional thinning and extension is considered, as shown in Figure 10. The analytical formula describing this morphology is given by

$$u_x = \alpha x^2 \left(y - \frac{l}{20}\right)^2, \quad (125a)$$

$$u_y = \beta \sqrt{x+2l} \left(y - \frac{l}{20}\right)^3, \quad (125b)$$

where the parameters $\alpha = 5 \times 10^{21}$ and $\beta = 1.5 \times 10^{19}$ are chosen. Under this setting, the beam experiences nonuniform distribution of strains across the cross section and along the length giving rise to electric polarisation.



Figure 10: Original and deformed shape of nanobeam

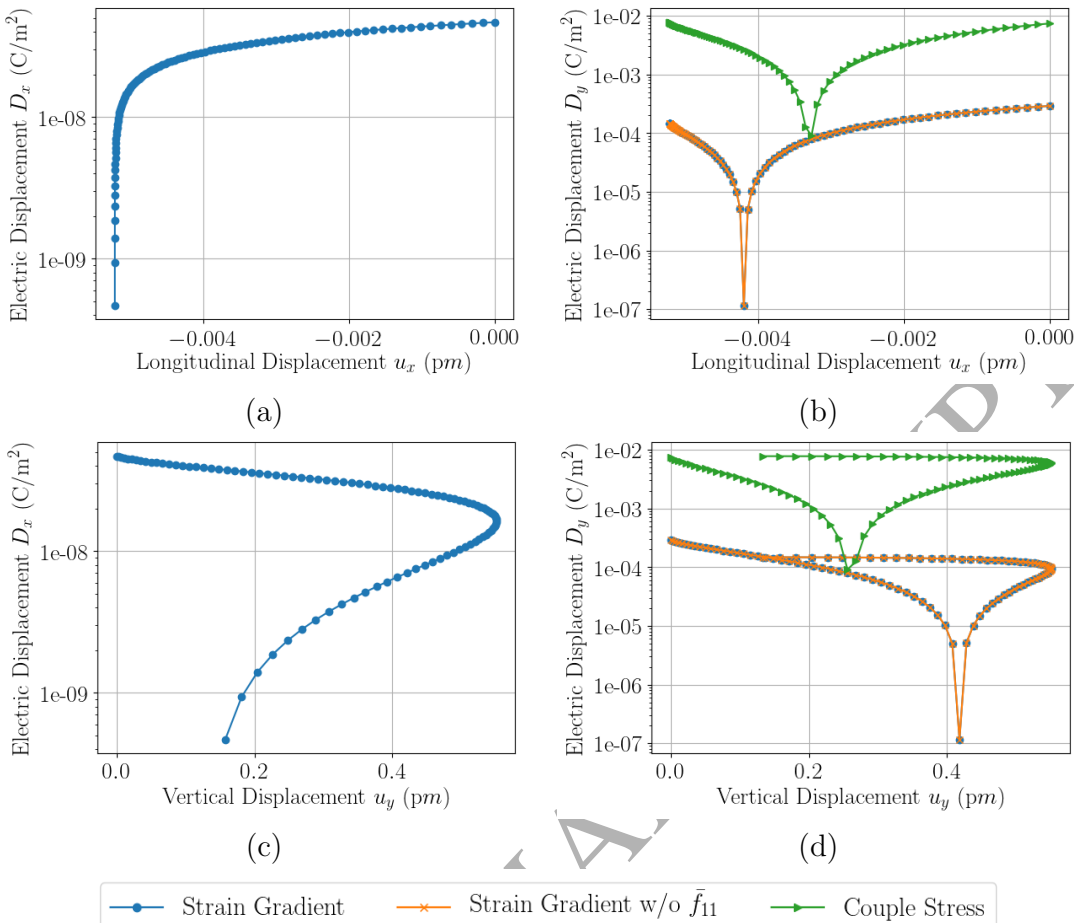


Figure 9: Comparison of couple stress based and strain gradient based flexoelectric models for the case of (124), when material constants are fitted according to (122)

Figure 11 compares the generated electric displacement of the couple stress model with that of the standard strain gradient model with and without consideration of the \bar{f}_{11} constant. As expected in this case the electric displacement component D_x is more pronounced compared to D_y , unlike the previous cases. The couple stress model generates up to an order of magnitude higher electric polarisation under this coupling mode and the profile of electric displacement is also very different from that of strain gradient model. The polarisation in the vertical y direction remains weak and \bar{f}_{11} parameter is discarded both couple stress and strain gradient models generate the same electric displacement component D_y . In general, although non-intuitive, it can be observed that in the case of extension the parameter \bar{f}_{11} plays no significant role.

From the analysis of three flexoelectric coupling cases in this section it can be concluded that, for both couple stress and strain gradient theories the bending/shear coupling mode is typically activated by the action of transverse electric field and the extension coupling mode is activated by the action of electric field aligned in parallel to the axis of extension. Under both these coupling modes the driving parameter is the flexoelectric constant \bar{f}_{12} . This is in contrast to piezoelectricity where different modes of coupling are typically driven by different material constants. If the same flexoelectric constant is chosen to simulate strain gradient and couple stress theory, the couple stress model will in general produce a higher electric polarisation that in some cases could be up to two orders of magnitude higher. It must be believed that for most problems of practical relevance analysed under such settings the couple stress flexoelectric model in general will produce a higher

electric polarisation. It is also worth noting that, simplified analytical solutions of strain gradient flexoelectricity overestimate the flexoelectric response in comparison to fully three-dimensional computational simulation as noted by [Abdollahi et al. \[2014, 2015\]](#). In the later sections we will see if this is the case for couple stress based flexoelectric models.

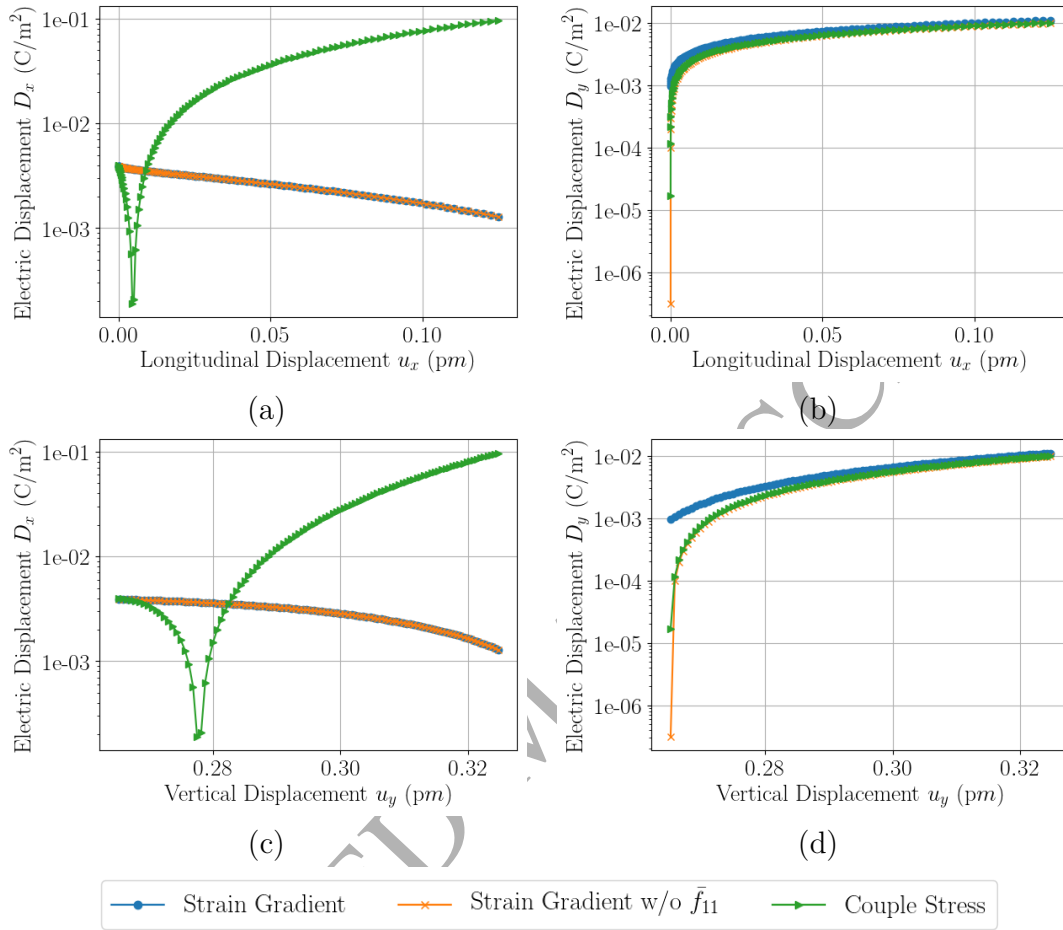


Figure 11: Comparison of couple stress based and strain gradient based flexoelectric models for the case of (125), when material constants are fitted according to (122)

6.2. Nanocompression of a flexoelectric conical pyramid

In this section, the nanocompression of a complex flexoelectric conical pyramid is chosen for numerical study. The objective is to examine the capability of the developed finite element framework in predicting the flexoelectric response when the geometrical representation of the problem is complex and when an analytical solution cannot be obtained. The numerical framework is thoroughly benchmarked against simple analytical solutions in Appendix C.1. The analysis of flexoelectric pyramidal structures have been carried by many other authors in the past as the differential thickness along the height of the pyramid produces a significant flexoelectric response Abdollahi et al. [2014, 2015]; Ghasemi et al. [2017]; Deng et al. [2018]. Furthermore, flexoelectric material constants are also typically experimentally characterised through either nanoindentation or bending experiments, using similar geometries. Abdollahi et al. [2014] has analysed the problem of nanocompression of the flexoelectric pyramid in depth showing that simplified solutions can in general overestimate the flexoelectric response and relying on computational methodologies can help provide better physical insight in to the design of such flexoelectric transducers.

To this end, a rather more complex flexoelectric conical pyramid is chosen for our study. The additional complexity of the problem emanates from the fact that the edges and facets of the pyramid are not straight sided but are rather described through NURBS functions. The geometry and the three-dimensional curved $p = 4$ tetrahedral mesh of the flexoelectric structure is shown in [Figure 12](#). To represent the geometry of the problem accurately, we employ the high order curvilinear finite elements recently developed by [Poya et al. \[2018\]](#) which uses a posteriori mesh morphing technique presented in [Poya et al. \[2016\]](#) to represent the CAD boundaries of the flexoelectric structure accurately (notice the curved elements representing the circle in the top conical frustum) without requiring a change in the mixed finite element functional spaces presented in [Appendix C](#).

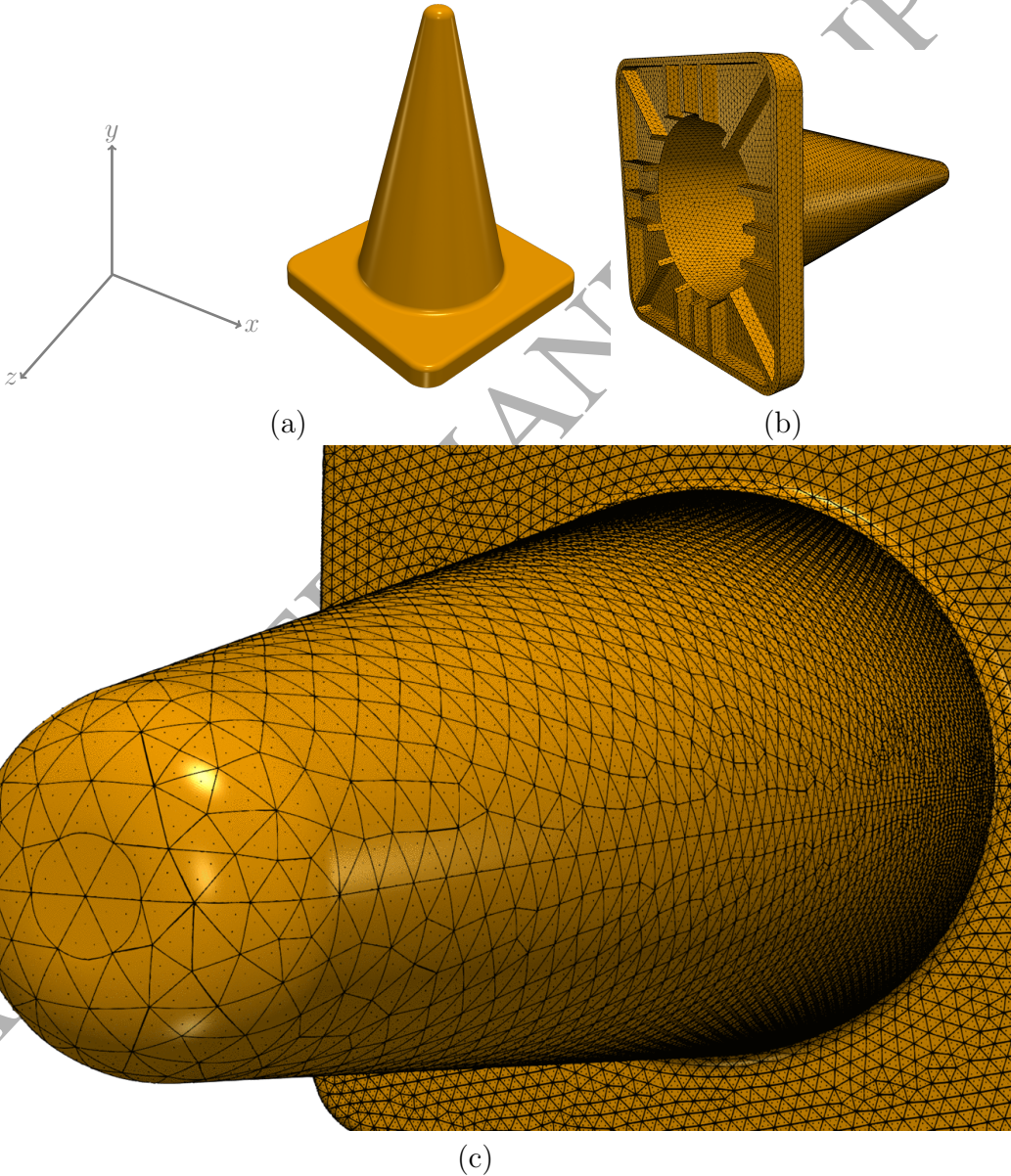


Figure 12: Geometry and quartic ($p = 4$) order curved mesh of the flexoelectric conical pyramid. The conical pyramid is being held by a plate-like support of size $100 \times 100\mu\text{m}^2$ and the total height of the pyramid is $130\mu\text{m}$. The thickness of pyramid is 150nm throughout the structure. The circle in top conical frustum represents the region where the compressive load is applied

Once again, we choose the Barium Titanate as the flexoelectric material of choice by neglecting the piezoelectric effect and only considering \bar{f}_{12} flexoelectric constant. A compressive load of 3mPa is applied as pressure on the circle in top conical frustum and the base of the plate-like support is mechanically fixed. The system has an open circuit configuration in that, only zero electric potential is applied at the base of the plate-like support. The problem consists of approximately 3.4M degrees of freedom excluding the condensed variables and approximately another 2.8M degrees of freedom are condensed out during each run of the analysis. The Lagrange multiplier formulation is used for this analysis and the simulation is performed dynamically using the Newmark's beta method with the density of the Barium Titanate given as $\rho = 6.02 \text{ g/cm}^3$. The total load is applied over a period of 30 seconds at a rate of 0.1mPa/sec.

[Figure 14](#) summarises various representative results of the analysis. First, a mesh refinement study has been performed to ensure that the results of the analysis are accurate. As can be observed the electromechanical coupling efficiency asymptotically approaches towards a reference solution with mesh refinement, confirming the stable approximation property of the developed finite element scheme. All the analyses are performed using the second finest mesh corresponding to [Figure 14a](#), where the number of elements in the computational mesh is kept fixed at 63794. Keeping the mesh size fixed a p refinement is then carried out from $p = 2$ to $p = 5$ respectively as shown in [Figure 14b](#). It can be observed that under p -refinement the convergence is much quicker and at $p = 3$ the reference solution is already obtained. As mentioned before, further analysis of the flexoelectric pyramid are however performed with keeping the polynomial refinement fixed at $p = 4$. [Figure 14c](#) shows the satisfaction of the couple stress constraint throughout the dynamic simulation time. As can be observed the constraint is numerically satisfied for the whole duration of the simulation. Finally, [Figure 14d](#) shows the effective electromechanical coupling efficiency (ECF) throughout the simulation time. Due to the linear nature of the problem, a constant ECF is obtained for the whole duration of simulation.

A common way to characterise size-dependent effect in flexoelectric theory is to measure the normalised effective piezoelectric constant. For complex problems such as the current one the approximate analytical solution for this constant reported in [Majdoub et al. \[2008\]](#) cannot be used and the more generic formula given below should be used

$$\bar{e} = \frac{\int_{\Omega} \mathbf{E}_c \cdot \epsilon \mathbf{E}_c}{\int_{\Omega} \mathbf{E}_e \cdot \epsilon \mathbf{E}_e}, \quad (126)$$

where \mathbf{E}_c represents the electric field when both piezoelectricity and flexoelectricity are present and \mathbf{E}_e represents the electric field when flexoelectricity is ignored. It is also established phenomenon that flexoelectricity modifies the inherent mechanical properties specially the bending modulus of the material [Sharma et al. \[2007\]](#); [Krichen and Sharma \[2016\]](#). The normalised effective stiffness of the system can be computed similarly as

$$\bar{Y} = \frac{\int_{\Omega} \boldsymbol{\varepsilon}_c : \mathbb{C} : \boldsymbol{\varepsilon}_c}{\int_{\Omega} \boldsymbol{\varepsilon}_m : \mathbb{C} : \boldsymbol{\varepsilon}_m}, \quad (127)$$

where $\boldsymbol{\varepsilon}_c$ represents the small strain tensor when flexoelectricity is present and $\boldsymbol{\varepsilon}_m$ represents the small strain tensor when flexoelectricity is ignored. [Figure 14e](#) shows the evolution of strain energy of the system with and without consideration of flexoelectricity characterising normalised effective stiffness of the system. We notice a rather constant normalised effective stiffness in the range of 2.2 ± 0.2 for the conical pyramid throughout the dynamic simulation due to the linear nature of the problem. Interestingly, the standard strain gradient models also produce a similar normalised

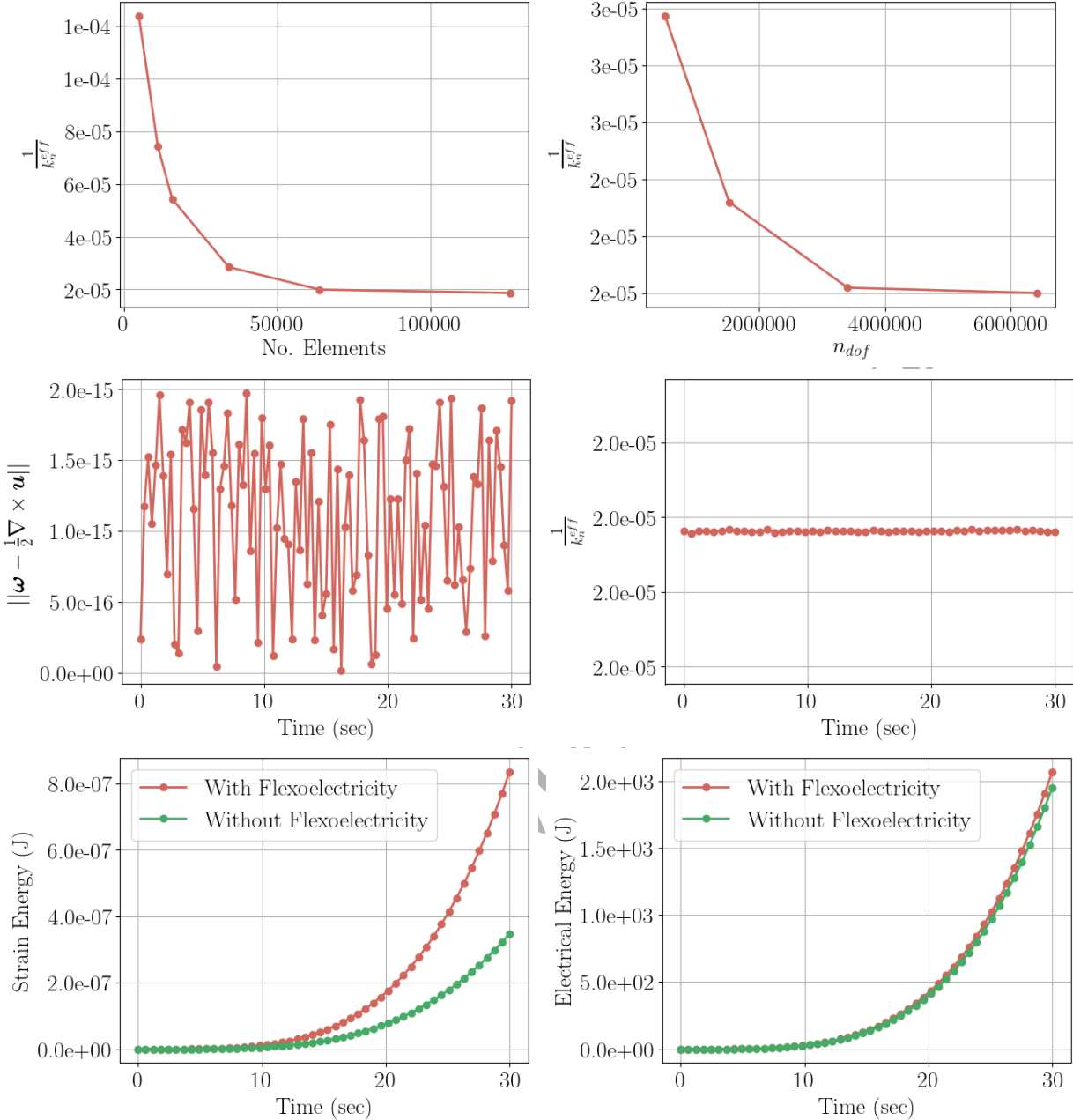


Figure 13: Various representative results of the analysis on conical pyramid, a) convergence of the solution with mesh refinement, b) satisfaction of couple stress constraint, c) evolution of strain energy with and without consideration of flexoelectricity characterising evolution of normalised effective stiffness, d) evolution of electrical energy and, e) evolution of effective electromechanical coupling coefficient, f) evolution of normalised effective stiffness

effective stiffness Abdollahi et al. [2014]. Similarly, Figure 14f shows the evolution of electrical energy with and without consideration of flexoelectricity characterising the normalised effective piezoelectric constant of the system. Note that all the piezoelectric material constants shown in Table 1 are now activated and deformation of the system is much more complex now as all coupling modes are active. A modest 4-6% increase in electrical energy is observed when flexoelectricity is activated. This is in contrast with respect to the results presented in Abdollahi et al. [2014, 2015]; Nanthakumar et al. [2017]; Ghasemi et al. [2017] wherein the flexoelectric constant is assumed to

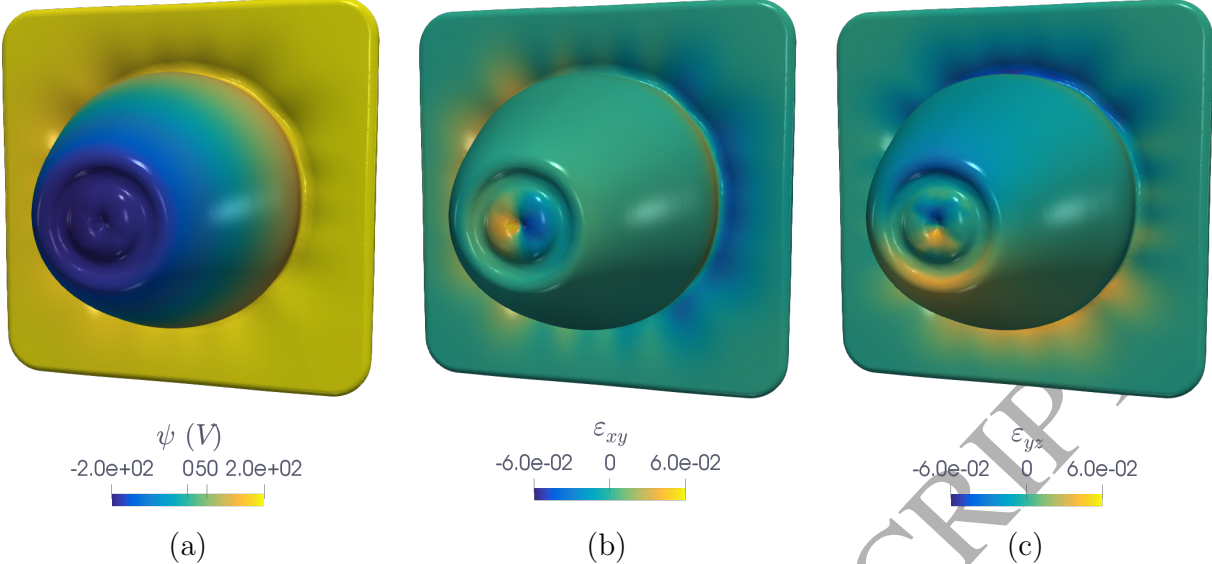


Figure 14: The final deformed conical pyramid configuration showing, a) electric potential ψ , b) strain component ε_{xy} and b) strain component ε_{yz} . 355M cells have been used to process a detailed resolution of the results. Deformations (not magnitudes) are magnified by a factor of 10 for aesthetics and clarity

be more than an order of magnitude higher than its actual value used here.

Figure 14 shows the final deformed configuration of the conical pyramid for $p = 4$ tetrahedral elements with an extremely detailed resolution wherein the results are extrapolated over 355M cells using high order finite element interpolation functions. It can be observed that both electric potential (primary variable) and strain components (derived variables) are well resolved at this level of detail. The deformation initially starts at the circular region in the top frustum of the pyramid. As the compressive pressure is increased the frustum is pushed inwards and the pyramid experiences necking right around the frustum. With further compression, a completely dished and grooved region starts to form around the frustum while the region immediately around the circle where the load is applied starts to bulge outwards. As shown in Figure 15 the base of the pyramid is severely pushed towards the plate support. Figure 15 further shows strain gradient measures, namely the vorticity vector and the curvature vector component. Interestingly, it can be observed in Figure 15c that the curvature evolves as a spin around the generated sink and starts to disperse near the grooved region. This is because the certain of the sink (y -axis) corresponds to the axis of rotation.

From the analyses performed in this section it can be concluded that, advanced computational tools help resolve the problem of flexoelectricity to an unprecedented detail beyond the realm of approximate closed form solutions. Certainly, the inclusion of anisotropy, necking and vortex formation is too complex to be handled otherwise. The use of high performance tensor contraction framework for coupled electromechanical problems developed by the authors Poya et al. [2017], make the developed finite element technique a viable candidate for solving extremely large scale problems on complicated geometries. Given that the normalised effective piezoelectric constant shows only a 4-6% increase due to flexoelectricity for this problem, we can assume that the computational model given its accuracy has modest estimations in comparison to analytical solutions (if available), an issue also present in standard strain gradient models Abdollahi et al. [2014]. However, as mentioned before, the major discrepancy in results of normalised effective piezoelectric constants between the current study and those of Abdollahi et al. [2014, 2015] is due to an order of magnitude higher flexoelectric constant chosen by the latter authors.

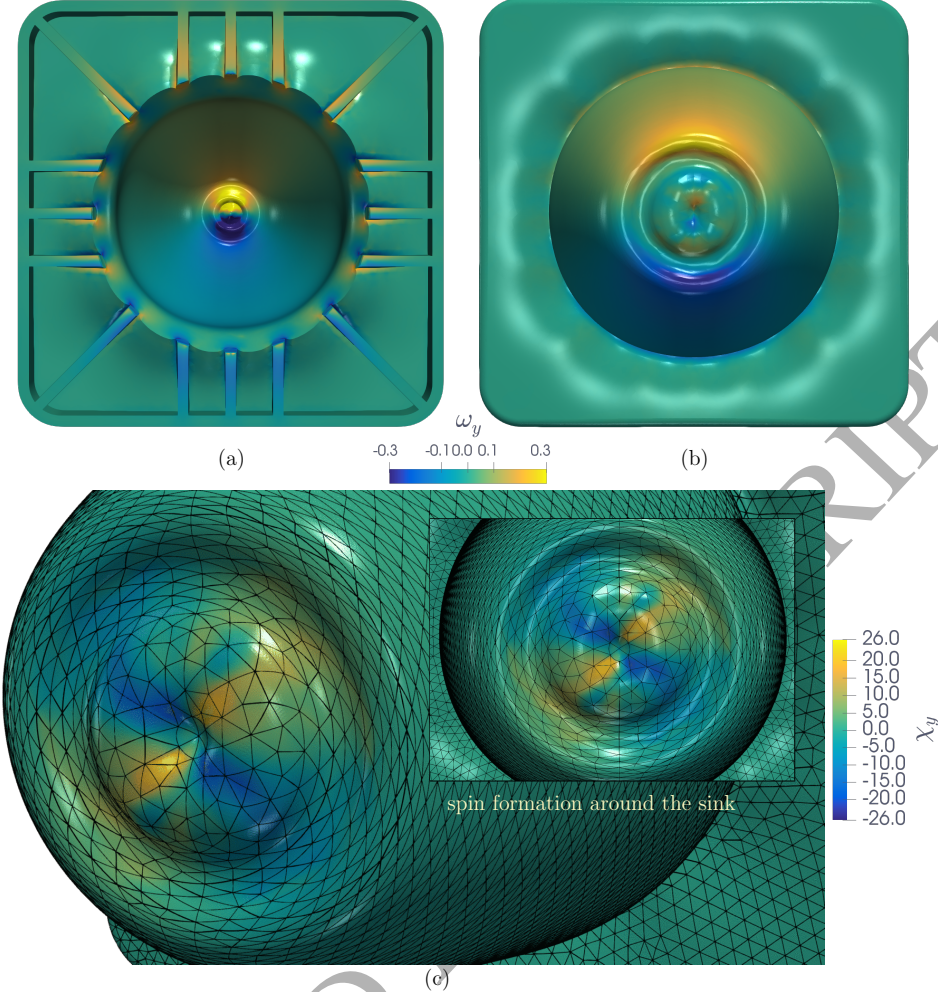


Figure 15: The final deformed conical pyramid configuration showing, a,b) axial vorticity vector component ω_y and, c) axial curvature vector component χ_y . The curvature forms a spin around the deformed sink. 355M cells have been used to process a detailed resolution of the results. Deformations (not magnitudes) are magnified by a factor of 10 for aesthetics and clarity

7. Conclusion

In this manuscript, a family of numerical models for the phenomenological linear flexoelectric theory for continua and their particularisation to the case of three-dimensional Timoshenko beams based on a skew-symmetric couple stress theory is presented. In contrast to the traditional flexoelectric models based on standard strain gradient wherein coupling between electric polarisation and strain gradients is assumed, we postulate an electric enthalpy in terms of linear invariants of curvature and electric field. This is achieved by introducing the axial or what is also called the *mean* curvature vector as a strain gradient measure. We have shown that this assumption has many important physical implications. Firstly, similar to the standard strain gradient models, for isotropic (non-piezoelectric) materials this approach allows constructing flexoelectric energies without breaking material's centrosymmetry. Secondly, unlike the standard strain gradient models, nonuniform distribution of volumetric part of strains (volumetric strain gradients) do not generate electric polarisation. We have shown that volumetric strain gradients have negligible contribution in generating electric polarisation. Thirdly, a state of plane strain generates out of plane deformation through strain gradient effects. Finally, under this theory, extension and shear coupling modes

cannot be characterised individually as they contribute to the generation of electric polarisation as a whole.

For the case of three-dimensional beams, we have shown that the skew-symmetric couple stress model in general, generate stresses spanned over the cross section rather than aligned with the longitudinal axis of the beam and as a result special care must be taken to integrate them over the cross section.

Four distinct variational principles are presented for both continuum and three-dimensional beam models namely, a displacement-potential formulation, a penalty formulation, a Lagrange-multiplier formulation and an augmented Lagrangian formulation. The three later formulations facilitate incorporation of strain gradient measures in to a standard finite element scheme while maintaining the C^0 continuity. To this end, the efficacy of high order finite elements along with the computational efficiency of mixed finite elements have been utilised to develop a series of low and high order mixed finite element schemes for couple stress based flexoelectricity and their corresponding results are benchmarked against available closed form solutions where good agreements have been found with the reference results. Furthermore, a detailed comparison of the developed couple stress based flexoelectric model with the standard strain gradient flexoelectric models has been performed for the case of Barium Titanate where a myriad of simple analytical solutions have been proposed in order to quantitatively describe the similarities and dissimilarities in effective electromechanical coupling under these two theories. As a physically insightful observation, it is observed that, if the same experimental flexoelectric constants are fitted in to both theories, the current couple stress theory in general, reports a much stronger electromechanical conversion efficiency of up to 200% under bending and up to two orders of magnitude under axial tension. This is mainly due to the fact that, most flexoelectric problems involve bending and flexural deformation and since in the present couple stress model multiple modes of deformations are combined, as a result, the axial curvature vector responsible for generating electric polarisation is much more pronounced for most of these cases. Finally, nanocompression of a complex flexoelectric conical pyramid for which analytical solution cannot be established has been numerically studied at an unprecedented level of detail to pinpoint the robustness and computational scalability of the framework. Under this experiment, the structure experiences necking and the curvature effect forms a vortex around the generated sink in the frustum. The geometry and the nature of the deformation certainly implies that studying flexoelectricity in these structures is not feasible without resorting to computational tools. We observe a modest normalised effective piezoelectric coefficient for this study while the normalised effective stiffness of the system reported by the couple stress model is similar to the ones reported by standard strain gradient models.

Appendix A. The indeterminate couple stress theory and its relation to the classical Cosserat theory

The theory in this section is a reiteration of the classical couple stress model briefly discussed here for the convenience of the reader. In classical linear elasticity due to symmetry of strains ($\boldsymbol{\varepsilon}$) an isotropic material is fully described with only two strain invariants. However, when the strain tensor is non-symmetric ($\tilde{\boldsymbol{\varepsilon}}$), at least three invariants are needed to describe an isotropic solid, Hence, the free energy takes the form, [Neff and Jeong \[2009\]](#); [Jeong and Neff \[2010\]](#)

$$\begin{aligned} W^{iso}(\tilde{\boldsymbol{\varepsilon}}, \tilde{\boldsymbol{\chi}}) &= W_{\tilde{\boldsymbol{\varepsilon}}}^{iso}(\tilde{\boldsymbol{\varepsilon}}) + W_{\tilde{\boldsymbol{\chi}}}^{iso}(\tilde{\boldsymbol{\chi}}) \\ &= \frac{\mu + \mu_c}{2} \tilde{\boldsymbol{\varepsilon}} : \tilde{\boldsymbol{\varepsilon}} + \frac{\mu - \mu_c}{2} \tilde{\boldsymbol{\varepsilon}} : \tilde{\boldsymbol{\varepsilon}}^T + \frac{\lambda}{2} (\text{tr}\tilde{\boldsymbol{\varepsilon}})^2 \end{aligned}$$

$$+ \frac{\zeta + \eta}{2} \tilde{\chi} : \tilde{\chi} + \frac{\zeta - \eta}{2} \tilde{\chi} : \tilde{\chi}^T + \frac{\alpha}{2} (\text{tr} \tilde{\chi})^2, \quad (\text{A.1})$$

where μ and λ are Lamé constants and μ_c, ζ, η and α are four additional material parameters known as Cosserat constants. The constant μ_c is called the Cosserat's coupled modulus. If we additively decompose $\nabla \mathbf{u}$ and $\nabla \boldsymbol{\omega}$ into their symmetric and skew-symmetric parts

$$\nabla \mathbf{u} = \nabla^{sym} \mathbf{u} + \nabla^{skew} \mathbf{u}, \quad \nabla \boldsymbol{\omega} = \nabla^{sym} \boldsymbol{\omega} + \nabla^{skew} \boldsymbol{\omega}, \quad (\text{A.2})$$

and substitute in (A.1), we obtain

$$\begin{aligned} W_{ce}^{iso}(\tilde{\epsilon}, \tilde{\chi}) &= \mu \|\nabla^{sym} \mathbf{u}\|^2 + \mu_c \|\hat{\boldsymbol{\omega}} - \nabla^{skew} \mathbf{u}\|^2 + \frac{\lambda}{2} \|\nabla \cdot \mathbf{u}\|^2 \\ &\quad + \zeta \|\nabla^{sym} \boldsymbol{\omega}\|^2 + \eta \|\nabla^{skew} \boldsymbol{\omega}\|^2 + \frac{\alpha}{2} \|\nabla \cdot \boldsymbol{\omega}\|^2. \end{aligned} \quad (\text{A.3})$$

At the limit when the Cosserat couple modulus $\mu_c \mapsto \infty$, the effect of microstructure would be too rigid to be incorporated in the strain energy $W_{\tilde{\epsilon}}^{iso}(\tilde{\epsilon})$ and one can constrain the rotations as

$$\hat{\boldsymbol{\omega}} - \nabla^{skew} \mathbf{u} = \mathbf{0} \quad \Rightarrow \quad \boldsymbol{\omega} = \frac{1}{2} \nabla \times \mathbf{u}, \quad (\text{A.4})$$

which renders

$$\nabla \cdot \boldsymbol{\omega} = \frac{1}{2} \nabla \cdot (\nabla \times \mathbf{u}) = 0, \quad (\text{A.5})$$

leaving the parameter α indeterminate. Also called the *Cosserat theory of constrained rotations*, this model was first introduced by [Mindlin and Tiersten \[1962\]](#), discussed in [Toupin \[1962\]](#), and elaborated lucidly by [Koiter \[1964\]](#); hence it is also referred to as the Mindlin-Toupin-Koiter theory. The strain and curvature tensors now become

$$\tilde{\epsilon} = \nabla \mathbf{u} - \nabla^{skew} \mathbf{u} = \nabla^{sym} \mathbf{u} = \epsilon, \quad (\text{A.6})$$

$$\tilde{\chi} = \nabla \boldsymbol{\omega} = \frac{1}{2} \nabla (\nabla \times \mathbf{u}) \quad (\text{A.7})$$

Hence, in couple stress theory, the strain tensor is symmetric and the curvature tensor as seen in (A.5) is solenoidal. Also note that in the modified couple stress theory [Yang et al. \[2002\]](#), the curvature tensor is symmetric, meaning that the parameter η in (A.1) also vanishes and the curvature energy considered is then the *weakest* possible in [Neff and Jeong \[2009\]](#); [Jeong et al. \[2009\]](#) sense.

Appendix B. Constitutive equations for isotropic and anisotropic couple stress flexoelectric materials

In this section, the constitutive equations for isotropic and anisotropic couple stress based linear flexoelectric material models are presented, based on [Hadjesfandiari \[2013\]](#). For the anisotropic case the constitutive equations are given both in terms of the curvature vector and its dual, [Table B.2](#). Note that the following relationships exist between material tensors and their duals

$$\hat{\mathcal{B}}_{ijkl} = \frac{1}{4} \xi_{ijm} \xi_{kln} \mathcal{B}_{mn}, \quad \mathcal{B}_{mn} = \xi_{ijm} \xi_{kln} \hat{\mathcal{B}}_{ijkl},$$

Description	Isotropic	Anisotropic
Enthalpy	$\Psi^{iso}(\varepsilon_{ij}, \chi_i, E_i) = \mu \varepsilon_{ij} \varepsilon_{ij} + \frac{\lambda}{2} \varepsilon_{kk} \varepsilon_{ll} + 8\eta \chi_i \chi_i - 4\bar{f} \chi_i E_i - \frac{1}{2} \epsilon_{ij} E_i E_j$	$\Psi^{anis}(\varepsilon_{ij}, \hat{\chi}_{ij}, E_i) = \frac{1}{2} \mathcal{C}_{ijkl} \varepsilon_{ij} \varepsilon_{kl} + \frac{1}{2} \hat{\mathcal{B}}_{ijkl} \hat{\chi}_{ij} \hat{\chi}_{kl} + \hat{\mathcal{D}}_{ijkl} \varepsilon_{ij} \hat{\chi}_{kl} - e_{ijk} E_i \varepsilon_{jk} - f_{ijk} E_i \hat{\chi}_{jk} - \frac{1}{2} \epsilon_{ij} E_i E_j$ or $\Psi^{*anis}(\varepsilon_{ij}, \chi_i, E_i) = \frac{1}{2} \mathcal{C}_{ijkl} \varepsilon_{ij} \varepsilon_{kl} + \frac{1}{2} \mathcal{B}_{ij} \chi_i \chi_j - \mathcal{D}_{ijk} \varepsilon_{ij} \chi_k - e_{ijk} E_i \varepsilon_{jk} - f_{ij} \chi_i E_j - \frac{1}{2} \epsilon_{ij} E_i E_j$
Force stress	$\sigma_{ij} = 2\mu \varepsilon_{ij} + \lambda \varepsilon_{kk} \delta_{ij}$	$\sigma_{ij} = \mathcal{C}_{ijkl} \varepsilon_{kl} + \hat{\mathcal{D}}_{ijkl} \hat{\chi}_{kl} - e_{kij} E_k$ or $\sigma_{ij} = \mathcal{C}_{ijkl} \varepsilon_{kl} + \mathcal{D}_{ijk} \chi_k - e_{kij} E_k$
Couple stress	$\mu_i = 8\eta \chi_i - 2\bar{f} E_i$	$\hat{\mu}_{ij} = \hat{\mathcal{B}}_{ijkl} \hat{\chi}_{kl} + \hat{\mathcal{D}}_{klj} \varepsilon_{kl} - f_{kij} E_k$ or $\mu_i = \frac{1}{2} (\mathcal{B}_{ij} \chi_j + \mathcal{D}_{jki} \varepsilon_{jk} - f_{ji} E_j)$
Electric Displacement	$D_i = \epsilon E_i + 4\bar{f} \chi_i$	$D_i = \epsilon_{ij} E_j + e_{ijk} \varepsilon_{jk} + f_{ijk} \hat{\chi}_{jk}$, or $D_i = \epsilon_{ij} E_j + e_{ijk} \varepsilon_{jk} + f_{ij} \chi_j$

Table B.2: Constitutive equations for isotropic and anisotropic couple stress based linear flexoelectric materials

$$\begin{aligned}\hat{\mathcal{D}}_{ijkl} &= \frac{1}{2} \xi_{mlk} \mathcal{D}_{ilm}, & \mathcal{D}_{ilm} &= \xi_{lkm} \hat{\mathcal{D}}_{ijkl}, \\ \hat{f}_{ijk} &= \frac{1}{2} f_{il} \xi_{kjl}, & f_{il} &= \hat{f}_{ijk} \xi_{kjl},\end{aligned}$$

with the following restrictions on material tensors

$$\begin{aligned}\mathcal{C}_{ijkl} &= \mathcal{C}_{klij} = \mathcal{C}_{jikl}, & \hat{\mathcal{B}}_{ijkl} &= \hat{\mathcal{B}}_{klji} = -\hat{\mathcal{B}}_{jikl}, & \hat{\mathcal{D}}_{ijkl} &= \hat{\mathcal{D}}_{jikl} = -\hat{\mathcal{D}}_{ijlk}, \\ e_{ijk} &= e_{ikj}, & \hat{f}_{ijk} &= -\hat{f}_{ikj}, & \epsilon_{ij} &= \epsilon_{ji},\end{aligned}$$

or equivalently in their vector form

$$\begin{aligned}\mathcal{B}_{ij} &= \mathcal{B}_{ji}, \\ \mathcal{D}_{ijk} &= \mathcal{D}_{jik}.\end{aligned}$$

Note that in general there is no restriction on flexoelectric tensor \mathbf{f} and for the most general case, there are 78 distinct material parameters. For isotropic materials, the number of distinct component reduces to 4 material constants and one characteristic length scale. These are the two Lamé constants (λ, μ), one permittivity coefficient (ϵ), one flexoelectric coefficient (\bar{f}) and the curvature coefficient η is related to μ through the characteristic length scale l_s , such that

$$\mathcal{B}_{ij} = 16\eta \delta_{ij}, \quad \eta = \mu l_s^2, \quad f_{ij} = \bar{f} \delta_{ij}, \quad \epsilon_{ij} = \epsilon \delta_{ij}.$$

Appendix C. Finite element discretisation of the variational forms

In this section we present a family of mixed finite element discretisation schemes for the couple stress flexoelectric theory of continua and beams. The point of departure is the respective variational formulations presented in the previous two sections in particular, the penalty formulation for continuum (32), the penalty formulation for beams (102), the Lagrange multiplier for continuum (36), the Lagrange multiplier for beams (106), the augmented Lagrangian formulation for continuum (40) and the augmented Lagrangian formulation for beams (106). The finite element

discretisation follows naturally by introducing a non-overlapping partition of the domain Ω into a series of one-dimensional (for beams) or two and/or three-dimensional (for continuum) elements, as shown in [Figure C.17](#) and [Figure C.16](#), respectively. Owing to the nature of the aforementioned variational formulations, C^0 continuity can be retained for all variables by choosing the standard p -version of the finite element method [Suri \[1996\]](#); [Chilton and Suri \[1997\]](#) for discretisation. For the penalty formulation this entails employing piece-wise continuous P_n interpolation functions for displacements \mathbf{u} while piece-wise discontinuous P_{n-1}^D interpolation functions for rotations $\boldsymbol{\omega}$ (where $n \geq 2 \in \mathbb{N}$ represents any arbitrary polynomial degree and D represents the discontinuous nature of the interpolation functions), subjected to the satisfaction of the inf-sup condition [Brezzi \[1974\]](#); [Chapelle and Bathe \[1993\]](#). Similarly, for Lagrange multiplier and augmented Lagrangian formulations piece-wise continuous P_n interpolation functions for displacements \mathbf{u} and electric potential ψ and piece-wise discontinuous P_{n-1}^D interpolation functions for the rotations $\boldsymbol{\omega}$ and the Lagrange multiplier \mathbf{s} can be employed. These arrangements are shown in [Figure C.16](#) for triangles, quadrilaterals, tetrahedra and hexahedra, where the standard terminology in finite element is used (i.e. P representing the polynomial degree of interpolation bases for triangles and tetrahedral elements and Q denoting the polynomial degree of interpolation bases for quadrilateral and hexahedral elements). Similar discretisation methodology can be followed in the case of beams. While $\{\boldsymbol{\omega}, \boldsymbol{\theta}, \psi, \boldsymbol{\beta}, \boldsymbol{\gamma}\}$ can be discretised using piece-wise continuous P_n interpolation functions, $\{\boldsymbol{\omega}_c, \boldsymbol{\omega}_p, \mathbf{s}_c, \mathbf{s}_p\}$ can be discretised using piece-wise discontinuous P_{n-1}^D interpolation functions, subjected to the satisfaction of the inf-sup condition. These arrangements are shown in [Figure C.17](#).

To keep the presentation succinct, the details of finite element implementations are not discussed here. Finite element implementations of couple stress models for purely mechanical continuum elements are discussed in [Chakravarty et al. \[2017\]](#); [Garg and Han \[2015\]](#) for penalty formulation and in [Deng et al. \[2018\]](#); [Kwon and Lee \[2017\]](#) for Lagrange multiplier formulation (see also [Hajesfandiari et al. \[2016, 2017\]](#) for boundary element treatment of the problem). The previous work of the authors also describe computational implementation of a series of mixed and high order finite element discretisations based on an enhanced set of variables in electromechanics for continuum and beam elements [Ortigosa and Gil \[2016a\]](#); [Poya et al. \[2018\]](#); [Ortigosa et al. \[2016\]](#); [Poya et al. \[2015\]](#). It is worth noting that, due to the discontinuous nature of couple stress related variables, their corresponding contributions can be locally condensed out using static condensation leading to an extremely efficient implementation of couple stress flexoelectricity that can be easily incorporated in to an existing piezoelectric finite element software [Poya et al. \[2017\]](#). Furthermore, since at least a quadratic interpolation is used for displacements, the geometry of flexoelectric structures can be represented accurately using the recently developed isoparametric curvilinear finite element technology presented in [Poya et al. \[2016, 2018\]](#).

Appendix C.1. Convergence study and further quantification of curvature-induced electromechanical coupling efficiency

In this section, the electromechanical coupling efficiency of the couple stress flexoelectric formulation is investigated using all the developed finite element techniques. The study albeit simple in nature, tests both the convergence properties of the finite element schemes and the quantification of flexoelectric based electric polarisation using the skew-symmetric couple stress theory. The problem involves mechanically loading a cantilever beam and monitoring the generated electric polarisation using the electromechanical coupling efficiency as a measure, as shown in [Figure C.18](#). This problem is analysed under strain gradient elasticity by [Nanthakumar et al. \[2017\]](#) and an analytical solution for the Electromechanical Coupling Efficiency (ECF) is given in [Majdoub et al.](#)

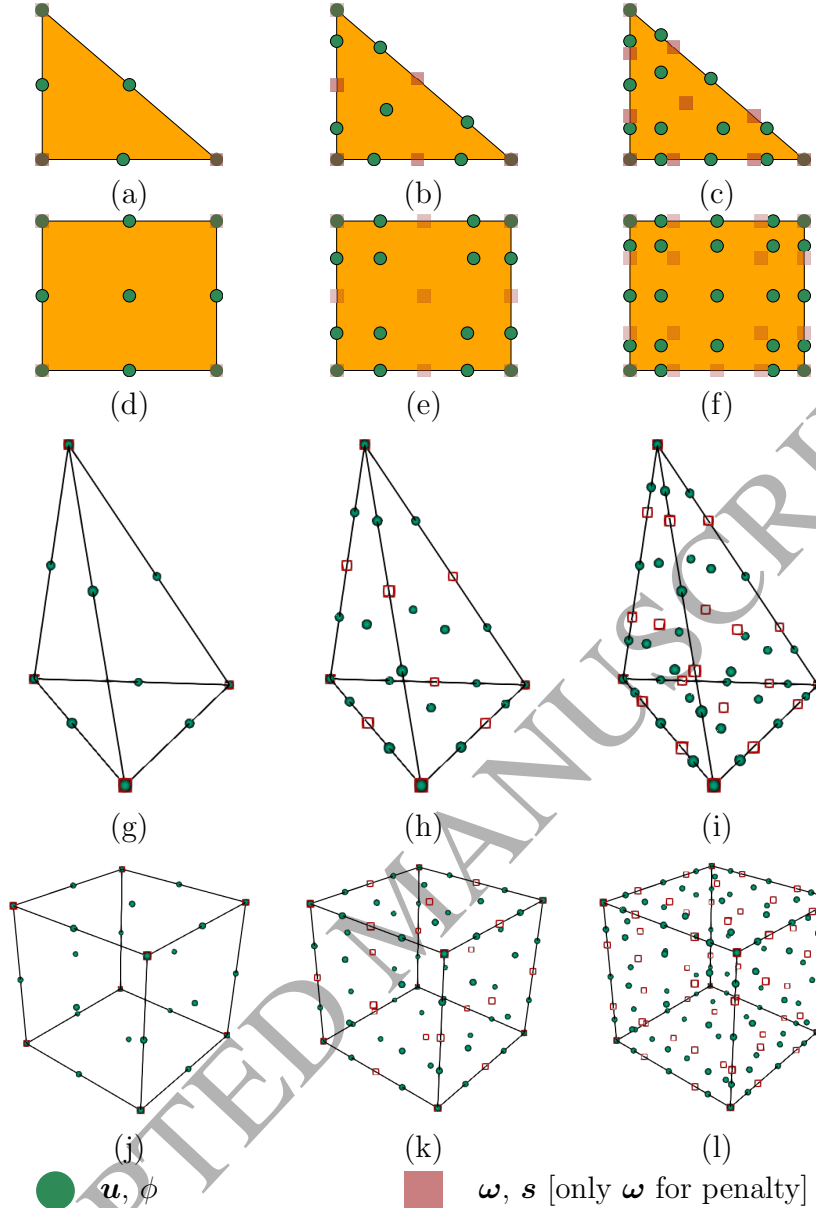


Figure C.16: A non-exhaustive list of the developed mixed finite elements for triangles: (a) $P_2-P_2-P_1^D-P_1^D/P_2-P_2-P_1^D$, (b) $P_3-P_3-P_2^D-P_2^D/P_3-P_3-P_2^D$, (c) $P_4-P_4-P_3^D-P_3^D/P_4-P_4-P_3^D$; quadrilaterals: (d) $Q_2-Q_1^D-Q_1^D/Q_2-Q_1^D$, (e) $Q_3-Q_3-Q_2^D-Q_2^D/Q_3-Q_3-Q_2^D$, (f) $Q_4-Q_4-Q_3^D-Q_3^D/Q_4-Q_4-Q_3^D$; tetrahedra: (g) $P_2-P_2-P_1^D-P_1^D/P_2-P_2-P_1^D$, (h) $P_3-P_3-P_2^D-P_2^D/P_3-P_3-P_2^D$, (i) $P_4-P_4-P_3^D-P_3^D/P_4-P_4-P_3^D$ and hexahedra: (j) $Q_2-Q_2-Q_1^D-Q_1^D/Q_2-Q_2-Q_1^D$, (k) $Q_3-Q_3-Q_2^D-Q_2^D/Q_3-Q_3-Q_2^D$, (l) $Q_4-Q_4-Q_3^D-Q_3^D/Q_4-Q_4-Q_3^D$. The developed framework encompasses $P_n-P_n-P_{n-1}^D-P_{n-1}^D$, $P_n-P_n-P_{n-1}^D$, $Q_n-Q_n-Q_{n-1}^D-Q_{n-1}^D$, $Q_n-Q_n-Q_{n-1}^D$ for any interpolation degree n .

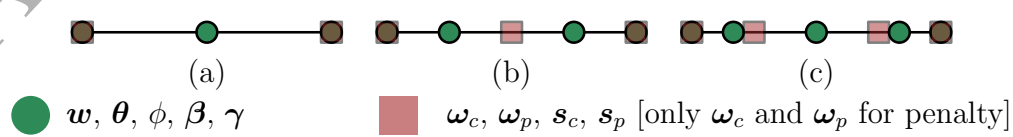


Figure C.17: A non-exhaustive list of the developed mixed finite elements for one-dimensional beam elements: (a) $P_2-P_2-P_2-P_2-P_1^D-P_1^D-P_1^D/P_2-P_2-P_2-P_2-P_1^D-P_1^D$, (b) $P_3-P_3-P_3-P_3-P_3-P_2^D-P_2^D-P_2^D/P_3-P_3-P_3-P_3-P_2^D-P_2^D$, (c) $P_4-P_4-P_4-P_4-P_4-P_3^D-P_3^D-P_3^D/P_4-P_4-P_4-P_4-P_3^D-P_3^D$. The developed framework encompasses $P_n-P_n-P_n-P_n-P_n-P_{n-1}^D-P_{n-1}^D-P_{n-1}^D$, $P_n-P_n-P_n-P_n-P_{n-1}^D-P_{n-1}^D-P_{n-1}^D$ for any interpolation degree n .

[2008] as

$$k_a^{eff} = \frac{\varpi}{1 + \varpi} \sqrt{\frac{\epsilon}{E} \left(e^2 + 12 \left(\frac{f}{h} \right)^2 \right)}, \quad (C.1)$$

where ϖ is the electrical susceptibility of the material (where $\varpi = 1408$ for the case of BaTiO₃), E the Young's modulus and ϵ , e and f the dielectric, piezoelectric and flexoelectric coupling coefficients of the material, respectively. L and h represent the length and the height of the beam, respectively; see also [Figure C.18](#). In the context of finite elements, the electromechanical conversion efficiency can be computed as the norm of the ratio of electrical energy to mechanical energy i.e.

$$\frac{1}{k_n^{eff2}} = \left\| \frac{W_{mech}}{W_{elect}} \right\|$$

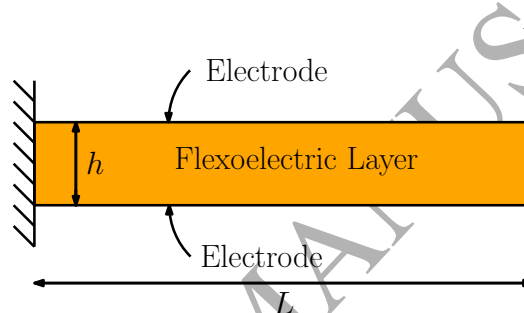


Figure C.18: Cantilever beam chosen for convergence study of the developed finite element discretisation techniques

However, given that the analytical solution for this problem was derived from the strain gradient model, for convergence studies, we choose to work with a reference solution obtained from an extremely fine discretisation. For the purpose of convergence studies, once again BaTiO₃ is chosen with material properties shown in [Table 1](#) by neglecting the piezoelectric effects i.e. setting $e_{31} = e_{33} = e_{15} = e = 0$. Only \bar{f}_{12} effect is considered i.e. $f = \bar{f}_{12}$. The length of the beam is kept at $0.8\mu m$ and the aspect ratio of the beam is varied from 10 to 50, while a constant load of $F = 100\mu N$ is applied on the free end of the beam.

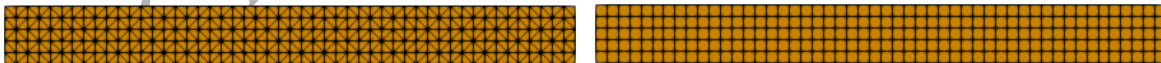


Figure C.19: Triangular and quadrilateral meshes (only aspect ratio 10 shown here) chosen for convergence study of the developed finite element discretisation techniques. Both meshes possess the same number of nodes

First a series of convergence studies are performed by using the quadratic mixed finite elements i.e. P2-P2-P1^D-P1^D/P2-P2-P1^D and Q2-Q2-Q1^D-Q1^D/Q2-Q2-Q1^D elements in a two-dimensional setting by successively refining the meshes, i.e. by performing the so-called h -refinement. To this end, two set of meshes are chosen namely a triangular mesh and a quadrilateral mesh, as shown in [Figure C.19](#) and the ECF is computed using the mixed finite elements and compared to the reference solution. The convergence properties of the mixed finite elements for the three variational formulations namely the penalty formulation, the Lagrange multiplier formulation and the augmented Lagrangian formulation is subsequently studied, by choosing the penalty parameter

to coincide with the Cosserat modulus $\kappa = \mu l_s^2 = 5 \times 10^{-7}$ GPa, where $l_s = 1\text{nm}$ is the length scale parameter. The chosen value of l_s is well within the range of the thickness chosen for epitaxial ferroelectric thin films.

Figure C.20 shows the h -convergence results of the different finite element discretisation techniques for penalty, Lagrange multiplier and augmented Lagrangian formulations for triangular and quadrilateral meshes, when the quadratic interpolation is used for displacements i.e. P2-P2-P1^D-P1^D/P2-P2-P1^D and Q2-Q2-Q1^D-Q1^D/Q2-Q2-Q1^D discretisations. It can be observed that the expected rate of convergence for electromechanical energy is achieved for all formulations with both triangular and quadrilateral elements Szabó and Babuška [1991]. Expectedly, the Lagrange multiplier approach performs the best, while the error incurred using the penalty approach is the highest. The augmented Lagrangian approach converges at the same rate, but the error incurred lies in between the penalty and the Lagrange multiplier approach. As the aspect ratio of the beam increases the incurred error typically increases. The performance of triangular and quadrilateral elements in general similar due the fact that both meshes have the same number of nodes and the triangular mesh is generated by a symmetric tessellation of the quadrilateral mesh. It should be noted that, since the couple stress theory imposes a constraint on the rotation part of the displacement gradients, bending locking becomes an apparent issue. The use of high order mixed finite elements in general resolves such bending problems Poya et al. [2018].

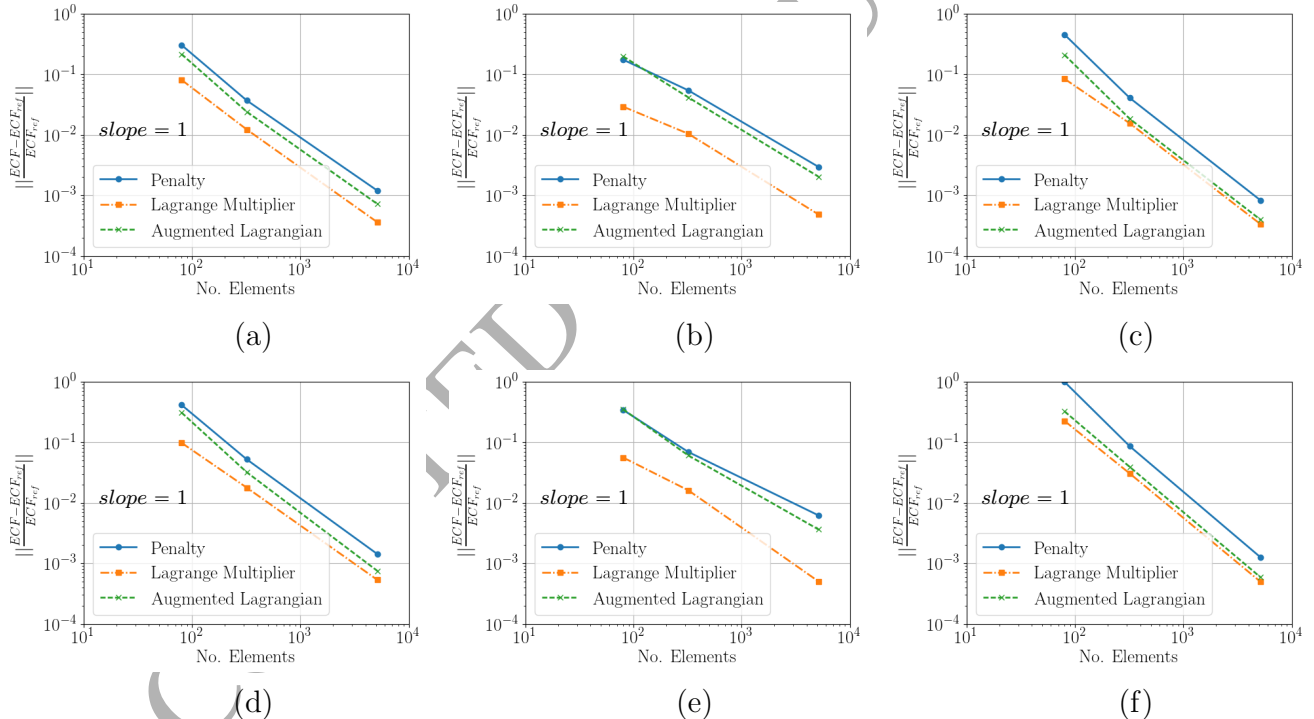


Figure C.20: Convergence of error in Electromechanical Coupling Efficiency (ECF) for different finite element discretisation techniques on triangular elements, a) aspect ratio 10, b) aspect ratio 25, c) aspect ratio 50, and quadrilateral elements, d) aspect ratio 10, e) aspect ratio 25, f) aspect ratio 50

Having confirmed the convergence of the quadratic mixed finite element for the two-dimensional case for triangular and quadrilateral meshes, the same problem is then analysed by fixing the refinement level (h) and successively increasing the order of finite element interpolation functions i.e. by performing the so-called p -refinement. In this context, we refer to p or q as the highest polynomial degree used for any variable (i.e. displacements and electric potential). This allows us to study the performance of higher order mixed finite elements shown in Figure C.16. To this end, two three-dimensional meshes are considered namely a tetrahedral mesh and hexahedral mesh, as

shown in Figure C.21.

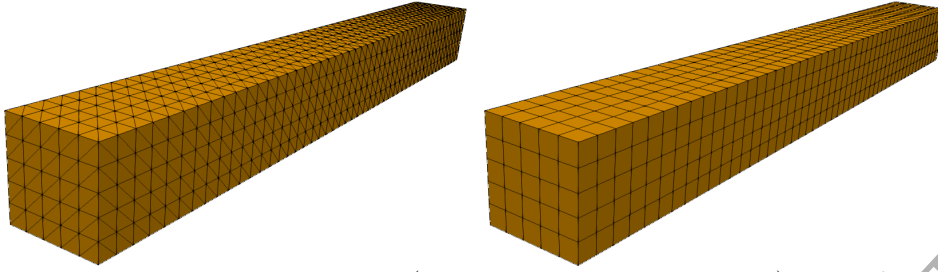


Figure C.21: Tetrahedral and hexahedral meshes (only aspect ratio 10 shown here) chosen for convergence study of the developed finite element discretisation techniques. Both meshes possess the same number of nodes

Figure C.22 shows the p -convergence results of the different finite element discretisation techniques for penalty, Lagrange multiplier and augmented Lagrangian formulations for triangular and quadrilateral meshes for aspect ratio 10. Once again, the expected rate of convergence for electromechanical energy is achieved for all formulations with both tetrahedral and hexahedral elements Szabó and Babuška [1991]. The Lagrange multiplier approach performs the best, followed by the augmented Lagrangian approach and the penalty, respectively. The performance of tetrahedral and hexahedral elements in general similar due the fact that both meshes have the same number of nodes and the tetrahedral mesh is generated by further tessellation of the hexahedral mesh. Note that this study confirms the rate of convergence for different choices of polynomial functional spaces for mixed finite elements up to $p = q = 6$, confirming their suitability for discretising the three aforementioned couple stress variational formulation.

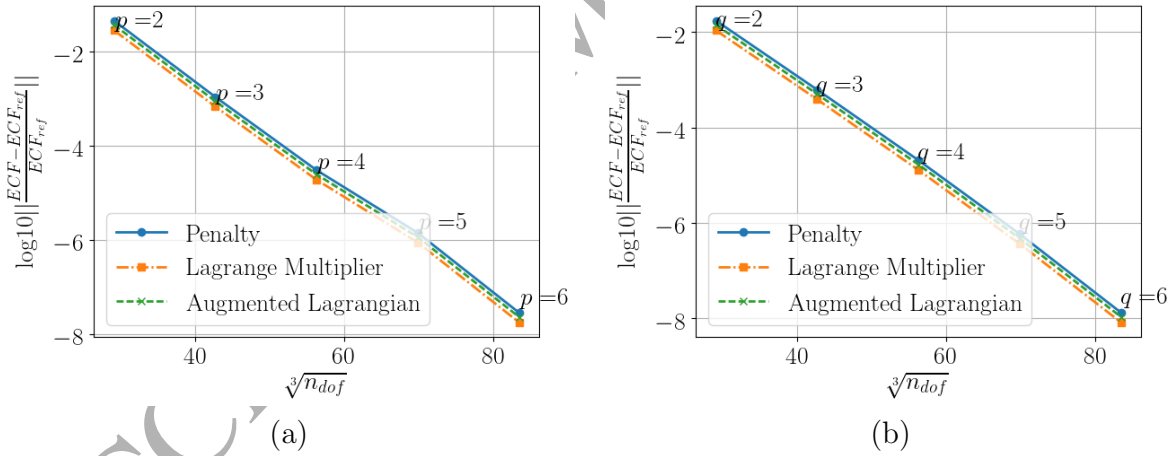


Figure C.22: Convergence of error in Electromechanical Coupling Efficiency (ECF) for different finite element discretisation techniques on tetrahedral and hexahedral elements for aspect ratio 10

Acknowledgments

The first author acknowledges the financial support received through the European Commission EACEA Agency, Framework Partnership Agreement 2013-0043 Erasmus Mundus Action 1b, as a part of the EM Joint Doctorate “Simulation in Engineering and Entrepreneurship Development (SEED)”. The second author acknowledges the financial support received through the European Training Network AdMoRe (Project ID: 675919). The third author acknowledges the financial

support provided by the Sêr Cymru National Research Network through Sêr Cymru II fellowship, funded by the European Regional Development Fund (ERDF).

References

- A. Erturk, D. J. Inman, *Piezoelectric Energy Harvesting*, first ed., John Wiley & Sons Inc., Chichester, England, 2011.
- N. E. duToit, B. L. Wardle, S. G. Kim, *Design considerations for MEMS-scale piezoelectric mechanical vibration energy harvesters*, Integrated Ferroelectrics 16 (2005) 121–160.
- M. Trindade, A. Benjeddou, R. Ohayon, *Finite element modelling of hybrid activepassive vibration damping of multilayer piezoelectric sandwich beams-part I: Formulation*, International Journal for Numerical Methods in Engineering 51 (2001a) 835–854.
- M. Trindade, A. Benjeddou, R. Ohayon, *Finite element modelling of hybrid activepassive vibration damping of multilayer piezoelectric sandwich beams-part II: System analysis*, International Journal for Numerical Methods in Engineering 51 (2001b) 855–864.
- J. Schröder, D. Gross, *Invariant formulation of the electromechanical enthalpy function of transversely isotropic piezoelectric materials*, Archive of Applied Mechanics 73 (2004) 533–552.
- R. Poya, A. J. Gil, P. D. Ledger, *A computational framework for the analysis of linear piezoelectric beams using hp-FEM*, Computers and Structures, 152 (2015) 155–172.
- W. A. Wooster, *Tensors and Group Theory for the Physical Properties of Crystals*, Clarendon Press, Oxford, England, 1973.
- P. Zubko, G. Catalan, A. Buckley, P. R. L. Welche, J. F. Scott, *Strain-gradient-induced polarization in SrTiO₃ single crystals*, Physical Review Letters 99 (2007) 167601.
- P. Zubko, G. Catalan, A. K. Tagantsev, *Flexoelectric Effect in Solids*, Annual Review of Materials Research 43 (2013) 387–421.
- T. Dumitrica, C. M. Landis, B. I. Yakobson, *Curvature-induced polarization in carbon nanoshells*, Chemical Physics Letters 360 (2002) 182–188.
- A. G. Petrov, Electricity and mechanics of biomembrane systems: Flexoelectricity in living membranes, Analytica Chimica Acta 568 (2006) 70 – 83. Molecular Electronics and Analytical Chemistry.
- R. Maranganti, N. D. Sharma, P. Sharma, *Electromechanical coupling in nonpiezoelectric materials due to nanoscale nonlocal size effects: Greens function solutions and embedded inclusions*, Physical Review B 74 (2006) 014110.
- S. V. Kalinin, V. Meunier, *Electronic flexoelectricity in low-dimensional systems*, Physical Review B 77 (2008) 033403.
- R. Maranganti, P. Sharma, *Atomistic determination of flexoelectric properties of crystalline dielectrics*, Physical Review B 80 (2009) 054109.
- M. Zelisko, Y. Hanlumyuang, S. Yang, Y. Liu, C. Lei, J. Li, P. M. Ajayan, P. Sharma, *Anomalous piezoelectricity in two-dimensional graphene nitride nanosheets*, Nature Communications 5 (2014) 4284.
- Q. Deng, L. P. Liu, P. Sharma, *Flexoelectricity in soft materials and biological membranes*, Journal of the Mechanics of Physics of Solids 62 (2014) 209–227.
- A. K. Tagantsev, *Piezoelectricity and flexoelectricity in crystalline dielectrics*, Physical Review B 34 (1986) 5883.
- W. Ma, L. E. Cross, *Large flexoelectric polarization in ceramic lead magnesium niobate*, Applied Physics Letters 79 (2001) 4420.
- W. Ma, L. E. Cross, *Flexoelectric polarization of barium strontium titanate in the paraelectric state*, Applied Physics Letters 81 (2002) 3440.
- G. Catalan, B. Noheda, J. McAneney, L. J. Sinnamon, J. M. Gregg, *Strain gradients in epitaxial ferroelectrics*, Physical Review B 72 (2005) 020102(R).
- W. Ma, L. E. Cross, *Flexoelectricity of barium titanate*, Applied Physics Letters 88 (2006) 232902.
- N. D. Sharma, R. Maranganti, P. Sharma, *On the possibility of piezoelectric nanocomposites without using piezoelectric materials*, Journal of the Mechanics and Physics of Solids 55 (2007) 2328–2350.
- N. D. Sharma, C. M. Landis, P. Sharma, *Piezoelectric thin-film superlattices without using piezoelectric materials*, Journal of Applied Physics 108 (2010) 024304.
- M. Gharbi, Z. Sun, P. Sharma, K. White, E.-B. S., *Flexoelectric properties of ferroelectrics and the nanoindentation size-effect*, International Journal of Solids and Structures 48 (2011) 249–256.
- S. Kriven, P. Sharma, *Flexoelectricity: A perspective on an unusual electromechanical coupling*, Journal of Applied Mechanics 83 (2016) 030801.
- P. V. Yudin, A. K. Tagantsev, *Fundamentals of flexoelectricity in solids*, Nanotechnology 24 (2013) 432001.

- Q. Deng, M. Kammoun, A. Erturk, P. Sharma, [Nanoscale flexoelectric energy harvesting](#), International Journal of Solids and Structures 51 (2014) 3218–3225.
- X. Jiang, W. Huang, S. Zhang, [Flexoelectric nano-generator: Materials, structures and devices](#), Nano Energy 2 (2013) 1079–1092.
- A. C. Eringen, G. A. Maugin, [Electrodynamics of Continua I: Foundations and Solid Media](#), Springer, Dordrecht, Heidelberg, London, New York, 1990.
- E. Cosserat, F. Cosserat, Théorie des corps déformables, Librairie Scientifique A. Hermann et Fils Paris (1909).
- R. D. Mindlin, H. F. Tiersten, [Effects of couple-stresses in linear elasticity](#), Archive for Rational Mechanics and Analysis 11 (1962) 415–488.
- R. D. Mindlin, [Micro-structure in linear elasticity](#), Archive for Rational Mechanics and Analysis 16 (1964) 51–78.
- R. D. Mindlin, [Second gradient of strain and surface-tension in linear elasticity](#), International Journal of Solids and Structures 1 (1965) 417–438.
- R. D. Mindlin, [Polarization gradient in elastic dielectrics](#), International Journal of Solids and Structures 4 (1968) 637–642.
- R. D. Mindlin, N. N. Eshel, [On first strain-gradient theories in linear elasticity](#), International Journal of Solids and Structures 4 (1968) 109–124.
- R. A. Toupin, [Elastic materials with couple-stresses](#), Archive for Rational Mechanics and Analysis 11 (1962) 385–414.
- R. A. Toupin, [Theories of elasticity with couple-stress](#), Archive for Rational Mechanics and Analysis 17 (1964) 85–112.
- A. C. Eringen, [Linear theory of micropolar elasticity](#), Indiana University Mathematics Journal 15 (1966) 909–923.
- A. C. Eringen, [Nonlocal polar elastic continua](#), International Journal of Engineering Science 10 (1972a) 1–16.
- A. C. Eringen, [Linear theory of nonlocal elasticity and dispersion of plane waves](#), International Journal of Engineering Science 10 (1972b) 425–435.
- A. C. Eringen, [On differential equations of nonlocal elasticity and solutions of screw dislocation and surface waves](#), Journal of Applied Physics 54 (1983) 4703.
- A. C. Eringen, [Theory of Micropolar Elasticity](#), In: Microcontinuum Field Theories Springer, Dordrecht, Heidelberg, London, New York (1999) 101–248.
- J. L. Erickson, C. Truesdell, [Exact theory of stress and strain in rods and shells](#), Archive for Rational Mechanics and Analysis 1 (1958) 295–323.
- D. C. C. Lam, F. Yang, A. C. M. Chong, J. Wang, P. Tong, [Experiments and theory in strain gradient elasticity](#), Journal of the Mechanics and Physics of Solids 51 (2003) 1477–1508.
- A. R. Hadjesfandiari, G. F. Dargush, [Couple stress theory for solids](#), International Journal of Solids and Structures 48 (2011) 2496–2510.
- W. T. Koiter, [Couple-stresses in the theory of elasticity: I and II.](#), Proc. Ned. Akad. Wetenschap B 67 (1964) 17–44.
- F. Yang, A. C. M. Chong, D. C. C. Lam, P. Tong, [Couple stress based strain gradient theory for elasticity](#), International Journal of Solids and Structures 39 (2002) 2731–2743.
- S. K. Park, X.-L. Gao, [Variational formulation of a modified couple stress theory and its application to a simple shear problem](#), Zeitschrift für angewandte Mathematik und Physik 59 (2008) 904–917.
- P. Neff, [The Cosserat couple modulus for continuous solids is zero viz the linearized Cauchy-stress tensor is symmetric](#), ZAMM - Zeitschrift für Angewandte Mathematik und Mechanik 86 (2006) 892–912.
- P. Neff, J. Jeong, [A new paradigm: the linear isotropic Cosserat model with conformally invariant curvature energy](#), ZAMM - Zeitschrift für Angewandte Mathematik und Mechanik 89 (2009) 107–122.
- J. Simo, D. Fox, T. Hughes, [Formulations of finite elasticity with independent rotations](#), Computer Methods in Applied Mechanics and Engineering 95 (1992) 277 – 288.
- P. Steinmann, [A micropolar theory of finite deformation and finite rotation multiplicative elastoplasticity](#), International Journal of Solids and Structures 31 (1994) 1063 – 1084.
- P. Steinmann, E. Stein, [A unifying treatise of variational principles for two types of micropolar continua](#), Acta Mechanica 121 (1997) 215–232.
- P. Neff, [A finite-strain elasticplastic cosserat theory for polycrystals with grain rotations](#), International Journal of Engineering Science 44 (2006) 574 – 594.
- S. Bauer, W. G. Dettmer, D. D. Perić, M. Schäfer, [Micropolar hyperelasticity: constitutive model, consistent linearization and simulation of 3D scale effects](#), Computational Mechanics 50 (2012) 383–396.
- A. Abdollahi, C. Peco, D. Millan, M. Arroyo, I. Arias, [Computational evaluation of the flexoelectric effect in dielectric solids](#), Journal of Applied Physics 116 (2014) 093502.

- A. Abdollahi, D. Millán, C. Peco, M. Arroyo, I. Arias, Revisiting pyramid compression to quantify flexoelectricity: A three-dimensional simulation study, *Physical Review B* 91 (2015) 104103.
- F. Deng, Q. Deng, S. Shen, A three-dimensional mixed finite element for flexoelectricity, *Journal of Applied Mechanics* 85 (2018) 031009.
- M. S. Majdoub, P. Sharma, T. Cagin, Enhanced size-dependent piezoelectricity and elasticity in nanostructures due to the flexoelectric effect, *Physical Review B* 77 (2008) 125424.
- M. S. Majdoub, P. Sharma, T. Cagin, Erratum: Enhanced size-dependent piezoelectricity and elasticity in nanostructures due to the flexoelectric effect, *Physical Review B* 79 (2009) 119904.
- S. Mao, P. K. Purohit, Insights into flexoelectric solids from strain-gradient elasticity, *ASME - Journal of Applied Mechanics* 81 (2014) 081004.
- J. Chen, Micropolar theory of flexoelectricity, *Journal of Advanced Mathematics and Applications* 1 (2012) 269–274.
- A. R. Hadjesfandiari, Size-dependent piezoelectricity, *International Journal of Solids and Structures* 50 (2013) 2781–2791.
- I. Takayoshi, Bending piezoelectricity in polytetrafluoroethylene, *Japanese Journal of Applied Physics* 13 (1974) 197.
- E. Fukada, G. M. Sessler, J. E. West, A. Berraissoul, P. Günther, Bending piezoelectricity in monomorph polymer films, *Journal of Applied Physics* 62 (1987) 3643.
- W. Ma, L. E. Cross, Flexoelectric effect in ceramic lead zirconate titanate, *Applied Physics Letters* 86 (2005) 072905.
- S. K. Park, X.-L. Gao, Bernoulli-Euler beam model based on a modified couple stress theory, *Journal of Micromechanics and Microengineering* 16 (2006) 2355.
- H. M. Ma, X.-L. Gao, J. N. Reddy, A microstructure-dependent Timoshenko beam model based on a modified couple stress theory, *Journal of the Mechanics and Physics of Solids* 56 (2008) 3379–3391.
- J. N. Reddy, Microstructure-dependent couple stress theories of functionally graded beams, *Journal of the Mechanics and Physics of Solids* 59 (2011) 2382–2399.
- J. N. Reddy, S. El-Borgi, Eringen's nonlocal theories of beams accounting for moderate rotations, *International Journal of Engineering Science* 82 (2014) 159–187.
- A. R. Srinivasa, J. N. Reddy, A model for a constrained, finitely deforming, elastic solid with rotation gradient dependent strain energy, and its specialization to von Krmn plates and beams, *Journal of the Mechanics and Physics of Solids* 61 (2013) 873–885.
- G. C. Tsiatas, A new Kirchhoff plate model based on a modified couple stress theory, *International Journal of Solids and Structures* 46 (2009) 2757–2764.
- J. Jeong, P. Neff, Existence, uniqueness and stability in linear Cosserat elasticity for weakest curvature conditions, *Mathematics and Mechanics of Solids* 15 (2010) 78–95.
- I.-D. Ghiba, P. Neff, A. Madeo, I. Münch, A variant of the linear isotropic indeterminate couple-stress model with symmetric local force-stress, symmetric nonlocal force-stress, symmetric couple-stresses and orthogonal boundary conditions, *Mathematics and Mechanics of Solids* 22 (2017) 1221–1266.
- M. Romeo, Polarization in dielectrics modeled as micromorphic continua, *Z. Angew. Math. Phys.* 66 (2015) 1233.
- L. Anqing, Z. Shenjie, Q. Lu, C. Xi, A flexoelectric theory with rotation gradient effects for elastic dielectrics, *Modelling and Simulation in Materials Science and Engineering* 24 (2016) 015009.
- R. de Borst, L. J. Sluys, Localisation in a Cosserat continuum under static and dynamic loading conditions, *Computer Methods in Applied Mechanics and Engineering* 90 (1991) 805–827.
- A. Madeo, I.-D. Ghiba, P. Neff, I. Münch, A new view on boundary conditions in the grilikoitermindlintoupin indeterminate couple stress model, *European Journal of Mechanics - A/Solids* 59 (2016) 294 – 322.
- W. Nowacki, Theory of Assymmetric Elasticity, second ed., Pergamon Press and PWN, Warsaw, Oxford, New York, Toronto, Sydney, Paris, Frankfurt, 1986.
- M. Braun, Linear Elasticity with Couple Stresses, In *Mechanics of Microstructured Solids* 2 50 (2010) 1–8.
- R. de Boer, *Vektor- und Tensorrechnung für Ingenieure*, Springer Inc., Berlin, 1982.
- J. Bonet, A. J. Gil, R. Ortigosa, A computational framework for polyconvex large strain elasticity, *Computer Methods in Applied Mechanics and Engineering* 283 (2015a) 1061–1094.
- J. Bonet, A. J. Gil, R. Ortigosa, On a tensor cross product based formulation of large strain solid mechanics, Under Review (2015b).
- J. Bonet, A. J. Gil, C. H. Lee, M. Aguirre, R. Ortigosa, A first order hyperbolic framework for large strain computational solid dynamics. Part I: Total Lagrangian isothermal elasticity, *Computer Methods in Applied Mechanics and Engineering* 283 (2015c) 689–732.

- A. J. Gil, R. Ortigosa, A new framework for large strain electromechanics based on convex multi-variable strain energies: Variational formulation and material characterisation, Computer Methods in Applied Mechanics and Engineering 302 (2016) 293 – 328.
- R. Ortigosa, A. J. Gil, A new framework for large strain electromechanics based on convex multi-variable strain energies: Finite element discretisation and computational implementation, Computer Methods in Applied Mechanics and Engineering 302 (2016a) 329 – 360.
- R. Ortigosa, A. J. Gil, A new framework for large strain electromechanics based on convex multi-variable strain energies: Conservation laws, hyperbolicity and extension to electro-magneto-mechanics, Computer Methods in Applied Mechanics and Engineering 309 (2016b) 202 – 242.
- A. J. Gil, P. D. Ledger, [A coupled \$hp\$ -finite element scheme for the solution of two-dimensional electrostrictive materials](#), International Journal for Numerical Methods in Engineering 91 (2012) 1158–1183.
- R. Lakes, Experimental methods for study of Cosserat elastic solids and other generalized continua, In Continuum Models for Materials with Micro-structure (1995) 1–22.
- P. Neff, I. Münch, I.-D. Ghiba, A. Madeo, On some fundamental misunderstandings in the indeterminate couple stress model. a comment on recent papers of A.R. Hadjesfandiari and G.F. Dargush, International Journal of Solids and Structures 81 (2016) 233 – 243.
- B. T. Darrall, G. F. Dargush, A. R. Hadjesfandiari, [Finite element Lagrange multiplier formulation for size-dependent skew-symmetric couple-stress planar elasticity](#), Acta Mechanica 255 (2014) 195–212.
- B. T. Darrall, A. R. Hadjesfandiari, G. F. Dargush, [Size-dependent piezoelectricity: A 2D finite element formulation for electric field-mean curvature coupling in dielectrics](#), European Journal of Mechanics A/Solids 49 (2015) 308–320.
- A. C. Eringen, [Theory of Micropolar Elasticity](#), Technical Report No. 1 Princeton University (1967) 1–152.
- H. G. Georgiadis, E. G. Velgaki, [High-frequency Rayleigh waves in materials with micro-structure and couple-stress effects](#), International Journal of Solids and Structures 40 (2003) 2501–2520.
- G. Deng, G. F. Dargush, [Mixed Lagrangian formulation for size-dependent couple stress elastodynamic and natural frequency analyses](#), International Journal for Numerical Methods in Engineering 109 (2017) 809–836.
- K. L. Sudeep, J. Bonet, J. Peraire, L. Casals, [A variationally consistent fractional time-step integration method for incompressible and nearly incompressible Lagrangian dynamics](#), International Journal for Numerical Methods in Engineering 63 (2005) 1371–1395.
- M. Şişmek, J. N. Reddy, [Bending and vibration of functionally graded microbeams using a new higher order beam theory and the modified couple stress theory](#), International Journal of Engineering Science 64 (2012) 37–53.
- M. Şişmek, J. N. Reddy, [A unified higher order beam theory for buckling of a functionally graded microbeam embedded in elastic medium using modified couple stress theory](#), Composite Structures 101 (2013) 47–58.
- X. Li, Y. Luo, Flexoelectric effect on vibration of piezoelectric microbeams based on a modified couple stress theory, Shock and Vibration 2017, Article ID 4157085 (2017).
- K. D. Hjelmstad, [Fundamentals of Structural Mechanics](#), International series in civil engineering and engineering mechanics. Springer Inc., New York, 2005.
- D. Berlincourt, H. Jaffe, Elastic and piezoelectric coefficients of single-crystal barium titanate, Phys. Rev. 111 (1958) 143–148.
- S. Nanthakumar, X. Zhuang, H. S. Park, T. Rabczuk, Topology optimization of flexoelectric structures, Journal of the Mechanics and Physics of Solids 105 (2017) 217 – 234.
- H. Ghasemi, H. S. Park, T. Rabczuk, A level-set based IGA formulation for topology optimization of flexoelectric materials, Computer Methods in Applied Mechanics and Engineering 313 (2017) 239 – 258.
- R. Poya, A. J. Gil, R. Ortigosa, R. Sevilla, J. Bonet, W. A. Wall, A curvilinear high order finite element framework for electromechanics: From linearised electro-elasticity to massively deformable dielectric elastomers, Computer Methods in Applied Mechanics and Engineering 329 (2018) 75 – 117.
- R. Poya, R. Sevilla, A. J. Gil, A unified approach for a posteriori high-order curved mesh generation using solid mechanics, Computational Mechanics 58 (2016) 457–490.
- R. Poya, A. J. Gil, R. Ortigosa, A high performance data parallel tensor contraction framework: Application to coupled electro-mechanics, Computer Physics Communications 216 (2017) 35 – 52.
- J. Jeong, H. Ramézani, I. Münch, P. Neff, [A numerical study for linear isotropic Cosserat elasticity with conformally invariant curvature](#), ZAMM - Zeitschrift für Angewandte Mathematik und Mechanik 89 (2009) 552–569.
- M. Suri, [Analytical and computational assessment of locking in the \$hp\$ finite element method](#), Computer Methods in Applied Mechanics and Engineering 133 (1996) 347–371.
- L. Chilton, M. Suri, [On the selection of a locking-free \$hp\$ element for elasticity problems](#), International Journal for Numerical Methods in Engineering 40 (1997) 2045–2062.

- F. Brezzi, On the existence, uniqueness and approximation of saddle-point problems arising from Lagrange multiplier, *Revue française d'automatique, informatique, recherche opérationnelle, Analyse numérique* 8 (1974) 129–151.
- D. Chapelle, K. Bathe, The inf-sup test, *Computers & Structures* 47 (1993) 537 – 545.
- S. Chakravarty, A. R. Hadjesfandiari, G. F. Dargush, A penalty-based finite element framework for couple stress elasticity, *Finite Element in Analysis & Design* 130 (2017) 65–79.
- N. Garg, C.-S. Han, Axisymmetric couple stress elasticity and its finite element formulation with penalty terms, *Archive of Applied Mechanics* 85 (2015) 587–600.
- Y.-R. Kwon, B.-C. Lee, A mixed element based on lagrange multiplier method for modified couple stress theory, *Computational Mechanics* 59 (2017) 117–128.
- A. Hajesfandiari, A. R. Hadjesfandiari, G. F. Dargush, Boundary element formulation for plane problems in size-dependent piezoelectricity, *International Journal for Numerical Methods in Engineering* 108 (2016) 667–694.
- A. Hajesfandiari, A. R. Hadjesfandiari, G. F. Dargush, Boundary element formulation for steady state plane problems in size-dependent thermoelasticity, *Engineering Analysis with Boundary Elements* 82 (2017) 210 – 226.
- R. Ortigosa, A. J. Gil, J. Bonet, C. Hesch, A computational framework for polyconvex large strain elasticity for geometrically exact beam theory, *Computational Mechanics* 57 (2016) 277–303.
- B. Szabó, I. Babuška, [Finite Element Analysis](#), John Wiley and Sons Inc., New York, 1991.